DEMOCRATIC AND POPULAR REPUBLIC OF ALGERIA
MINISTRY OF HIGHER EDUCATION AND RESEARCH

SAAD DAHLAB BLIDA UNIVERSITY - 1

Faculty of Science
Computer Science Department
LRDSI Laboratory

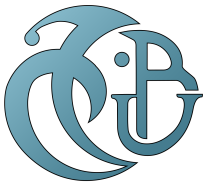

DOCTORAL THESIS OF THE THIRD CYCLE

Option: Data Science and Computing

Functional and Structural Analysis of fMRI/MRI Images of The Brain Using Graph Matching According to a Parallel and Distributed Approach

---

Realized by:
Hichem Felouat

Supervisor:
Pr. Saliha Oukid-Khouas

In Front of The Jury :

Narhimene Boustia	Professor, University of Blida 1	President
Okba Kazar	Professor, University of Biskra	Examiner
Adel Kermi	Associate Professor, E.S.I Algiers	Examiner
Nadjia Benblidia	Professor, University of Blida 1	Examiner
Saliha Oukid-Khouas	Professor, University of Blida 1	Supervisor

Algeria, Blida, 2021

I dedicate my thesis work:

To my dear parents

To all my family
All my friends . . .

Acknowledgements

First, I would like to express my deep gratitude to my advisor Pr. Saliha Oukid-Khouas, for guiding me throughout these five years. You were extraordinarily available for advice, provided great directions of research, showed great patience when it came to teaching me how to write, how to prove things, how to gain insight on what we were doing. Working at your side taught me rigor, perseverance, and hard work, and I hope to live up to your teachings in the future.

I warmly thank Pr. Okba Kazar, Pr. Adel Kermi and Pr. Nadjia Benblidia who accepted to review this thesis, as well as Pr. Narhimene Boustia for accepting to be the president of my defense jury.

My sincere thanks goes to the members of LRDSI Laboratory, it is an honor for me to work with these brilliant and kind researchers in this team.

Finally, I thank my friends from every horizon, my family, my parents, brothers, and sisters, computer science club Jijel members, my scout family, without whom none of this would have been possible.. . .

Hichem Felouat
hichemfel@gmail.com

Abstract

The complexity and diversity of the methods used in neuroimaging constitute areas of innovation and discovery in science with new algorithms and new methods for the collection and analysis of brain images. They continue to open up new avenues for understanding the brain; how it is structurally and functionally organized, how it develops, and its measurements relate to knowledge, behavior, and even genetics.

The analysis of brain images allows for a deep understanding of cognitive tasks and the disease process. In particular, the analysis of anatomical MRIs in the field of computational anatomy, which is interested in the modeling of aspects relating to the structure of the brain. The processing and manipulation of functional images cover modeling the causal relationships over time of functional data, which involves testing functional and connectivity hypotheses. The analysis of MRI images then consists of collecting and analyzing structural connectivity. The modeling of the interactions and the connectivity between the regions of the brain often calls upon the mapping mechanism and graphical calculation tools. Brain mapping approaches are increasingly used on different spatial and temporal scales. In order to understand the organization of the human brain, it becomes necessary to integrate and combine the different information modalities in order to develop a multimodal model of the brain. Atlases are a topographical means of integrating this information into a meaningful form.

In this thesis, the aim is to propose an approach based on graphs, in order to represent the different structures of the brain as well as the connectivity between them in the form of a network. It also involves adapting the analysis methods using mapping techniques between graphs. The use of graphs as a model to represent spatial and temporal information contained in brain images appears to be widespread in the field of functional/structural analysis of the brain and computational anatomy. The graph representation also seems suitable for the construction of 3D graphic models for multidimensional visual analysis of the brain. However, the algorithms for processing, learning, identification, clustering, etc..., which are often based on computational intelligence techniques, prove to be very expensive because of the complexity of the matching graph which constitutes a routine of the basis for the mapping mechanism in these algorithms. The other aim of this thesis is to propose calculation tools that optimize the different algorithms thanks to parallelization/distribution mechanisms on high performance computing virtual machines in order to reduce the complexity of the mapping operation in the graphs (by graph matching).

Key words:

Graph Matching, Functional Brain Analysis, Structural Brain Analysis, Digital Brain Atlas, MRI, fMRI, Neural Networks, Brain Regions, Graphical Visualization, Clustering, Graph Mining, Non-Invasive Exploration.

Résumé

La complexité et la diversité des méthodes utilisées en neuroimagerie, constituent des domaines d'innovation et de découverte en science avec de nouveaux algorithmes et de nouvelles méthodes pour la collecte, l'analyse des images du cerveau. Elles continuent d'ouvrir de nouvelles perspectives pour la compréhension du cerveau ; comment il est organisé structurellement et fonctionnellement, comment il se développe et sont reliées ses mesures à la connaissance, au comportement, et même à la génétique. L'analyse des images du cerveau permettent une compréhension profonde des tâches cognitives et du processus de maladie. En particulier, l'analyse des IRM anatomiques du domaine de l'anatomie computationnelle, qui s'intéresse à la modélisation des aspects relatif à la structure du cerveau. Le traitement et la manipulation des images fonctionnelles couvrent la modélisation des relations causales dans le temps des données fonctionnelles, qui consiste à tester des hypothèses fonctionnelles et de connectivité. L'analyse des images IRM consiste alors à collecter et analyser la connectivité structurelle. La modélisation des interactions et la connectivité entre les régions du cerveau fait souvent appel au mécanisme de mappinget à des outils de calcul graphique. Les approches de mapping du cerveau sont de plus en plus utilisées selon les différentes échelles spatiales et temporelles. Afin d'appréhender l'organisation du cerveau humain, il devient nécessaire d'intégrer et combiner les différentes modalités d'information afin d'élaborer un modèle multimodal du cerveau. Les atlas constituent un moyen topographique d'intégrer ces informations sous forme significative.

Dans cette thèse, il s'agit de proposer une approche basée sur les graphes, afin de représenter les différentes structures du cerveau ainsi que la connectivité entre elles sous forme d'un réseau. Il s'agit également d'adapter les méthodes d'analyse à l'aide des techniques de mapping entre graphes. L'utilisation des graphes comme modèle de représentation des informations spatiales et temporelles contenues dans des images du cerveau semble très répandue dans le domaine de l'analyse fonctionnelle/structurelle du cerveau et de l'anatomie computationnelle.La représentation en graphe semble également adaptée pour la construction de modèles graphiques 3D pour une analyse visuelle multidimensionnelle du cerveau. Cependant, les algorithmes de traitement, d'apprentissage, d'identification, de clustering . . . , lesquels sont souvent basés sur des techniques d'intelligence computationnelle, s'avèrent très coûteux à cause de la complexité du graphe matching qui constitue une routine de base pour le mécanisme de mapping dans ces algorithmes. Dans ce travail, il s'agit de proposer des outils de calcul qui optimisent les différents algorithmes grâce à des mécanismes de parallélisation/distribution sur des machines virtuelles de calcul haute performance afin de réduire la complexité de l'opération de mapping dans les graphes (de graph mathching).

Mots clés: *Graphe Matching, Analyse Fonctionnelle du Cerveau, Analyse Structrelle du Cerveau, Atlas Numérique du Cerveau, Images IRM, Image IRMf, Réseaux Neuronaux, Régions Cérébrales, Visualisation Graphique, Clustering, Graphe Mining, Exploration non Invasive.*

الملخص

يشكل تعقيد وتنوع الأساليب المستخدمة في التصوير العصبي مجالا للإبتكار والإكتشاف في العلوم باستخدام خوارزميات و طرق جديدة لجمع و تحليل صور الدماغ و الإستمرار في فتح آفاق جديدة لفهمه. كيف يتم تنظيمه هيكليا ووظيفيا، وكيف يتطور ، و تتعلق قياساته بالمعرفة و السلوك و حتى علم الوراثة.

يسمح تحليل صور الدماغ بالفهم العميق للمهام المعرفية و حالة المرض. على وجه الخصوص ، تحليل الصور بالرنين المغناطيسي التشريحي في مجال علم التشريح الحسابي والذي يهتم بنمذجة الجوانب المتعلقة ببنية الدماغ. تغطي معالجة الصور الوظيفية و تحليلها نمذجة العلاقات السببية مع مرور الوقت للبيانات الوظيفية و التي تتضمن اختبار الفرضيات الوظيفية والتوصيلية. ثم إن تحليل صور الرنين المغناطيسي التشريحي يمكن من جمع و تحليل الإتصال الهيكلي للدماغ. غالبا ما تستخدم نمذجة التفاعلات والإتصال بين مناطق الدماغ آلية رسم الخرائط وأدوات الحساب الرسومية. تستخدم مناهج رسم خرائط الدماغ بشكل متزايد في مختلف المقاييس المكانية والزمانية. من أجل فهم تنظيم الدماغ البشري أصبح من الضروري دمج وتركيب أساليب المعلومات المختلفة من أجل تطوير نموذج متعدد الوسائط للدماغ. الأطالس (جمع أطلس) هي وسيلة طوبوغرافية لدمج هذه المعلومات في شكل ذي معنى.

الهدف من هذه الأطروحة هو إقتراح نهج قائم على الرسوم البيانية من أجل تمثيل الهياكل المختلفة للدماغ وكذلك الإتصال الوظيفي بينها في شكل شبكة. إنها أيضا مسألة تكييف طرق التحليل بإستخدام تقنيات رسم الخرائط بين الرسوم البيانية. يبدو أن إستخدام الرسوم البيانية كنموذج لتمثيل المعلومات المكانية والزمانية الواردة في صور الدماغ منتشر للغاية في مجال التحليل الوظيفي و البنيوي للدماغ والتشريح الحسابي. و يبدو تمثيل الرسم البياني مناسبا أيضا لبناء نموذج بياني ثلاثي الأبعاد للتحليل البصري متعدد الأبعاد للدماغ. و مع ذلك ، فإن خوارزميات المعالجة و التعلم والتعرف والتجميع و ما إلى ذلك و التي غالبا ما تستند إلى تقنيات الذكاء الحسابي أثبتت أنها باهظة الثمن بسبب تعقيد مطابقة الرسم البياني الذي يشكل أساسا روتينيا لآلية رسم الخرائط في هذه الخوارزميات. الهدف الأخر من هذا العمل هو اقتراح أدوات حسابية تعمل على تحسين الخوارزميات المختلفة بفضل آليات التنفيذ المتوازي و التوزيع على أجهزة إفتراضية للحوسبة عالية الأداء من أجل تقليل تعقيد عملية رسم الخرائط ومطابقاتها في الرسوم البيانية.

الكلمات المفتاحية :
مطابقة الرسم البياني ، التحليل الوظيفي للدماغ ، التحليل البنيوي للدماغ ، أطلس الدماغ الرقمي ، صور الرنين المغناطيسي ، صور الرنين المغناطيسي الوظيفي ، الشبكات العصبية ، مناطق الدماغ ، التصور الرسومي ، التجميع ، التنقيب في الرسم البياني ، الإستكشاف غير الغازي.

Contents

List of Figures

List of Tables

List of Algorithms

List of Abbreviations

CNS	The **C**entral **N**ervous **S**ystem
PNS	The **P**eriphera **N**ervous **S**ystem
GM	The **G**ray **M**atter
WM	The **W**hite **M**atter
NMR	The **N**uclear **M**agnetic **R**esonance
RF	The **R**adio **F**requency
MRI	The **M**agnetic **R**esonance **I**maging
FID	The **F**ree **I**nduction **D**ecay
TR	The **R**epetition **T**ime
TE	The **E**cho **T**ime
fMRI	The **f**unctional **M**agnetic **R**esonance **I**maging
EEG	The **E**lectro **E**ncephalo **G**raphy
ECoG	The **E**lectro **Co**tico **G**raphy
sEEG	The **s**tereotactic **E**lectro **E**ncephalo **G**raphy
MEG	The **M**agneto **E**ncephalo **G**raphy
PET	The **P**ositron **E**mission **T**omography
SPECT	The **S**ingle **P**hoton **E**mission **T**omography
nIRS	The **n**ear **I**nfrared **S**pectroscopy
ASL	The **A**rterial **S**pin **L**abeling
BOLD	The **B**lood **O**xygen **L**evel **D**ependent
CBF	The **C**erebral **B**lood **F**low
rs-fMRI	The **r**esting **s**tate **f**unctional **M**agnetic **R**esonance **I**maging
t-fMRI	The **T**ask-based **f**unctional **M**agnetic **R**esonance **I**maging
NIfTI	The **N**euroimaging **I**n**F**ormatics **T**echnology **I**nitiative
CSF	The **C**erebro **S**pinal **F**luid
ROIs	The **R**egions **O**f **I**nterest
GLM	The **G**eneral **L**inear **M**odel
MNI	The **M**ontreal **N**eurological **I**nstitute
SNR	The **S**ignal to **N**oise **R**atio
FWHM	The **F**ull **W**idth **H**alf **M**aximum
HRF	The **H**emodynamic **R**esponse **F**unction

FWER	The **F**amily **W**ise **E**rror **R**ate
FDR	The **F**alse **D**iscovery **R**ate
RSNs	The **R**esting **S**tate **N**etworks
DMN	The **D**efault **M**ode **N**etwork
ALFF	The **A**mplitude of **L**ow-**F**requency **F**luctuations
ReHo	The **Re**gional **Ho**mogeneity
FCD	The **F**unctional **C**onnectivity **D**ensity
ICA	The **I**ndependent **C**omponent **A**nalysis
PCA	The **P**rincipal **C**omponent **A**nalysis
KPCA	The **k**ernel **P**rincipal **C**omponent **A**nalysis
AAL	The **A**utomated **A**natomical **L**abeling
FC	The **F**unctional **C**onnectivity
GED	The **G**raph **E**dit **D**istance
mcs	The **m**aximum **c**ommon **s**ubgraph
MCS	The **M**inimum **C**ommon **S**upergraph
HITS	The **H**yperlink-**I**nduced **T**opic **S**earch
NSD	The **N**etwork **S**imilarity **D**ecomposition
ASD	The **A**utism **S**pectrum **D**isorder
ABIDE I	The **A**utism **B**rain **I**maging **D**ata **E**xchange **I**
GCNs	The **G**raph **C**onvolutional **N**etworks

General Introduction

The human brain is more complex than any other known structure in the universe. The study of the human brain has been one of the challenges of neuroimaging /neuroscience and still is. Evidence of this is the large number of papers that have been published during the last years to study brain structure and function. The brain is the center of the central nervous system and it centralizes the control over the other organs of the body and contains about 100 billion neurons and 1000 billion glial cells, the adult brain weighs between 1250 and 1450 g. It is composed of neurons and glia, cells that provide support to the neurons. Neurons' signal is transmitted by electrical impulses along their axons in the form of electrochemical pulses called action potentials. They communicate with other cells via synapses, membrane-to-membrane structures that permit to pass an electrical or chemical signal between the cells. Neuron bodies together with capillary blood vessels form gray matter tissue and neuron axons form white matter tissue. Gray matter is associated with processing and cognition.

Neuroimaging is the discipline that deals with the in vivo depiction of anatomy and function of the central nervous system in health and disease, it was considered the domain of radiologists with a specific interest in the nervous system. It produces images of the brain by noninvasive techniques in order to understand the brain structures and functions, the relationship between brain activity in certain brain areas and specific mental functions and diagnosis of various neurological diseases of the brain. This thesis focuses on two complementary technologies; magnetic resonance imaging (MRI) and functional magnetic resonance imaging (fMRI).

Structural Magnetic Resonance Imaging (MRI) is today one of the most widely used and versatile medical imaging modalities. MRI is nowadays the reference tool for the diagnosis and the investigation of neurological diseases, including the investigation of trauma and disease-related brain changes for some considerable time. It is based on the physical phenomenon of nuclear magnetic resonance (NMR). The main advantages of MRI are that it is noninvasive, it does not use any harmful radiation, it produces truly 3D images of high-resolution, and it offers contrast mechanisms for imaging many kinds of tissues and tissue properties which is especially useful for soft tissues. It, therefore, meets the criteria for structural analysis well.

Functional Magnetic Resonance Imaging (fMRI) is a powerful brain imaging modality, it allows us to better understand how the brain work by recording with very little intrusion the brain activity of an active human subject with a good time (1s) and spatial resolution (1mm). fMRI measures the changes induced by cerebral activity. The most widely used fMRI modality

is BOLD for blood oxygen level dependent and, as the name indicates, it reflects the changes in oxygen concentration in the blood. When there is brain activity, oxygen is consumed and its concentration in the blood decreases; then there is an inflow of oxygenated blood to replenish the tissue, increasing blood oxygen concentration. Deoxygenated blood causes magnetic distortions that can be measured by an MRI scanner. The field of fMRI is becoming data-intensive, as the number of publicly available studies is constantly growing, and as several acquisition campaigns on large cohorts have provided tens of thousand hours of brain records.

Graphs are a powerful and universal tool widely used in information processing. Numerous methods for graph analysis have been developed. In particular, graph representations are extremely useful in image processing and understanding. A graph is a set of elements, called nodes, and a set of links, called edges, linking together a subset of nodes by pairs. This representation of information can be applied in a wide range of domains, going from transportation with for example the complex network of airline routes (where the nodes represent the airports and the edges the direct flight routes between two airports) to sociology (friendship, professional relationship), biology (protein interactions, epidemic spreading) and many more. Complex networks have also found applications in neuroimaging and neuroscience. Indeed, the brain can be regarded as a network, where nodes represent brain regions, and edges represent the anatomical or functional connections between brain regions. Recent research has shown that graph-theory based complex network analysis provides a powerful framework for examining the topological properties of brain networks. Graph theory has drawn a lot of attention in the field of brain MRI/fMRI analysis during the last decade, mainly due to the abundance of tools that it provides to explore the interactions of elements in a complex graph like the brain. In these fields, the construction of a representative brain graph for each individual is critical for further analysis. Additionally, graph matching is an essential step for inference and classification analyses on brain graphs. Graph matching is the process of finding a correspondence between the nodes and the edges of two or more graphs that satisfies some (more or less stringent) constraints ensuring that similar substructures in one graph are mapped to similar substructures in the others. In realistic applications, the matching is done by comparing the model graph which is stored in a file and an input graph that is given at the run time.

Organization of The Manuscript

The aim of this thesis is to give a compact insight to the state-of-the-art of the brain MRI/fMRI analysis by using graph matching in a parallel and distributed approach including the necessary introduction to the principles of MRI/fMRI and graph theory.

In the first chapter, we introduce the general goals and the type of data that were studied in this thesis. This is useful to understand the various directions that we took. An overview of brain anatomy and magnetic resonance imaging is provided, we started by providing some insight into the human brain structure and function. Then, we introduced the principles of nuclear magnetic resonance (NMR) and its properties. Next, we briefly introduced the magnetic

resonance imaging (MRI) method; how to get the signal, the image contrast and some artifacts can be generated by a wide variety of factors resulting from the scanner hardware itself. Finally, we introduced functional magnetic resonance imaging (fMRI) and we summarize the existing neuroimaging techniques, focusing on the ones that are going to be used in the context of this thesis (BOLD fMRI).

In the second chapter, we described some of the most common MRI steps normally applied to raw MR images in order to improve their quality (Preprocessing) and the main approaches to MRI analysis of the brain.

In the third chapter, we presented a brief overview of the most common classical methods used for the preprocessing and analysis of fMRI in both task data and resting-state data.

In the fourth chapter, we provided an overview of graph matching, we focused on three main components. Firstly, an introduction to graph theory, we mainly concentrate on the fundamental concepts. Secondly, an overview of graph matching and the most important methods used. Thirdly, we provided some methods based on graph matching techniques that may be successfully applied to neuroimaging data for understanding the brain structure or its structural and functional connectivity.

The human brain cortex is very complex structure containing folds (gyri) and fissures (sulci). The sulcus is one of the most important features in order to know the different functions areas of the brain. The exact identification of sulci on the human brain using MRI images is helpful in many studies and applications related to brain diseases and human behavior. Automatic labeling of cortical sulci with all this complexity and inter-subject variability is considered non-trivial task. In the fifth chapter, we proposed a new graph-based approach of automatic labeling of cortical sulci with parallel and distributed algorithms using graph matching and generalized median graph. The generalized median graph of a set of graphs is a way to represent a set of graphs by a comprehensive graph that minimizes the sum of the distances to all graphs. We used a dataset of MRI images weighted in T1 and with voxel dimensions of $1mm^3$. Our dataset is grouped into two sets, the first one is the training set used for the construction of the generalized median graph and the second set is used for the evaluation of the performance of the proposed approach. In order to describe the sulci, we used the characteristics of shape, orientation, and location. The estimation measures are used to evaluate the automatic labeling accuracy for each sulcus by each test subject are the true positive rate (TPR), false-positive rate (FPR), and the similarity index (SI). Our method achieves an average SI = 0.796 for the normal graph match algorithm and SI = 0.802 for the parallel graph match algorithm compared to other methods. The results that we obtained prove that our approach is accurate and acceptable in this field which uses graph matching for automatic labeling of cortical sulci.

In the sixth chapter, we proposed a study where its purpose is to apply graph convolutional networks (GCNs) for feature extraction and classification of patients with autism spectrum disorder (ASD). The number of people with (ASD) increases every year and poses a threat to the

life and future of many children which makes this study very important. We used the resting-state fMRI data from a large multi-site dataset called Autism Brain Imaging Data Exchange I (ABIDE I) to validate our proposed approach. Based on functional connectivity (FC), we represented the brain through a complex network where the regions of the brain represent the nodes in the network and the correlation coefficient between two regions represents the weight of the edge connects them. The data were preprocessed, and we constructed a functional connectivity graph for each subject by parcellation of the whole brain into 392 distinct regions using the (CC400) atlas. The graph measures were then calculated and used as features for both nodes and edges to classify these subjects by graph convolutional networks classifier proposed in this study. The results we achieved in our experiments were with accuracy of 70% to identify patients with autism spectrum disorder from healthy individuals, which proved the accuracy and robustness of our approach in classifying brain diseases.

Publications

- Graph Matching and Generalized Median Graph for Automatic Annotation of Cortical Sulci [5]
- Graph matching approach and generalized median graph for automatic labeling of cortical sulci with parallel and distributed algorithms [6]
- Graph Convolutional Networks and Functional Connectivity for Identification of Autism Spectrum Disorder [7]

Chapter 1

Overview of Brain Anatomy and Magnetic Resonance Imaging

1.1 Introduction

The study of the human brain has been an important focus of attention in science since the 19th century and still is. This is demonstrated by the large number of initiatives that have been created during the last years to study brain function, this allowed neuroscientists to significantly improve the study of the human brain. In this chapter, we introduce an overview of brain anatomy and magnetic resonance imaging. We will start by providing some insight into human brain structure and function. Then, we will introduce the principles of nuclear magnetic resonance (NMR) and its properties. Next, we briefly introduce the magnetic resonance imaging (MRI) method; how to get the signal, the image contrast and some artifacts can be generated by a wide variety of factors resulting from the scanner hardware itself. Finally, we introduce the functional magnetic resonance imaging (fMRI) and we summarize the existing neuroimaging techniques, focusing on the ones that are going to be used in the context of this thesis (BOLD fMRI).

1.2 The Nervous System

The nervous system is the system responsible for sensations, thinking and the control of our body. To accomplish these functions, it collects sensory information from the whole body and transmits it through the nerves to the spinal cord and the brain. These can respond immediately to sensory information and send signals back to the muscles or internal organs, causing a response

called motor response. The nervous system is divided into two major sections : the central nervous system (CNS) and the peripheral nervous system (PNS), Figure[1] 1.1.

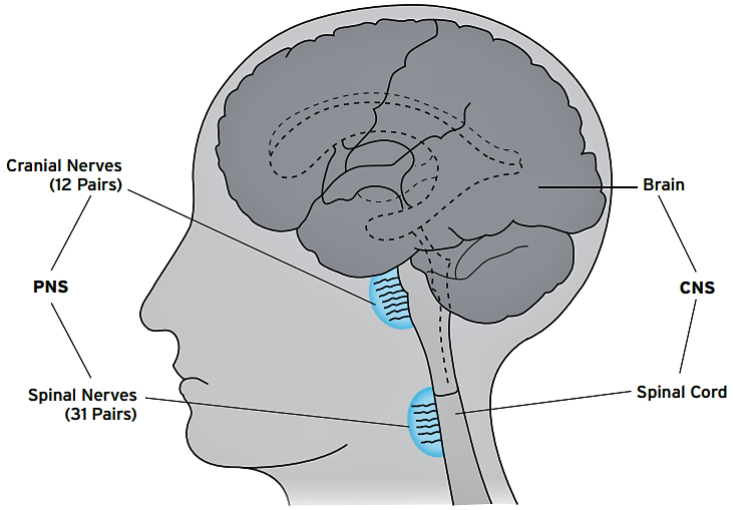

FIGURE 1.1: The central and peripheral nervous systems [1].

1.2.1 The Central Nervous System

The central nervous system is the set of nerve centers that are responsible for ensuring the proper functioning of the various centers of regulation. All the sensitive information arrives and all the motor information leaves. Anatomically, it consists of the brain and spinal cord.

The Brain

The brain is the largest part of the central nervous system which is the center of thinking and memory and monitoring the various vital processes in the human body. The brain contains about 100 billion neurons and 1000 billion glial cells, the adult brain weighs between 1250 and 1450 g. The brain consists of three gross divisions, the cerebrum, the brain stem, and the cerebellum, Figure 1.2.

1. **The cerebrum :** is the large gray part located at the top of the brain which houses the highest cognitive functions and the place where consciousness arises and the ability to do different things such as speech, learning and organizing the movements of the body. It consists essentially of two hemispheres, the left hemisphere and the right hemisphere separated by a groove is known as the longitudinal fissure. The surface tissue of the

[1] Basic Brain Anatomy 94170_02_6272.*indd*

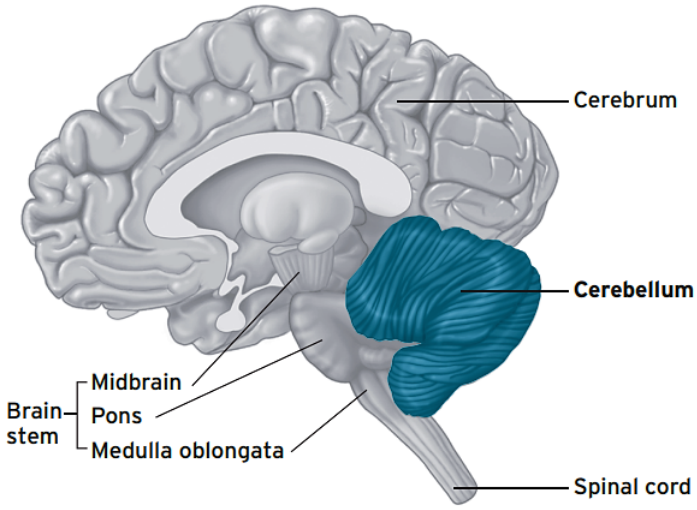

FIGURE 1.2: Brain sections : the cerebrum, the brain stem, and the cerebellum [1].

cerebrum is known as the cerebral cortex which has two parts, the gray matter (GM) and the white matter (WM), Figure [2] 1.3.

(a) **The gray matter (GM) :** is responsible for the processing and regulating of information within the nervous system. It is present in the cortex and some subcortical structures such as the cerebellum, thalamus, basal ganglia, and the spinal cord. The cerebral cortex is a very complex structure containing gyri (singular: gyrus) and sulci (singular: sulcus) that are the most important features in order to know the location, structures, and different functions of many other areas of the brain, Figure 1.3. The basal ganglia are a group of brain neurons located deep in the cerebral cortex, which runs certain vital functions such as movement and fine-tuning the activity of brain circuits, as well as memory.

(b) **The white matter (WM) :** is located in the inner part of the brain, which is responsible for the transmission of impulses from one area of the brain to another, Figure 1.3. It consists of links called Axons, which covered by a protein layer called the Myelin to protect signals transmitted from interference and noise.

(c) **The axon :** makes the white matter looks white and there are three kinds of axons. The association fibers are axons connecting the cerebral cortex regions in the same cerebral hemisphere of the brain. The commissural fibers are axons connecting the cerebral cortex regions in the two hemispheres of the brain. The projection fibers are axons connecting the brain to the spinal cord.

(d) **The major cerebral lobes :** the cerebrum consists of two cerebral hemispheres where each cerebral hemisphere performs specific functions in the body. The right cerebral hemisphere is responsible for processing the sensory information coming

[2] www.mayfieldclinic.com/pe-anatbrain.htm

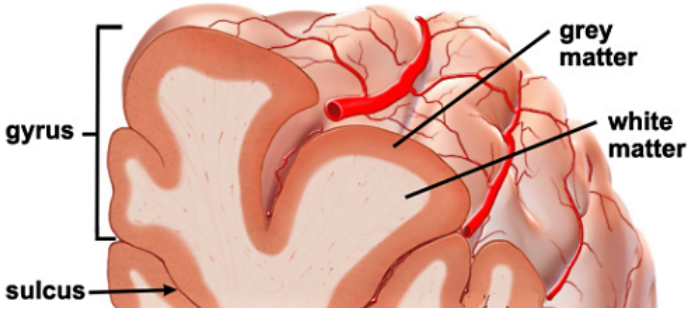

FIGURE 1.3: The cortex contains gray matter, white matter, gyrus, and sulcus.

up from the left side of the body and controlling the movement in it, and the same role is done by the left hemisphere with the right side of the body. Each cerebral hemisphere is subdivided into four lobes: the frontal, parietal, temporal, and occipital lobes, Figure 1.4. Each cerebral lobe in each cerebral hemisphere houses various major functions of the brain and specializes in certain functions, Figure[3] 1.5.

2. **The brain stem :** is the region of the brain that connects the cerebrum with the spinal cord, which consists of the midbrain, medulla oblongata, and the pons, Figure 1.2. The brain stem houses many of the control centers for vital body functions such as breathing, swallowing, heart rate, blood pressure, consciousness, and whether one is awake or sleepy.

3. **The cerebellum :** is known as a small brain because it is similar to the brain and has two hemispheres like it, which is located at the back of the brain, underlying the occipital and temporal lobes of the cerebral cortex, Figure 1.2. The cerebellum receives information from the sensory systems, the spinal cord, and other parts of the brain and then regulates motor movements. It performs several functions related to movement and coordination, including maintaining balance and posture, coordination of movement, motor learning and has some role in thinking.

4. **The cerebral meninges :** are three layers of protective tissue surrounding the brain and separates the brain from the skull. The dura mater envelopes the brain and spinal cord as well as protects the brain from displacement. The pia mater is the innermost layer of the meninges and adhere closely to the brain. The arachnoid mater is the middle layer of the meninges that plays a major role in the distribution of blood to the cerebral cortex.

The Spinal Cord

The spinal cord consists of bundles of nerve fibers that are mainly made up of white matter and gray matter, which begins at the end of the brain stem and continues down almost to the bottom

[3]Credit: Nucleus Medical Art, Inc./Getty Images. http://dana.org

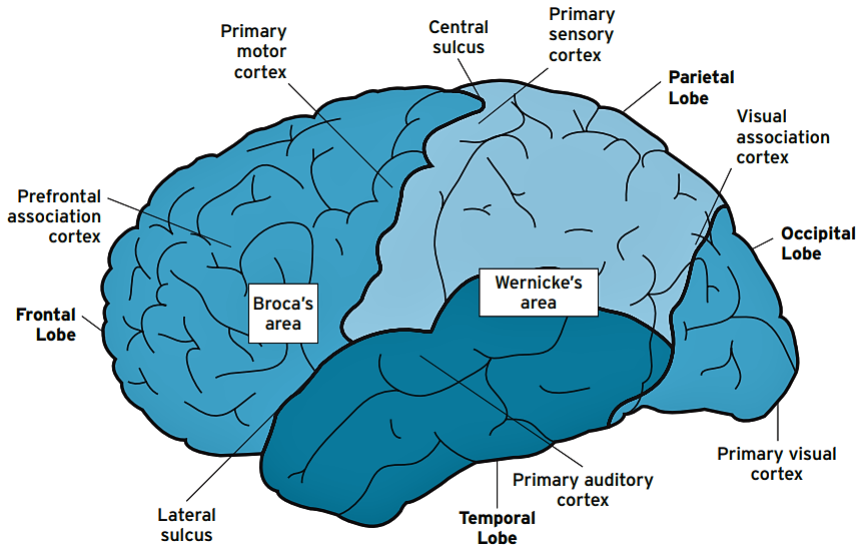

FIGURE 1.4: Diagram of the lateral view of the human brain[1].

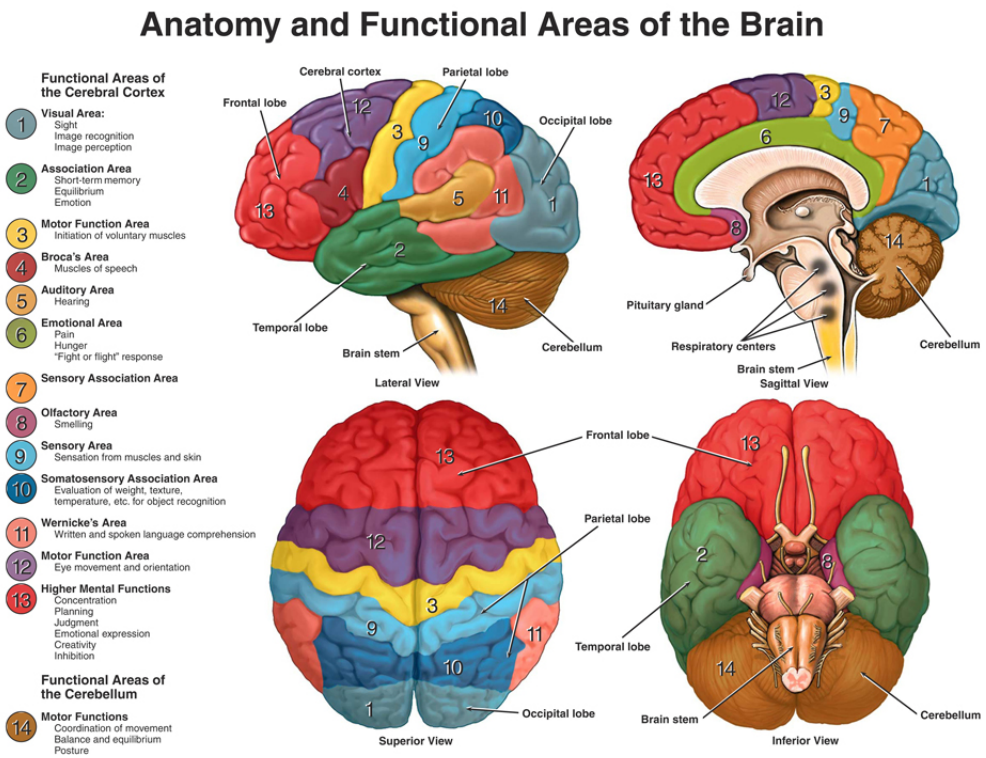

FIGURE 1.5: Main functional and anatomical areas of the brain.

of the spine in the form of a cylinder. The spinal cord transfers the sensory impulses coming from the body to the brain and transmits the motor impulses from the brain to the body.

1.2.2 The Peripheral Nervous System

The peripheral nervous system (PNS) consists of the nerves that connect the central nervous system (CNS) to the rest of the body, allowing the brain and spinal cord to receive and transmit sensory and motor information to other parts of the body which allow us to respond and react to the stimuli that come from our environment, Figure 1.1. The PNS consists of 12 pairs of cranial nerves and 31 pairs of spinal nerves. The cranial nerves are nerves attached to the brain stem with the head, neck, and face, which are primarily responsible for their sensory and motor functions. The spinal nerves transmit sensory and motor information between the spinal cord and the rest of the body, which contributes to control of the rest of the body that is not reached by the cranial nerves.

1.2.3 The Nerve Cells

The brain is made up of billions of nerve cells, which is consists of two basic cells types. The neurons and the glial cells.

The Neuron

Neurons are cells responsible for communication and integration into the nervous system, which transmit information to other nerve cells, muscle or gland cells by electrical stimulation. Typically, neurons have three basic parts, Figure[4] 1.6.

1. **The cell body (soma) :** consists of a membrane surrounding the cytoplasm and the nucleus of the cell inside. It is responsible for most of the protein and energy production of the cell to drive activities, it also carries the genetic information of the neuron and maintains its structure. The soma is generally circular but there are other forms such as the pyramid shape and can be classified according to their shape.

2. **The dendrites :** are branch-like structures extending away from the cell body, which receive information from other neurons and transmit that information to the soma.

3. **The axon :** is a tube-like structure and it is the transmitting part of the neuron that carries information from the cell body to other neurons.

[4] www.simple.wikipedia.org/wiki/Neuron

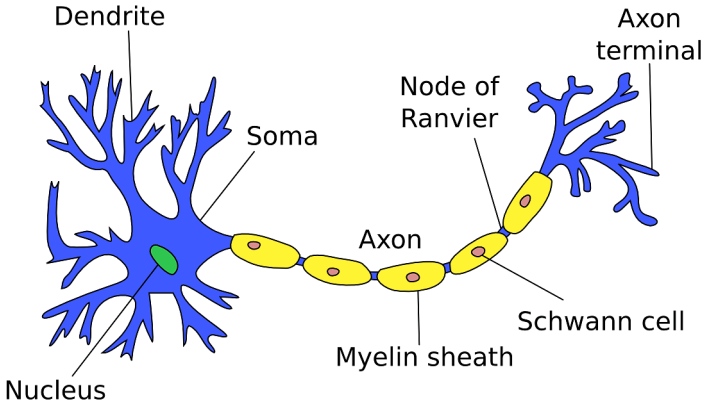

FIGURE 1.6: The basic structural elements of a neuron.

The Glial Cell

Glial cells playing a supporting role of neurons, where ensuring the isolation of nerve tissue, metabolic functions, skeletal support and protection from foreign bodies in case of injury. They also play an active role in the transmission of nerve impulses, accelerating nerve conduction by acting as an insulating sheath for certain axons. Indeed, there are many more glial cells in the brain than there are neurons, the most important types of glial cells are Microglia, Astrocytes, Oligodendrocytes, and Ependymal.

1.3 Nuclear Magnetic Resonance (NMR)

Nuclear magnetic resonance is a technique that was discovered independently by Felix Bloch and Edward Purcell in 1946 [8] [9], they were both awarded the Nobel prize for Physics in 1952 for the discovery. The principle of magnetic resonance is when we placed a particle in an external magnetic field can be excited by absorbing photons and return back to the equilibrium state after some time with releasing the absorbed photons, by release photons we can obtain information about the physical and chemical properties of the exciting elements [10].

1.3.1 Spin

The atoms consist of three fundamental particles: electrons that have a negative charge and are located in the orbits surrounding the nucleus. Protons have a positive charge, and neutrons have no charge, both protons and neutrons are located in the nucleus of the atom. Nuclei with unpaired protons or neutrons have a positive charge and generate a property called angular momentum or

spin. The spin produces a nuclear magnetic moment and the nuclei behave as a small magnetic dipole with a random orientation in space.

1.3.2 Net Magnetization

The spin is considered as a small magnetic and has a magnetic moment vector of equal magnitude. It can be positive and negative and are randomly oriented in all directions. Spins of opposite signs cancel out. The vector of these spin vectors produces a zero-sum; that is, no net magnetization is observed.

When an external magnetic field $\mathbf{B}_0$ (oriented in the z-direction) is applied, each spin aligns parallel or anti-parallel to the direction of the applied field and begin to rotate perpendicular to, or precess about, the magnetic field $\mathbf{B}_0$. The anti-parallel state has higher energy than the parallel state. Slightly greater number of spins align along that $\mathbf{B}_0$ direction, and therefore, the vector sum of all the spin vectors is greater than zero and is aligned along the +z-direction, the direction of $\mathbf{B}_0$, that vector is called the net magnetization vector $\mathbf{M}_0$, Figure 1.7.

The net magnetization vector $\mathbf{M}_0$ is the summation of all the magnetic moments or spins.

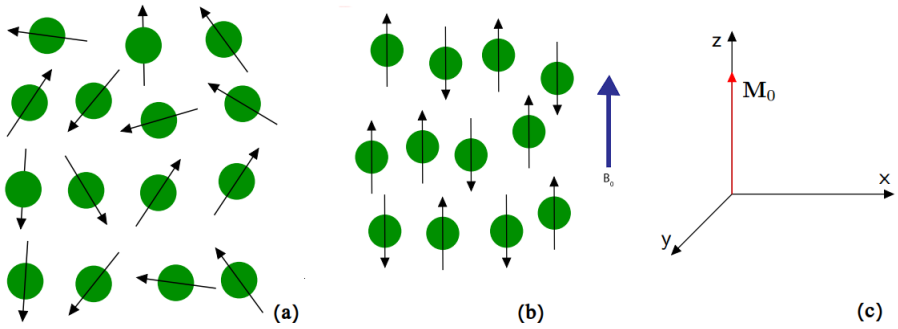

FIGURE 1.7: Spin behavior in an external magnetic field. (a) The spins initially oriented randomly in space. (b) become aligned either parallel or anti-parallel to an externally applied magnetic field $\mathbf{B}_0$. (c) The net magnetization vector $\mathbf{M}_0$ in the equilibrium state.

1.3.3 Radio-frequency Excitation

The spins can switch from the lower energy state to the higher energy state by transmitting a radio-frequency pulse (RF pulse) at the resonance frequency energy is added to the system. During the pulse, the protons absorb a portion of this energy at a particular frequency. The particular frequency absorbed is proportional to the magnetic field $\mathbf{B}_0$. When the spins switch to the higher energy state by photon absorption, which causes $\mathbf{M}_0$ to rotate away from its equilibrium orientation. The net magnetization will be composed of the longitudinal component

$\mathbf{M}_Z$ which is aligned with the orientation of the main magnetic field $\mathbf{B}_0$, and the transversal part $\mathbf{M}_T$ that refers to the magnetization in the plane perpendicular to the longitudinal direction, Figure 1.8.

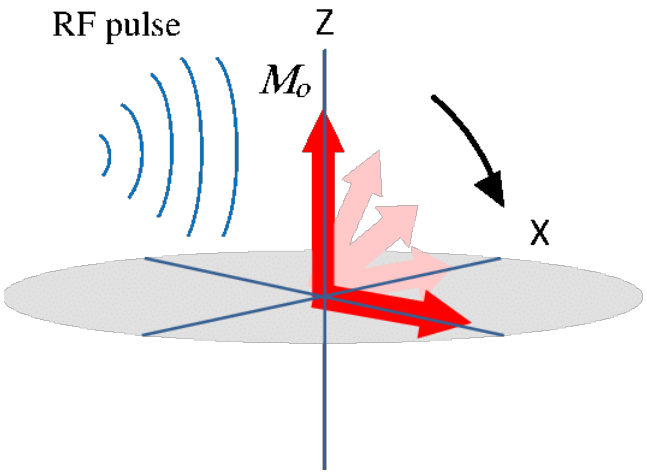

FIGURE 1.8: When a radio-frequency pulse is applied at the appropriate frequency, the spins absorb it and $\mathbf{M}_0$ rotates into the transverse plane.

1.3.4 Relaxation

When the radio-frequency pulse is turned off, the protons immediately begin to realign themselves and return to their original equilibrium orientation. Some of the energy absorbed by the spins from the applied radio-frequency pulse is lost to its surroundings in constant times called relaxation times. There are two relaxation times can be measured, known as $\mathbf{T}_1$ (spin-lattice) and $\mathbf{T}_2$ (spin-spin). While both times measure the spontaneous energy transfer by an excited proton, they differ in the final disposition of the energy [11], Figure [5] 1.9.

T1 Relaxation: describes the decay constant for the net magnetization vector $\mathbf{M}_Z$ recovers to its equilibrium state in the direction of $\mathbf{B}_0$. The magnetization recovers to 63% of its equilibrium value after one time constant $\mathbf{T}_1$.

T2 Relaxation: describes the decay constant for the net magnetization vector $\mathbf{M}_T$ recovers to its initial magnetization at time zero. The transverse magnetization vector drops to 37% of its original magnitude after one time constant $\mathbf{T}_2$.

[5] www.radiologycafe.com

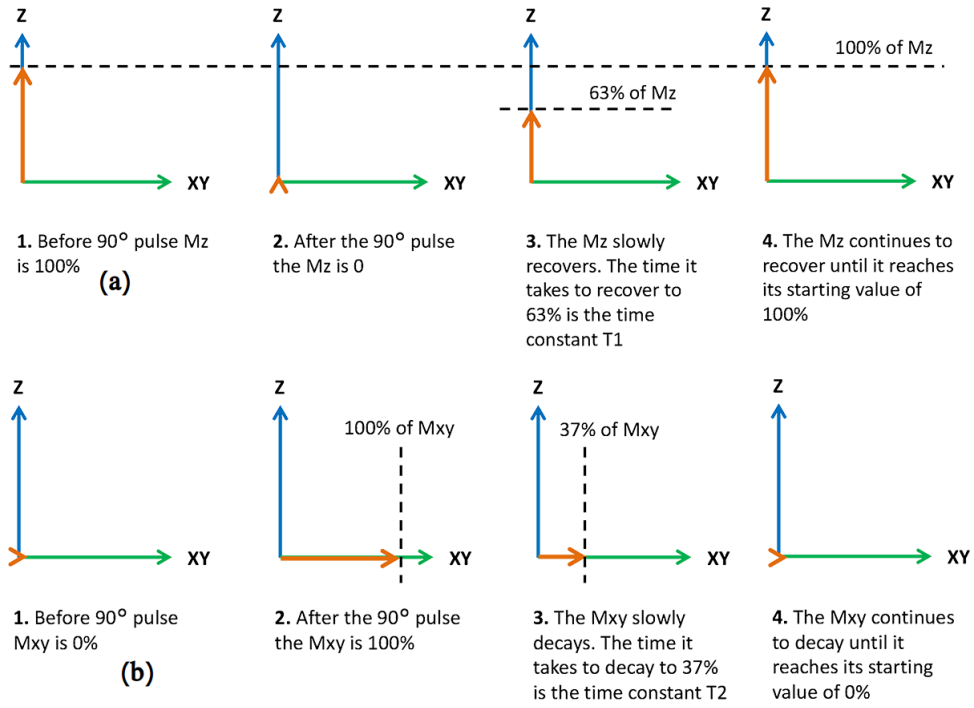

FIGURE 1.9: Relaxation of the net magnetization vector after excitation by radio-frequency pulse. (a) $\mathbf{T}_1$ relaxation. (b) $\mathbf{T}_2$ relaxation.

1.4 Principles of Magnetic Resonance Imaging (MRI)

Magnetic Resonance Imaging is a non-invasive imaging technology that produces three-dimensional detailed anatomical images. It is often used for disease detection, diagnosis, and treatment monitoring. It is based on the physical phenomenon of nuclear magnetic resonance (NMR). The first developments in Magnetic Resonance Imaging were in 1973 by Paul Lauterbur [12]. Richard Ernst introduced an improved method of image acquisition in 1975 [13], which is used until today. The first images of humans were made in 1979. Today, MRI has become a major technique of modern medical imaging in order to investigate the anatomy and physiology of the body, and to detect pathologies including tumors, inflammation, neurological conditions such as stroke, disorders of muscles and joints, and abnormalities in the heart and blood vessels among others. MRI primarily focus on the hydrogen atoms, because living tissue consists mostly of water and fat which contain many hydrogen atoms and, therefore, most atoms in the human body are hydrogen atoms.

In this section, we describe the main technique for producing MRI and image acquired imperfections by MRI. For more information, refer to [11] [14].

1.4.1 Gradient Fields

Gradient magnetic fields are used primarily for localization of the MR signal, these magnetic fields are much weaker than $\mathbf{B}_0$ and oriented linearly across the x, y, or z-direction, Figure [6] 1.10. In the presence of a gradient field, each proton will resonate at a unique frequency that depends on its exact position within the gradient field [11]. During the acquisition, the current in the gradient coils is switched on and off rapidly, causing, in turn, quick changes in amplitude and polarity of the gradient magnetic fields in order to encode the spatial position of the NMR signal. The MR image is simply a frequency and phase map of the protons generated by unique magnetic fields at each point throughout the image. Paul Lauterbur and Sir Peter Mansfield discovered this idea of using the gradient fields to spatially locate the protons and separate the signal from different parts of the body. They received the Nobel prize in Medicine for this accomplishment in 2003.

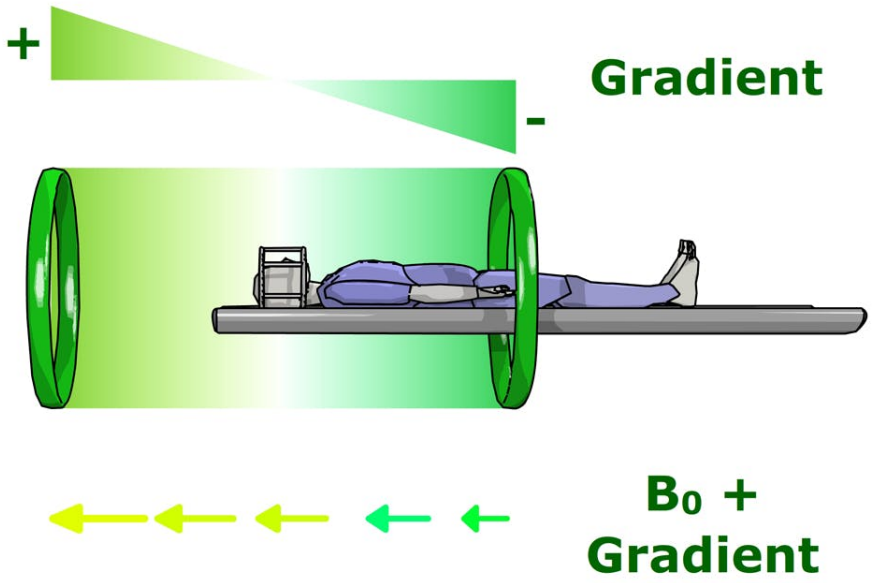

FIGURE 1.10: Applying the gradient magnetic fields on the z-axis. The gradient was represented by two triangles joined at the top of the image, which has two components, the positive component added to $\mathbf{B}_0$ and the negative component subtracted from $\mathbf{B}_0$.

Slice Selection

The initial step in MRI is the localization of the radio-frequency pulse excitation to a region of space, which is accomplished through the location of the axial slice within the object being imaged. This is known as slice selection. The way this is done is by applying a one-dimensional,

[6] www.imaios.com

linear magnetic field gradient during the period that the radio-frequency pulse is applied so that the resonance frequency of the spins becomes linearly dependent on the spatial position, Figure [7] 1.11. The gradient direction (x, y, z or a combination) determines the slice orientation while the gradient amplitude together with certain radio-frequency pulse characteristics determine both the slice thickness and slice position.

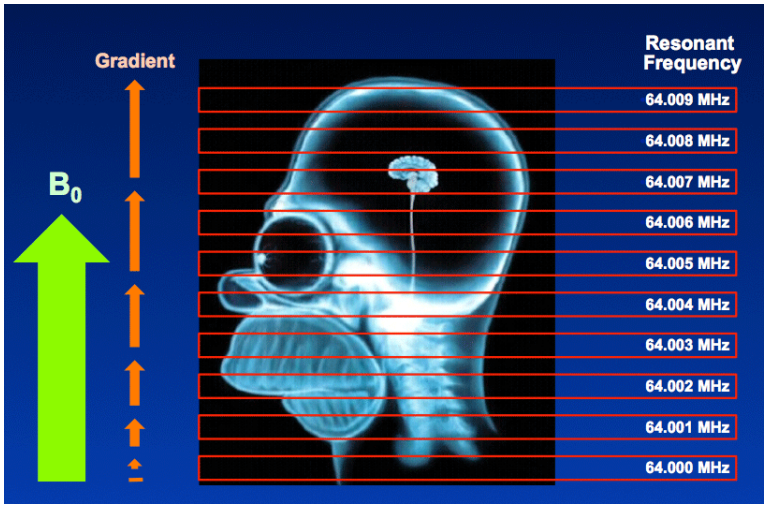

FIGURE 1.11: Magnetic field gradient applied in the z-direction causes the resonant frequencies to vary by a few thousand Hz from slice to slice.

Free Induction Decay (FID)

After the RF pulse turned off, the protons immediately begin to re-radiate the absorbed energy, the signal we detect is called a Free Induction Decay (FID). The free induction decay (FID) is a damped oscillation at the resonance frequency recorded when the net magnetization is tipped into the transverse plane [8]. The amplitude of the FID signal becomes smaller over time as net magnetization returns to equilibrium. The FID contains all of the information in the NMR spectrum, but it is difficult for us to discern the information in this format. Fourier transformation of the FID, a time domain signal, produces the frequency domain NMR spectrum. The resonance frequencies of the signals in the transformed spectrum correspond to the frequency of oscillations in the FID [9].

[7] www.mriquestions.com
[8] www.mriquestions.com
[9] www.libretexts.org

K-space

The k-space is usually a grid of raw data represents the locations of the acquired signals which have been encoded with frequency and phase encoding along the x, and y directions of the form(K_x, K_y). The k-space represents the spatial frequency information in two or three dimensions of an object [15] [16]. The relationship between k-space data and image data is the Fourier transformation [17] [18] [19] [20]. The individual points (K_x, K_y) in k-space do not correspond one-to-one with individual pixels (x,y) in the image. Each k-space point contains spatial frequency and phase information about every pixel in the final image. Conversely, each pixel in the image maps to every point in k-space. The k-space representation of the MR image is therefore akin to the diffraction patterns generated by x-ray crystallography, optics, or holography, Figure[10] 1.12.

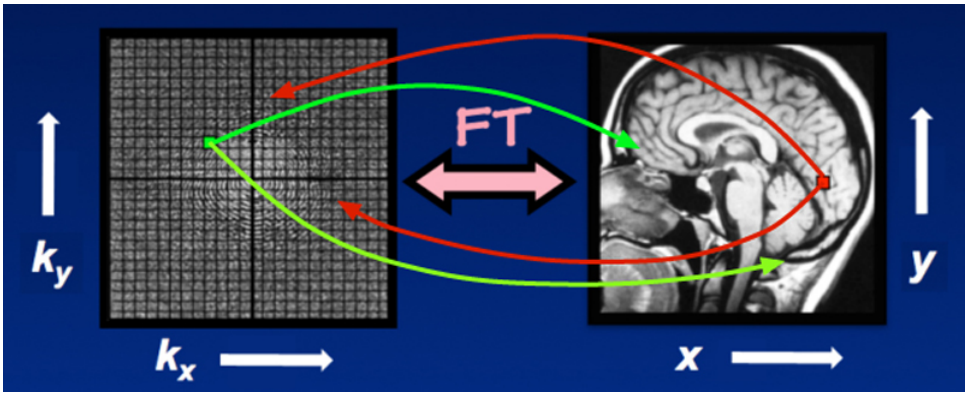

FIGURE 1.12: Each point in k-space maps to every point in the image, and vice-versa.

1.4.2 Image Contrast

The contrast in most MRI is more complex and is influenced by several characteristics of tissues and other materials. Actually, MRI image contrast is a mixture of several parameters, which can be classified into intrinsic and extrinsic parameters. Intrinsic parameters relate directly to the tissue. Extrinsic parameters relate to the physical characteristics of the imager and the details of the pulse sequence used for imaging. The control of the imaging pulse sequence allows one contrast mechanism to be emphasized while the others are minimized. The ability to choose different contrast mechanisms by tailoring the appropriate pulse sequence and choosing the right pulse sequence parameters is what gives MRI its tremendous flexibility.

There are two principal timing variables: repetition time (TR) and echo time (TE), where the variations in the value of TR and TE have an important effect on the control of image contrast characteristics , Figure 1.13. Repetition time (TR) measured in ms, is the time between

[10] www.mriquestions.com

successive RF excitation pulses applied to a given volume of tissue. Echo time (TE) measured in ms, is the time between the excitation pulse and the echo (signal maximum).

Short values of TR and TE are common in images exhibiting T1 contrast (T1-Weighted Image). Long values of TR and TE are common in images exhibiting T2 contrast (T2-Weighted Image). Long TR values and short TE values are common for density weighted contrast (Proton Density Weighted Image).

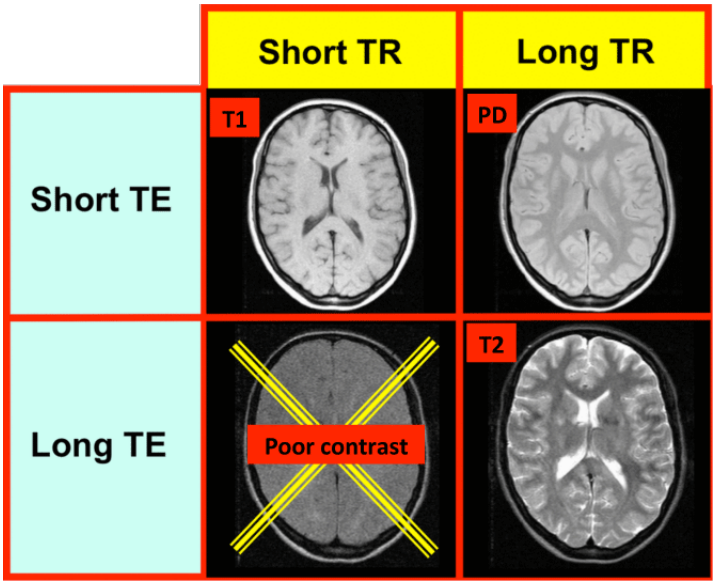

FIGURE 1.13: Image contrast and the effect of repetition time and echo time.

Contrast Agents

In MRI, some areas of the body, adjacent tissues have similar MRI appearance, and contrast agents are needed for adequate differentiation. Contrast agents are chemical substances used in magnetic resonance imaging (MRI) scans. When injected into the body, contrast agents enhances and improves the quality of the MRI images as well as to help in the diagnosis of pathologies, such as tumors and infection, Figure[11] 1.14.

1.4.3 Artifacts

Artifacts in MRI can be generated by a wide variety of factors resulting from the MR scanner hardware itself, the interaction of the patient with the hardware, or poorly optimized measurement sequences [21]. The knowledge of the artifacts and their sources is extremely important in order

[11] www.aappublications.org

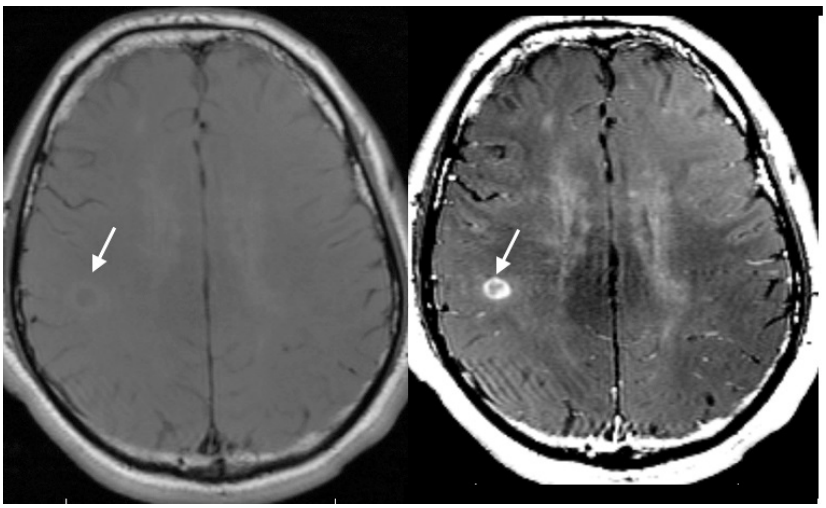

FIGURE 1.14: Effect of contrast agent on images: Left image, no contrast agent present. Right image, contrast agent present. Signal increase due to the presence of the agent.

to avoid false diagnoses and to learn how to eliminate them [22]. Some of the most important artifacts are described below.

Motion Artifacts

Motion is one of the most common artifacts in MR imaging, causing either ghost images or diffuse image noise in the phase-encoding direction [23]. Motion artifacts occur as a result of the movement of the tissue during the data acquisition period, caused by breathing, cardiac movement, patient's movement, which create ghost artifacts [22], Figure 1.15. They can be reduced by patient immobilization, cardiac/respiratory gating, signal suppression of the tissue causing the artifact, saturation bands, or drugs that slow down the intestinal peristalsis. One can also reduce motion artifacts by using echo planar imaging, a very fast MR imaging technique [24].

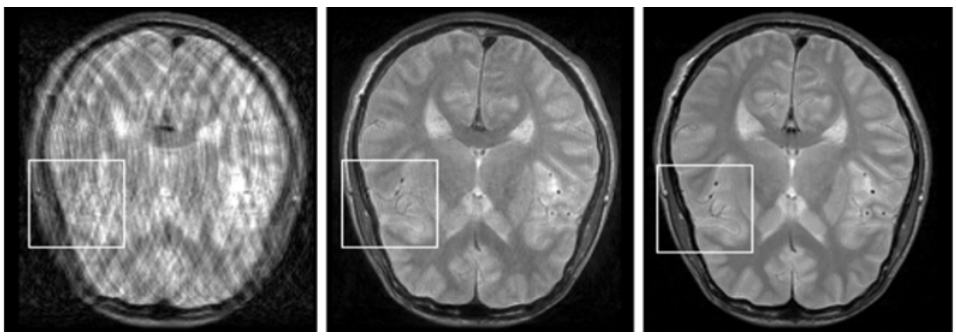

FIGURE 1.15: Motion artifacts in brain MRI due to head movement during the examination. Left: motion corrupted image. Middle: less motion. Right: no motion image.

Aliasing Artifacts

The techniques used for spatial localization assign a unique frequency and phase to each location within the image. These are determined by the acquisition matrix and the desired field of view in the phase encoding and readout directions. Aliasing artifacts occur when tissue outside the chosen field of view [11]. One can eliminate them by increasing the field of view [23].

Chemical Shift Artifacts

Chemical shift artifacts occur as dark or bright bands at the lipid-water interface and are seen especially in case of fluid-filled structures surrounded by fat. These artifacts arise due to the difference in water and fat resonate at different frequencies [25]. MRI systems usually adjust their reference frequency to that of water, with the result that where localization depends on frequency, as in slice selection or frequency encoded readout, the fat signal will be spatially displaced from the water signal, effectively producing a shifted image. This can result in areas of signal void or brighter signal, owing to the overlap of water and fat signals in the readout direction [14].

1.5 Principles of Functional Magnetic Resonance Imaging (fMRI)

Functional magnetic resonance imaging (fMRI) is a widely used method for functional brain imaging and has become a standard tool for mapping the working brain activation patterns, both in health and in disease. It is non-invasive and allows to better understand how the brain works by recording with very little intrusion the brain activity of an active human or animal subject with a good time ($1s$) and spatial resolution ($1mm^3$). fMRI simultaneously models the spatial and temporal patterns of brain functional networks (4D). The brain can be imagined as a set of (3D) cubes in the fMRI, where each cube is called as voxel and represents the three spatial dimensions (X, Y, Z). Time is the fourth dimension and is called the time-series, each voxel has its own time-series. It may be used to examine the brain's functional anatomy, (determine which parts of the brain are handling critical functions), evaluate the effects of a stroke or other diseases, or to guide brain treatment. fMRI may detect abnormalities within the brain that cannot be found with other imaging techniques. fMRI is based on the same technology as magnetic resonance imaging (MRI). It uses a strong magnetic field and radio waves to create detailed images of the body. But instead of creating images of organs and tissues like MRI, fMRI looks at blood flow in the brain to detect areas of activity. The fMRI technique was invented in 1990 by a group at

Bell Laboratories led by Seiji Ogawa [26] [27]. A startling amount of progress has been made in the few years since then. In this section, we will briefly discuss the principles of fMRI.

1.5.1 Functional Neuroimaging Modalities

Nowadays, there are several functional brain imaging methods [28]. Each of these modalities makes it possible to study brain structures, as well as their function. Some of the most commonly used functional imaging techniques are sensitive to indirect changes in blood oxygenation or measure direct or indirect electrical activity. Therefore, the selection of a functional brain imaging modality depends on the experimental hypothesis that one wants to test. Different modalities have different trade-offs in terms of spatial and temporal resolution, Figure 1.16, [29]. In this subsection, we will discuss briefly some of the main functional neuroimaging modalities available today.

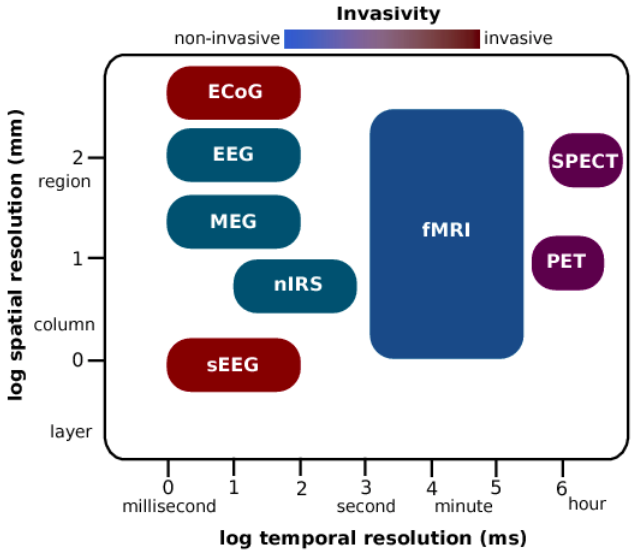

FIGURE 1.16: Spatial and temporal resolutions of the different modalities commonly used for functional imaging. fMRI is a non-invasive technique that gives a spatial resolution of 1 to 3 milliliters with a temporal resolution of 1 to 3 seconds.

Electroencephalography (EEG)

The EEG measures electrical activity on the scalp. It represents direct measures of neural activity. In particular, scalp recorded EEG has been used extensively in research, clinical neurophysiology, and practice. EEG can determine changes in brain activity that might be useful in diagnosing brain disorders, especially epilepsy or another seizure disorder, EEG also

can identify the causes of other problems, such as sleep disorders and changes in behavior. It has a high temporal resolution but a poor spatial resolution compared to other modalities such as fMRI.

Invasive versions of EEG improve spatial resolution by placing electrodes on the exposed surface of the brain to record electrical activity from the cerebral cortex as Electrocorticography (ECoG) imaging or by using depth electrodes localized with a stereotactic technique as Stereotactic EEG (sEEG) imaging.

Magnetoencephalography (MEG)

MEG is a non-invasive technique that measures the magnetic field induced by neural electrical activity. The synchronized currents in neurons create magnetic fields that can be detected using very sensitive magnetometers and gradiometers. Although the EEG and the MEG are produced by the same physiological process, the MEG displays an improved spatial resolution compared to EEG, due to the fact that the magnetic fields are less deformed than the electric fields by the skull and the scalp.

Positron Emission Tomography (PET)

PET is a type of nuclear medicine procedure based on the detection of radioactive tracers introduced in the body of the subject. PET is actually a combination of nuclear medicine and biochemical analysis. It can provide detailed information about biochemical or physiological processes with a precise anatomical context. This scan used mostly in patients with brain or heart conditions and cancer, it can sometimes detect disease before it shows up on other imaging tests.

Single Photon Emission Computed Tomography (SPECT)

SPECT is a noninvasive nuclear imaging test. It uses radioactive tracers that are injected into the blood to produce pictures of the body. It can be used for functional brain imaging by using a specific tracer. Doctors use SPECT to help diagnose seizures, stroke, stress fractures, infections, coronary artery, and tumors in the spine.

Near-Infrared Spectroscopy (nIRS)

nIRS is a spectroscopic method that uses the near-infrared region of the electromagnetic spectrum to non-invasively probe the concentration and oxygenation of hemoglobin in the brain, muscle, and other tissues and is used e.g. to detect changes induced by brain activity, injury, or disease.

Functional Magnetic Resonance Imaging (FMRI)

fMRI techniques are now a primary tool for basic studies of the organization of the working human brain. The primary form of fMRI measures the oxygen change in blood flow. This is known as the Blood oxygen level-dependent (BOLD) contrast, which is indirectly related to brain activity. Other increasingly popular fMRI method is arterial spin labeling (ASL), which uses arterial water as a tracer to measure cerebral blood flow. In this work, we focus on BOLD functional MRI modalities.

1.5.2 Blood Oxygen Level Dependent (BOLD) Signal

The working brain requires a continuous supply of glucose and oxygen (O_2), which must be supplied by cerebral blood flow (CBF). The human brain receives approximately 15% of the total cardiac output of blood and yet accounts for only 2% of the total body weight [30]. During brain activity, the energy consumption is increased and so is oxygen consumption, and this metabolic activity is implicitly related to oxygen consumption. We can indirectly measure neural activity by acquiring a signal depending on local metabolic demands (oxygenation consumption) of active neurons. This is the core concept behind the Blood Oxygen Level Dependent signal [26] [31].

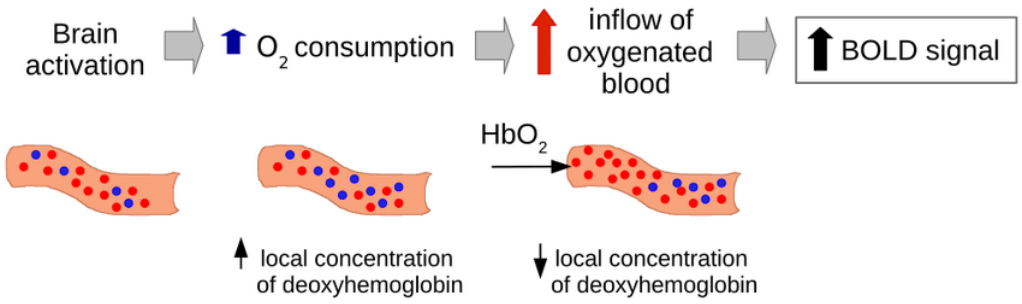

FIGURE 1.17: The BOLD signal measures the ratio between oxy and deoxy-hemoglobin in the blood. This ratio changes during brain activity.

Cerebral blood flow needs hemoglobin, a protein present in blood cells that has the ability to bind oxygen. The Blood Oxygen Level Dependent (BOLD) signal measures the ratio between

oxygenated and deoxygenated hemoglobin, Figure 1.17 [32]. Both hemoglobin states have different magnetic properties and produce different local changes in magnetic susceptibility where oxyhemoglobin has no unpaired electrons and is weakly diamagnetic. When oxygen is released to form deoxyhemoglobin, 4 unpaired electrons are exposed at each iron center, causing the molecule to become strongly paramagnetic, Figure[12] 1.18. The presence of deoxyhemoglobin in the blood (less than 2% in arterial blood to greater than 40% in venous blood) modifies the magnetic resonance signal of the protons of the water molecules surrounding the blood vessels. The difference of magnetic susceptibility between the blood vessel and the surrounding tissues creates inhomogeneities in the magnetic field that are quantified by the magnetic resonance scanner [27].

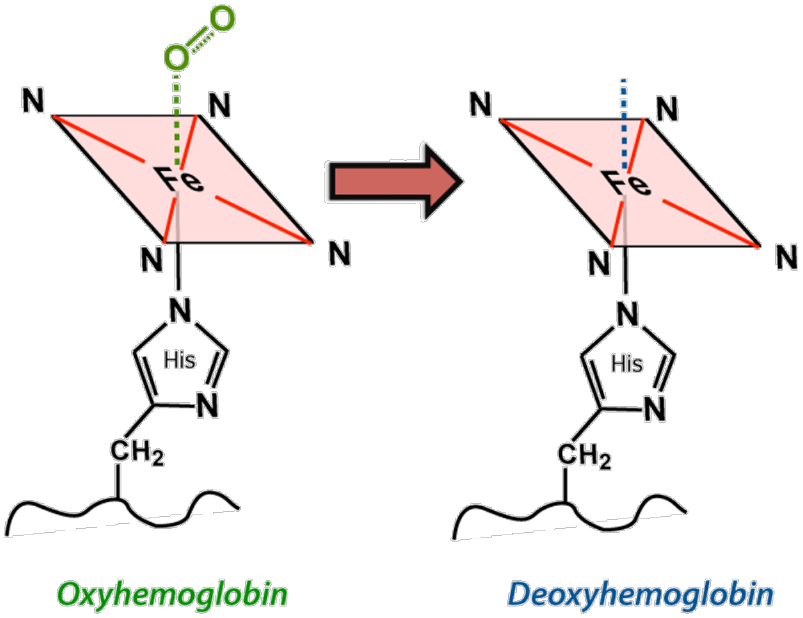

FIGURE 1.18: Deoxyhemoglobin is strongly paramagnetic due to 4 unpaired electrons at each iron center.

1.5.3 Resting-State fMRI

Resting-state fMRI was first described by Biswal et al in 1995 [33] and has since then been widely used in fMRI analysis for various neurologic, neurosurgical, and psychiatric disorders [34]. rs-fMRI does not require subjects to perform a task or respond to stimuli. Subjects are asked to rest in the scanner a few minutes with their eyes closed or staring at a fixed point while whole-brain BOLD data is collected; as it is cheap to acquire and contains much intrinsic information about brain functioning.

[12] http://mriquestions.com/

Rs-fMRI has permitted the discovery of at least 20 distinct patterns of brain connections called resting-state networks (RSNs). These networks have provided significant insights into the cognitive organization of the brain in health and disease. The functional network which has been the most studied by resting-state fMRI is the default mode network. This network has been shown to be spontaneously activated without stimulation and linked with mind wandering [35]. The functional networks uncovered from resting-state data have been used for neurosurgical planning [36]. It has also been used to identify bio-markers for certain diseases: epileptogenic networks in epileptic patients, Alzheimer disease, Parkinson disease, Autism spectrum disorder, distinguish patients with mild cognitive impairment from controls, patients with disorders of consciousness and psychiatric [37].

1.5.4 Task-based fMRI

Task-based functional magnetic resonance imaging (t-fMRI) is a non-invasive technique has been well established for mapping brain activation and network activities when individuals are asked to perform a given task. It has been a powerful tool to study functional networks and cognitive behaviors of the human brain. t-fMRI has significantly advanced our knowledge of brain regions and networks that are functionally involved in specific cognitive or perceptive tasks [38].

1.6 Conclusion

In this first chapter, we have presented the principal structures of the human brain. We have then presented the principle of nuclear magnetic resonance. Next, we briefly introduced both magnetic resonance imaging and functional magnetic resonance imaging, in so far as it allows us to understand the basic anatomical and functional features of the brain and how to use magnetic resonance in order to take structural and functional images of the brain to complete our thesis. In the next two chapters, we will present the main approaches for MRI and fMRI analyses.

Chapter 2

Brain MRI Analysis

2.1 Introduction

Magnetic resonance imaging is today one of the most widely used and versatile medical imaging modalities. Currently, several technical developments have made it possible to derive quantitative measurements from these data. In this chapter, we will describe some of the most common MRI steps normally applied to raw MR images in order to improve their quality (Preprocessing) and the methods used in the analysis process.

2.2 Brain MRI Preprocessing

MRI images are normally affected by different types of artifacts that must be minimized before applying any analysis process in order to improve the expected results.

2.2.1 Conversion to NIFTI

Most medical imaging devices store images in variations of the complicated DICOM format. DICOM is too complex and is missing attributes useful for neuroimaging. For this reason and in the first step, MR images are converted to the commonly used format of the Neuroimaging Informatics Technology Initiative (NIfTI) [39]. The NIfTI makes up for DICOM shortcomings and was designed for scientific analysis of brain images. The format is simple, compact, versatile and follows the Talairach/MNI coordinate system. Many scientific tools expect medical images to be stored in the simpler NIfTI format.

2.2.2 Denoising

The visual quality of magnetic resonance images plays an important role in accuracy of clinical diagnosis which can be seriously degraded by existing noise during the acquisition process [40]. The aim of MRI denoising step is that of reducing the noise power while maintaining the original resolution of the useful features and is an important MRI preprocessing step used for the analysis process, Figure 2.1 [41].

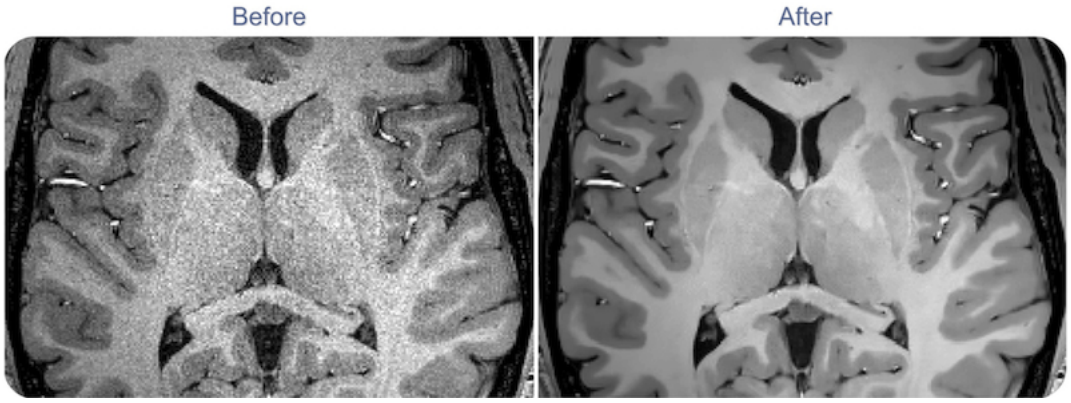

FIGURE 2.1: Left: original noisy T1-weighted image. Right: denoised image using a filter.

Despite the MRI noise can be effectively reduced by simply averaging several acquisitions directly into the scanner, but this technique significantly increases the acquisition time. A variety of techniques have been presented in the literature on denoising MR images and each technique has its own assumptions, advantages, and limitations which can be grouped based on filtering approach, transform approach and statistical approach. Figure 2.2 gives an overview of various methods for denoising MR images presented in the literature [40].

2.2.3 Co-register

Co-registering an MRI is the process of mapping different images into the same coordinate system so equivalent points of the different images share the same location in a standard space as MNI space or atlas [41]. Co-registration is necessary in order to be able to compare or integrate data from multiple sources or to apply some analysis pipeline and is most widely used to standardize images and measurements to brain atlases [42]. It can be useful to correct for motion, differences in sequence measurements, and sequence localization disagreements when selecting regions of interest [43].

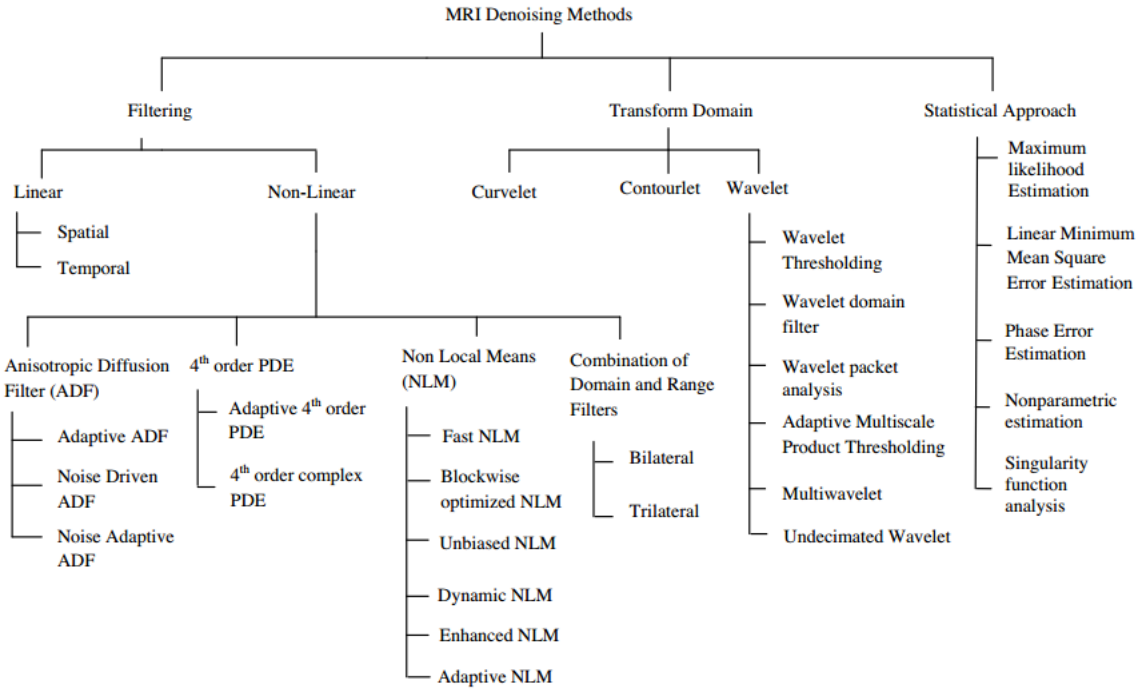

FIGURE 2.2: Classification of MRI denoising method.

2.2.4 Bias Correction

Magnetic resonance images often exhibit non-uniformities of image intensity resulting from magnetic field variations rather than anatomical differences and this non-uniformity of image intensity is known as a bias field. These variations are often seen as a signal gain change that varies slowly spatially. This can result in white matter measurements in one part of the image with the same intensity as gray matter measurements elsewhere and it can lead to serious misclassifications by intensity-based segmentation algorithms that assume a uniform intensity.

Bias correction refers to a procedure to estimate the bias field from the measured image so that its effect can be eliminated, Figure 2.3 [44]. These artifacts often caused by the imperfection of imaging devices or by magnetic susceptibility changes at the boundaries between anatomical tissue and air. There are two main types of methods for bias correction: prospective and retrospective methods [45].

2.2.5 Skull Stripping

Skull stripping in brain MRI is an essential step to analyze images of the brain where non-brain tissues such as the skull, scalp, and dura are removed from images of the brain, Figure 2.4. It is also a very important preprocessing step, which ensures better segmentation and assures

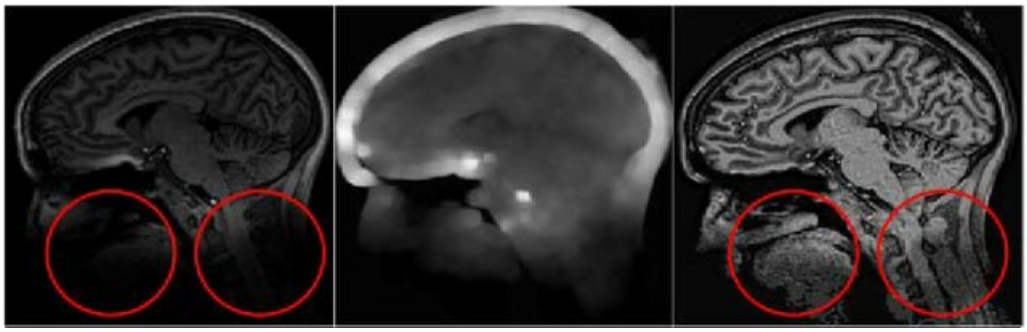

FIGURE 2.3: Bias-correction results on an MRI image. Left: original images. Middle: estimated bias fields. Right: the bias-corrected.

accurate diagnosis of brain diseases and the probability of misclassification of abnormal tissues is also reduced [46].

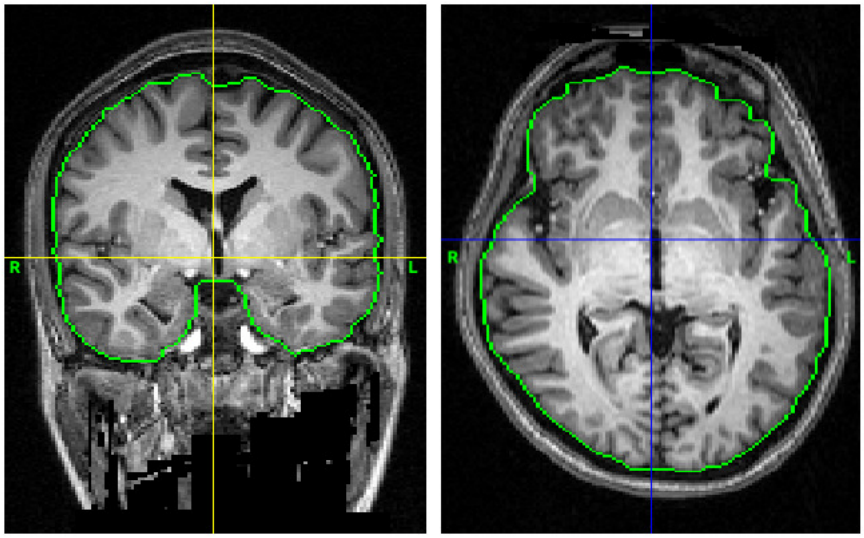

FIGURE 2.4: Result of skull stripping.

2.2.6 Intensity Normalization

Intensity normalization plays an important role in normalizing the tissue intensity ranges on which most automatic image analysis methods base their distributional assumptions. During acquisition, MR images do not share similar intensities across scanners. Even within the same scanner and setting, there is variability in the intensity patterns of the acquired images on different sessions [41]. This intensity variability will greatly undermine the performance of subsequent MRI processing, and it is significantly difficult to obtain quantitative measures directly from the data. Most simple approaches to normalized MR intensities rely on the use of histogram matching techniques, which is the transformation of an image so that its histogram matches a specified histogram [47] [48].

2.2.7 Extraction of Cerebral Hemispheres

Extraction of Cerebral Hemispheres refers to the extraction of the left and right cerebral, which is an important step in many different analyses of the brain, Figure 2.5. It is needed to separate the hemispheres for volumetric and morphological analysis. It also contains many important interhemispheric structures [49].

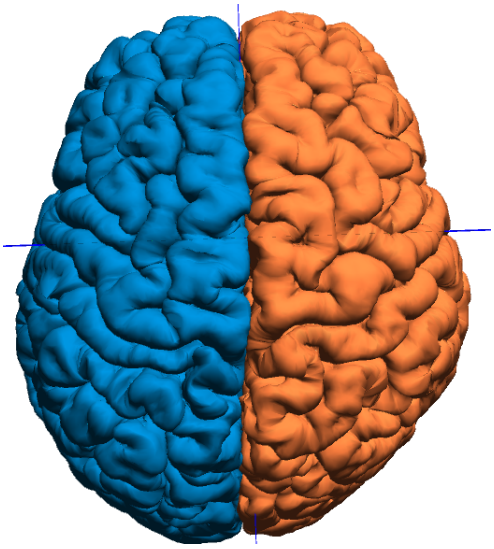

FIGURE 2.5: Result of the extraction of the cerebral hemispheres.

2.2.8 Tissue Segmentation

Tissue segmentation of the brain MRI consists of the assignment of a tissue type to each voxel of the MRI scan. Generally, the brain tissue segmented into one of the three main tissue types that are the gray matter (GM), the white matter (WM) and the cerebrospinal fluid (CSF), Figure 2.6.

The brain has a particularly complex structure and its precise tissue segmentation is very important for describing anatomical phenotypes and individual variations. Measuring how diseases affect the shape and size of the structures that make up the brain. Obtaining morphometric biomarkers for the diagnosis, prognosis, and disease monitoring. Assign anatomical locations at functional activations. There are various segmentation approaches been developed and reported in the literature. An overview of the most popular methods commonly used for brain MRI tissue segmentation in [50].

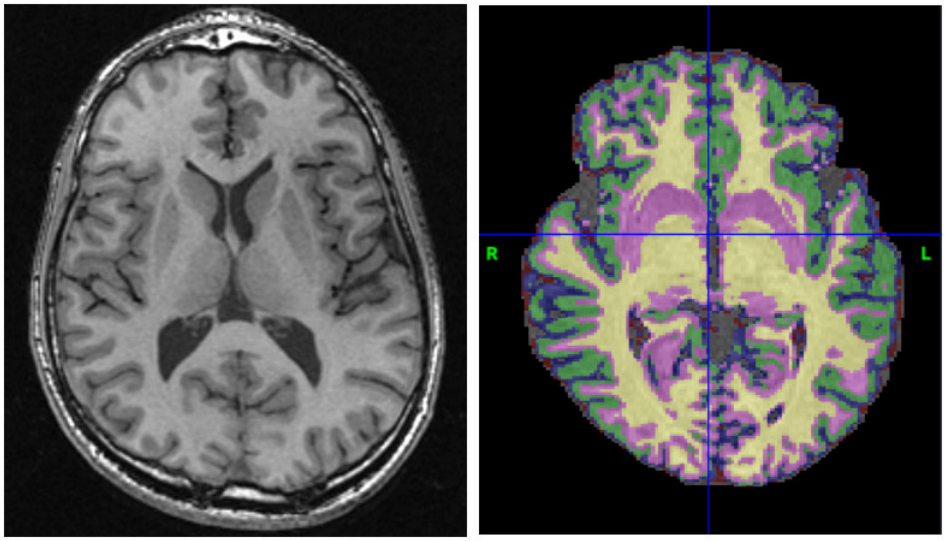

FIGURE 2.6: Brain tissue segmentation. Left: the original T1-MRI. Right: the result of tissue segmentation.

2.2.9 Surface Atlas Registration

The human cerebral cortex is placed in a highly folded leaf, most of the cortical surface area buried in folds and folding patterns considerably variable across subjects. To study cortical structure and function, we need to register the cortical surface as an atlas, Figure 2.7 for providing the common spaces for quantitative comparison of subjects and group analysis of functional data, in order to compensate for differences in position, size, and shape of brain structures across individuals.

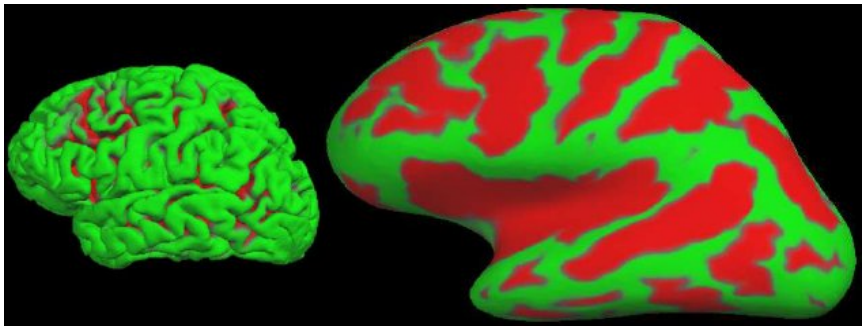

FIGURE 2.7: Surface atlas registration where green indicates a gyrus and red indicates a sulcus.

2.2.10 Reconstruction of Cortical Surfaces

Reconstruction of cortical surfaces from magnetic resonance images is an important means to study the structure and function of the brain cortex, Figure 2.8. It is also an important step in

quantitative analysis of the human brain structure, we can mention, analysis of cortical folding patterns, brain morphometry, and in cortical thickness studies. The cortical surface model must be geometrically accurate and topologically correct in order to provide valid and accurate quantitative measures of brain structure [51]. There has been a significant effort towards the development of methods for the reconstruction of the cortical surface. Most of these methods are either voxel-based or deformation-based [52].

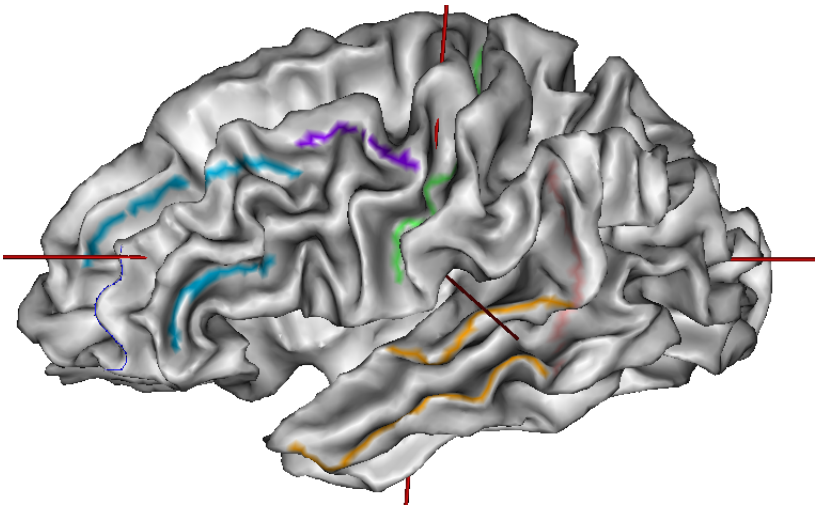

FIGURE 2.8: Result of cortical surface reconstruction.

2.3 Brain MRI Analysis

Magnetic resonance imaging (MRI) has become a powerful diagnostic tool by providing high-quality images, thanks to new advances in technology [53]. The strength of MRI lies in the excellent anatomical details it provides as well as the high soft-tissue contrast and the possibility of enhancing different tissue types using different acquisition protocols. Automatic diagnostic tools aid in the diagnosis by providing quantitative measures of morphology, function, and other biomarkers in different tissues. This is due to the difficulty of diagnosing some pathologies with the human eye because of their limited ability to detect the heterogeneous intrinsic properties of certain tissues. In this section, we will present the main approaches to MRI analysis of the brain.

2.3.1 Regions Of Interest (ROIs)

The thin outer layer of the brain cerebrum is of particular interest due to its vital role in cognition, vision, and perception. It is arranged in areas based on criteria such as cytoarchitecture, functional

specialization or axonal connectivity. Parceling the cortex into such areas and characterizing their interaction is the key to provide biomarkers that can be used to study the neurobiology of various diseases and understanding how the brain works.

There are two types of methods for ROIs definition: Manual ROIs definition is still considered the gold standard in many applications, but it is difficult to perform for the whole cortex because it consumes a lot of time and requires a high level of anatomical expertise. Automatic or semi-automatic methods of ROIs definition have been developed to parcellate cortical surfaces into ROIs automatically or semi-automatically. Those methods are useful for large-scale studies because they do not require significant manual intervention. Approaches used clustering based on local regional statistics [54], supervised techniques [55], approaches use a cortical surface-based feature to find surface correspondence as sulci [56], Conventional approaches [57]. In other research, you will discover that researchers are using the parcellation that refers to parceling the cortical surface into sub-regions, Figure 2.9. Cortical surface parcellation helps to establish relationships by classifying brain tissue and cortex into different functional regions.

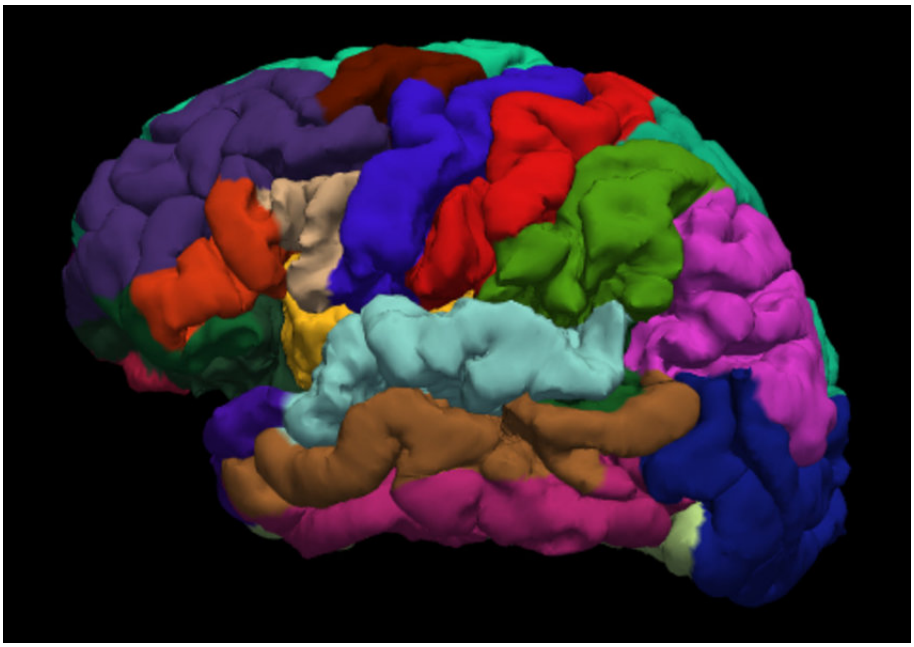

FIGURE 2.9: Cortical surface parcellation with Freesurfer software.

2.3.2 Gyri and Sulci Labeling

The cerebral cortex of the human brain is highly complicated and folds itself into gyri and sulci during brain development. A precise description of the anatomy of the brain makes it possible to understand its structure and functioning. It is crucial for possible surgical interventions and brain diseases predicted. Automated labeling of the cerebral gyri on the cerebral surface is a fundamental work for helping us to diagnose cerebral diseases, Polymicrogyria [58], Brain

atrophy [59], and Alzheimer's disease [60]. The changes in sulci width or depth can be related to changes in the cortical gray matter or white matter volumes. Therefor, studying sulci shape is very important to intervene before some diseases occur as Alzheimer's disease and mild cognitive impairment [61], also it is helpful in many studies and applications related to brain diseases, human behavior and allowed to distinguish different functional areas of the brain [62], Figure [1] 2.10.

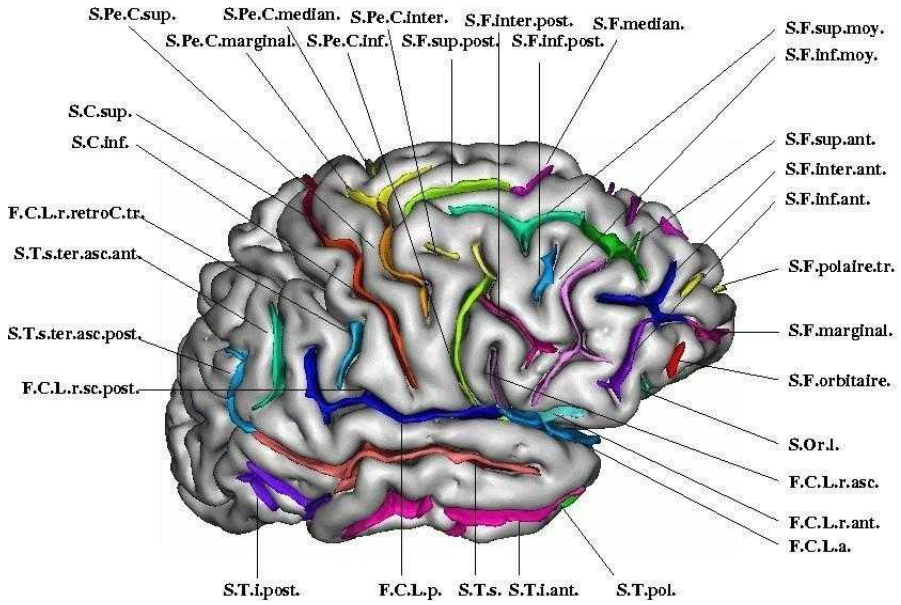

FIGURE 2.10: Example of sulci labeling.

2.3.3 Feature Extraction and Selection

The brain MRI features are the characteristics of the whole or a part of the brain which contains the maximum information needed to analyze the brain images. Feature extraction methodologies are applied to extract the most prominent features from the image that represents the different classes of objects. The objective behind feature extraction is reducing the original data by computing certain properties or features that differentiate one input pattern from another. There are various types of features such as shape-based (circularity, irregularity, area, perimeter, shape Index, etc), color-based (mean, variance, standard variance, median intensity, skewness, kurtosis, etc) and texture-based feature (contrast, correlation, entropy, energy, homogeneity, cluster shade, sum of square variance), etc [63]. Texture analysis is an important parameter of human visual perception and machine learning systems. It is used effectively to improve the accuracy of the diagnosis system by selecting prominent features. Texture analysis and its statistical features were stated in [64] [65].

[1] http://brainvisa.info/web/index.html

Feature Selection:

is a process applied for selecting appropriate features from all extracted features for building robust learning models by removing most irrelevant and redundant features from the data. Feature selection helps improve the performance of learning models by: Alleviating the effect of the curse of dimensionality, Enhancing generalization capability, Speeding up the learning process and Improving model interpretability [63].

2.3.4 Prediction and Classification

In recent years, machine learning and deep learning have shown record-shattering performance in a variety of computer vision problems, such as visual object recognition, detection and segmentation. These methods have also been utilized in the medical image analysis domain, Figure 2.11 [66]. Generally, studies of machine learning and deep learning are applied in medical image analysis for disease prediction, diagnosis, and prediction of treatment response [67].

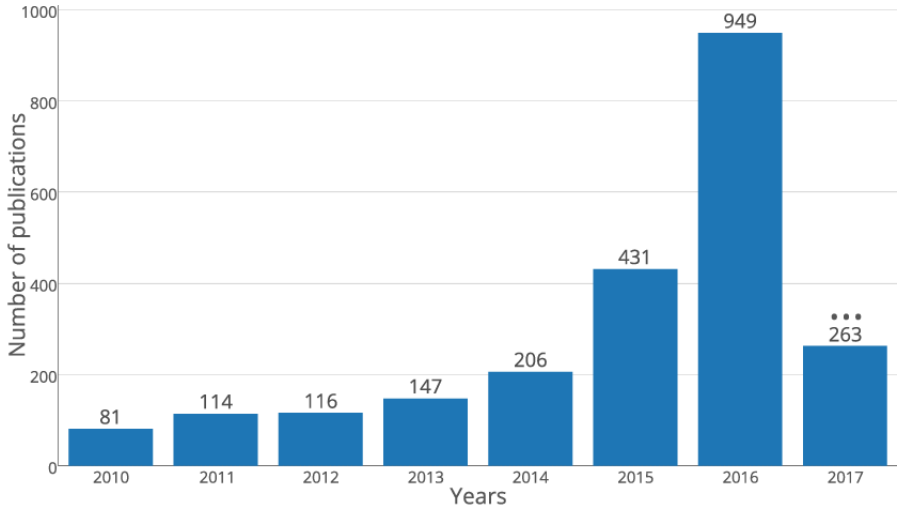

FIGURE 2.11: Number of publications per year in IEEE-Xplore containing "deep learning" and "medical imaging" keywords from 2010 to 2017. (Queried: June 6th, 2017).

We now mention some work related to the use of prediction and classification in the three categories previously. Predicting the onset or progression of the disease: Use machine learning and deep learning methods to predict disease risk have been developed in various fields of medicine [68] [69]. Used machine learning models to predict the onset of Alzheimer's disease or the conversion from mild cognitive impairment to Alzheimer's disease [70] [71]. Predict the first onset of major depression in adolescence [72]. Diagnosis: or classification is the most widely and frequently applied area of machine learning and deep learning studies in brain MRI analysis.

Brain tumor classification methods [73] [74] [75] [76]. Parkinson's disease and Progressive Supranuclear Palsy [77]. Schizophrenia [78]. Brain lesions [79] [80]. Predicting treatment response: predicting the treatment of major depressive disorder [81]. Prediction of individual response to electroconvulsive therapy [82].

2.3.5 Voxel-Based Morphometry Analysis

The human brain structure is in a state of constant change and adaptation. This may be driven either by normal developmental or aging processes or by the effects of learning, training, and new occurrences in daily life [83]. The identification of structural changes in the brain on magnetic resonance imaging (MRI) scans is increasingly important in the study of neurological and psychiatric diseases [84] [85] [86] [87] [88]. Traditional techniques for identifying structural changes in brain MRI are based on the visual assessment by experienced radiologists and manual measurements of structures of interest. However, automated techniques have been developed to allow these structural changes to be assessed on large sets of subjects without the need for time-consuming manual measurements or subjective visual assessments. Voxel-based morphometry is one of those automated techniques that has been gaining popularity since its introduction [89] [90], Figure 2.12 [91].

Voxel-based morphometry of MRI data comprises segmentation into gray matter, white matter, and cerebrospinal fluid partitions, anatomical standardization of all the images to the same stereotactic space using linear affine transformation and further non-linear warping, smoothing and finally performing a statistical analysis. The output from the method is a statistical parametric map. It has become a common tool for computational brain anatomy studies. It allows a comprehensive measurement of structural differences within a group or across groups, not just in specific structures, but throughout the entire brain [87] [92] [90]. Statistical analysis is based on the General Linear Model (GLM) to identify regions of gray/white matter concentration that are significantly related to the particular effects understudy, and residual variability applied to each voxel independently. Standard parametric statistical procedures are used to test hypotheses that are expressed as linear functions of the GLM estimated regression parameters [89].

2.3.6 Texture Analysis

Although MRI offers excellent anatomic details due to its high soft-tissue contrast and the possibility to enhance different types of tissues using different acquisition protocols. However, the diagnosis of some pathologies remains difficult due to the limited ability of the human eye to detect the heterogeneous intrinsic properties of certain tissues and a wrong diagnosis can lead to improper patient treatment. In order to assist the radiologist in the diagnosis, there are

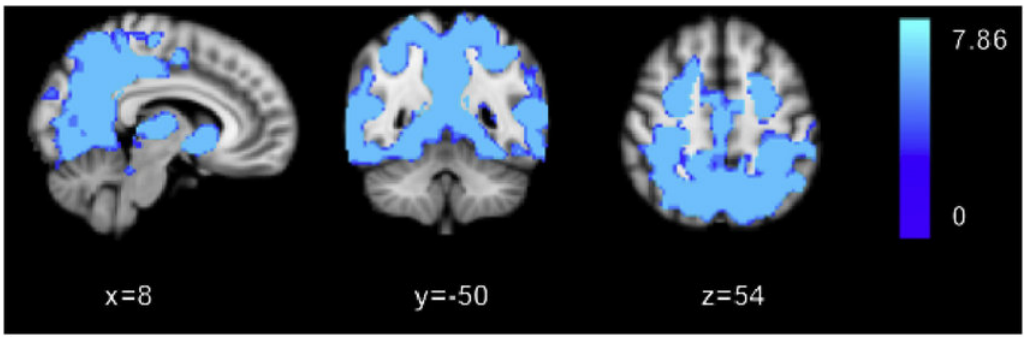

FIGURE 2.12: Voxel-based morphometry maps displaying reduced grey matter density in posterior cortical atrophy (PCA) patients. Colour bar indicates T-values of statistically significant voxels.

numerous tools and approaches providing quantitative measurements of morphology, function and other biomarkers in different tissues. Texture analysis is one such significant tool in medical applications. It has gained attention in the past years and has become an important tool in the computer-assisted diagnostic process [53] [93].

The texture of images refers to the spatial arrangement of patterns that provides the visual appearance of coarseness, randomness, smoothness, etc. It consists of the calculation in digitized images of mathematical parameters characteristic of the texture, using the data of each pixel in all regions of interest. The analysis of texture parameters is a useful way of increasing the information obtainable from medical images and have been used as input parameters in machine learning approaches for human tissue classification, discrimination between different types of tumors [94] [95], classification of diseases like Alzheimer's [96] or Friedreich ataxia [97], brain segmentation [98] [99]. There are two main types of texture analysis: statistical methods and structural methods [100]. The structural methods represent the texture by the primitives and their related rules. The advantage of these methods is that they provide a good symbolic description of the image. Statistical methods study relationships between one pixel and its neighborhood. They are used in order to characterize fine structures with no apparent regularity: the higher the order of the structure, the higher must be the number of pixels considered. So, the texture is described by the statistical distribution of gray levels. These methods normally achieve higher discrimination indexes than structural and are the most widely used methods in medical imaging [101].

2.3.7 Structural Connectivity

Significant advances in multi-modal magnetic resonance imaging techniques, analysis, and modeling have been made to investigate brain changes or group differences. Gray matter areas are responsible for information processing and are physically interconnected via axonal pathways in the white matter, thus producing functional networks of sub-cortical areas associated with specific tasks.

The brain can be modeled as a network where the nodes represent the sub-cortical gray matter areas and the edge model relationships (connectivity) between the nodes [102] [103]. A network whose edges are characterized by properties related to white matter pathways is defined as a structural network or structural connectivity. The combination of MRI with other types of medical images as fMRI and diffusion MRI (DMRI) has been conducted to improve our understanding of brain mechanisms, and interactions between structural and functional networks [104] [105]. Using MRI and DMRI for producing a structural connectivity network in which the nodes are represented by the regions of interest and the number of tractography between a pair of regions represents the edges, Figure 2.13 [106].

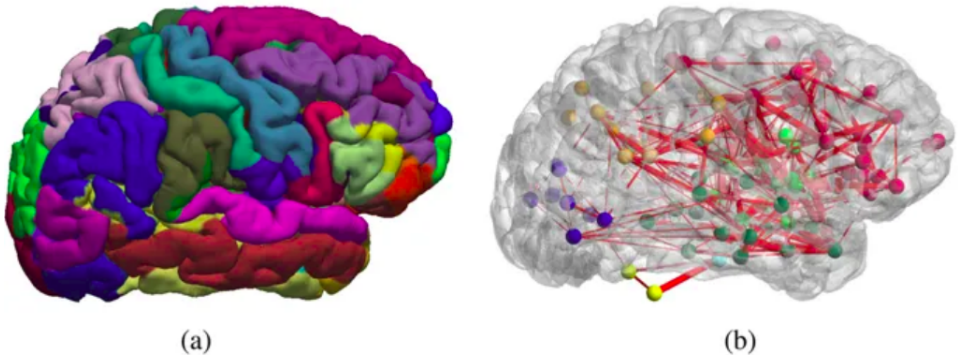

FIGURE 2.13: (a) Extraction of regions of interest. (b) Measure the number of tractography between a pair of regions to produce a structural connectivity network.

2.4 Conclusion

MRI analysis has become a powerful tool in the diagnosis of brain diseases. Improvements in image measurement and preprocessing can, therefore, have a significant impact on clinical diagnosis, image analysis, and computer-assisted diagnosis. Thus, in this chapter, we have presented the preprocessing steps and methods of analysis that will be used to draw conclusions from MRI experiments in the following chapters.

Chapter 3

Brain fMRI Analysis

3.1 Introduction

Functional magnetic resonance imaging (fMRI) is a powerful non-invasive tool for defining activity in the healthy and diseased human brain, used in several domains, for example, Neuroimaging, Neuroscience, Neurology, Psychology, and Psychiatry. fMRI can provide high-quality visualization of the location of activity in the brain resulting from sensory stimulation or cognitive function. It, therefore, allows the study of how the healthy brain functions, how it is affected by different diseases, how it attempts to recover after damage and how drugs can modulate the activity or post-damage recovery. After the fMRI experiment has been designed and implemented, the resulting data must be passed through several analysis steps before we can get results related to the activity of different brain regions during performing specific tasks. In this chapter, we will give a brief overview of the most commonly used preprocessing and analysis methods.

3.2 Brain fMRI Preprocessing

Preprocessing is necessary in fMRI analysis in order to take raw data from the scanner and prepare it for the analysis step. The purpose of the preprocessing is to remove various kinds of artifacts in the data, and to condition the data, in order to maximize the sensitivity of later statistical analysis, and also, in some situations, to increase the statistical validity. This section describes the various preprocessing steps which occur prior to the statistical analysis step.

3.2.1 Image Reconstruction

After converting k-space data into images, we sometimes get problematic data as scanner artifacts. We must therefore first check if the data is not corrupted by artifacts such as spikes or incomplete brain coverage, ensuring no missing regions and correct any distortion. Then fMR images are converted to the commonly used format of the Neuroimaging Informatics Technology Initiative (NIfTI). Note: The brain is a 3D object and is represented as a group of cubes (3D) in fMRI, each cube being called voxel. Thus, the fMR image has a voxel image (3D image) and a temporal dimension (Time series). That is why fMRI data is 4D data.

3.2.2 Motion Correction

People always move in the scanner even with padding around the head, there is still some motion, this leads to reduces the statistical significance of the activation maps and increases the prevalence of false activation, Figure 3.1. Motion correction is, therefore, an essential tool for successful fMRI data analysis [107]. Need each voxel to correspond to a consistent anatomical point for each point in time, that is mean to find a common orientation for all images within a given session and resampling the original data to this reference orientation. This is usually achieved by performing a separate 3D image registration of each image in the series with a chosen reference image, can use either one original volume, mean of several, standard space image, etc. The major component of motion is due to the rigid movement of the head in the scanner. For more detail on physiological noise, see [108] [109].

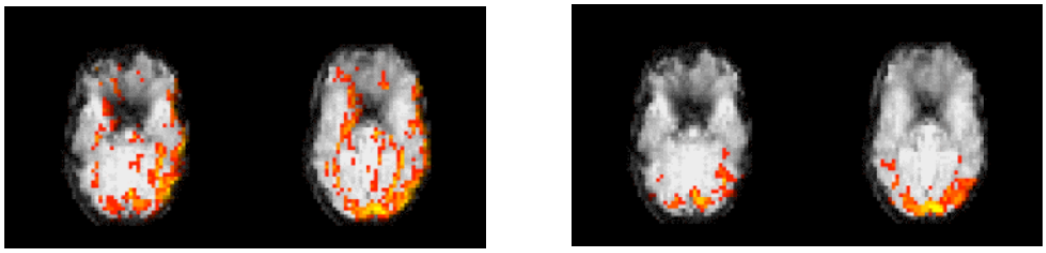

FIGURE 3.1: Motion affects the statistical analysis, reduces the statistical significance of the activation maps and increases the prevalence of false activation. Left: without motion correction. Right: with motion correction.

3.2.3 Slice Timing Correction

Functional volumes are normally acquired slice-by-slice. The slices are not acquired at the same time, each slice is scanned at a slightly different time over the repetition time (TR) [110]. The

timing in all voxels is not the same, if this change in timing is not properly taken into account, the timing of the stimulus and the response will not be matched and, therefore, the statistical analysis will not be able to adjust the model with optimal accuracy, Figure 3.2 [111]. Slice timing correction aims to correct differences in timing across different slices in the image to fit a uniform model on the whole brain by adjusting the voxel time series so that a common reference timing exists for all voxels. The reference time is often chosen as that corresponding to the first slice. The temporal consistency is usually achieved by shifting the time series of values slightly forward or backward in time and then applying some form of interpolation. We must know the slice order and the repetition time. Slice timing correction methods can not correct for spatial variability within the slice for that ideally, a combined approach to both slice timing and motion correction is required [112].

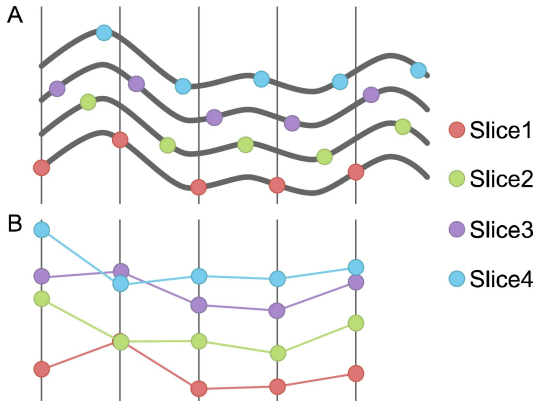

FIGURE 3.2: The slice-timing problem: the same signal sampled at different offsets produces signals that are not alike. (A) Five adjacent slices acquired with interleaved acquisition all sample the same underlying bold signal. (B) Without correction, reconstruction yields five different signals despite having the same underlying shape.

3.2.4 Spatial Normalization

The brain of each individual subject is different in size and shape. Such structural variability of brains imposes obstacles on intersubject brain function studies in how to determine regional correspondence from brain to brain despite their divergence. To perform the group analysis, one has to align each brain into a common space (coregistration or normalization). In coregistration, the fMRI data (time series) are overlaid on the subject's own anatomic brain images [113]. In normalization, the fMRI data (time series) are warped onto a generic brain template, Figure [1] 3.3, [114]. A reference anatomical template used for fMRI registration is the Montreal Neurological Institute (MNI).

[1] Adapted from Chris Rorden : www.mriquestions.com

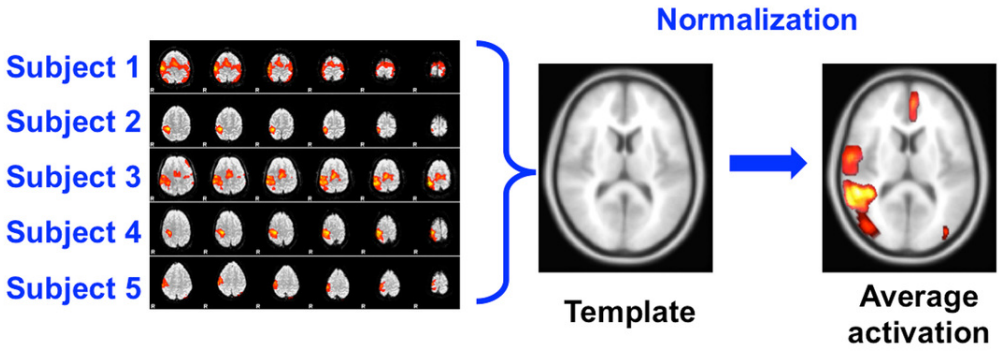

FIGURE 3.3: Normalization warps fMRI data from one or more subjects into a common anatomic template.

3.2.5 Spatial Smoothing

The noise is the unavoidable random variations in the intensity of the image that are present even when no stimulation is applied and any reduction of random noise in the image will improve the ability of a statistical technique to detect true activation. The use of spatial smoothing increases the signal-to-noise-ratio (SNR), by reducing undesired noise. The signal-to-noise ratio is a measure used in science and engineering that compares the level of the desired signal to the level of background noise. Spatial smoothing means that each voxel intensity is replaced by a weighted average of neighboring intensities. This has the effect of a low pass filter meaning that high frequencies of the signal are removed from the data while enhancing low frequencies. The result is that it improves the SNR but will reduce the resolution of each image, Figure 3.4. It is, therefore, necessary to find a balance between the improvement of the SNR and the maintenance of the resolution of the functional image. The most common method of carrying out spatial smoothing is to convolve each volume with a Gaussian filter. The width of this filter usually expressed in millimeter (mm) determines the extent of the blurring that takes place. The full-width-half-maximum (FWHM) for fMRI images is most common.

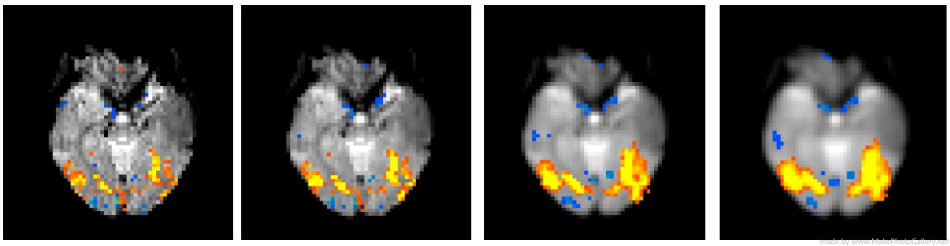

FIGURE 3.4: The effect of different smoothing kernels. from left to right: no Smoothing, 4 mm FWHM, 6 mm FWHM and 8 mm FWHM.

3.2.6 Temporal Filtering

Time series from each voxel of fMRI data often contains signal drifts, which is thought to be caused by physiological noise (cardiac cycle, breathing) as well as by physical (scanner-related) noise. If not taken into account, these signal drifts reduce substantially the power of statistical data analysis. They also invalidate event-related averaging, which assumes stationary time courses, i.e. time courses with a constant signal level. The main point of temporal filtering is to remove unwanted components of a time series (removal of high frequencies, low frequencies or both) without damaging the signal of interest. High-pass filtering and Low-pass filtering attempts to remove respectively all slowly varying unwanted signals and high-frequency noise in each voxel's time series, Figure 3.5.

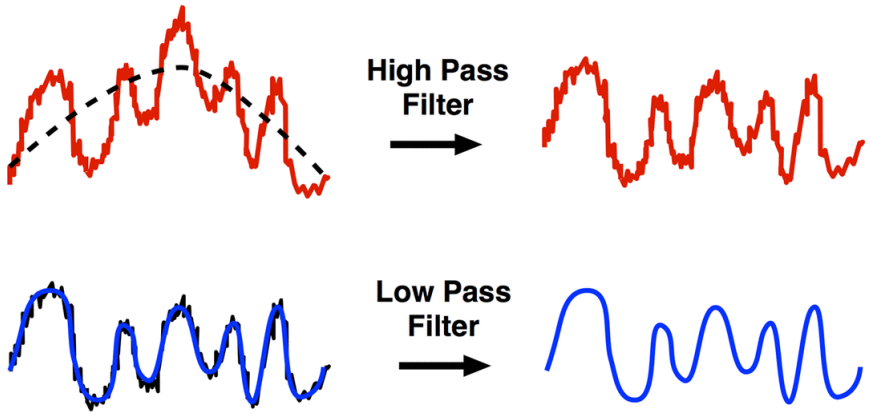

FIGURE 3.5: An example of how to remove unwanted components of a time series. High-pass filtering and Low-pass filtering.

3.2.7 Intensity Normalization

The variations of Intensity in fMRI data are caused by scanner-related artifacts, noise, and partial volume effects. Intensity normalization of fMRI scans has been a very useful preprocessing step, especially when conducting across subject fMRI studies. It attempts to rescale the mean intensity of the fMRI signal in order to compensate for variations of global signal both within sessions and between sessions.

3.3 Statistical Analysis of the fMRI Data

The purpose of fMRI analysis is to detect, in a robust, sensitive and valid way, the parts of the brain that show increased intensity at the points in time when stimulation has been applied to locate brain regions activated by a certain task, determine distributed networks that correspond to brain function and make predictions about psychological or disease states. The statistical analysis is carried out to determine which voxels are activated by the stimulation. In this section, we give a very brief overview of different approaches to obtaining activation maps.

3.3.1 Hemodynamic Response Function (HRF)

The brain consumes the oxygen transported by the hemoglobin and turns oxyhemoglobin into deoxyhemoglobin. Performing a cognitive task causes an oversupply of the oxygenated blood in the active region, and results in a decrease of deoxyhemoglobin. The oversupply process is called the hemodynamic response and enables to relate the oxygenation level to neural activity [115] [116]. The primary goal of fMRI research is to use the information provided by the BOLD signal to make conclusions about the underlying unobserved neuronal activation. Therefore, the construction of the hemodynamic response function (HRF) of the signal response to an external stimulus is the essential step in the statistical analysis of fMRI data for identifying activation regions [117].

The BOLD signal does not increase instantaneously after the stimulus presentation nor does it return to baseline immediately after the stimulus ends. Instead, the BOLD signal peaks approximately 5 seconds after stimulation, and is followed by an undershoot that lasts as long as 30 seconds. The HRF typically demonstrates a small initial dip, followed by a tall peak, and then a variable post-stimulus undershoot, Figure [2] 3.6. Glover [118] proposed to define the HRF as a sum of two gamma probability density functions, where the first gamma probability density function models the shape of the initial stimulus-response and the second gamma probability density functions models the undershoot :

$$h(t) = \frac{t^{\alpha_1 - 1}\beta_1^{\alpha_1} e^{-\beta_1 t}}{\gamma(\alpha_1)} - c\frac{t^{\alpha_2 - 1}\beta_2^{\alpha_2} e^{-\beta_2 t}}{\gamma(\alpha_2)} \tag{3.1}$$

where γ is the gamma function and α_1, α_2, β_1, β_2 control the shape and scale, respectively, and c determines the ratio of the response to undershoot.

[2] www.mriquestions.com

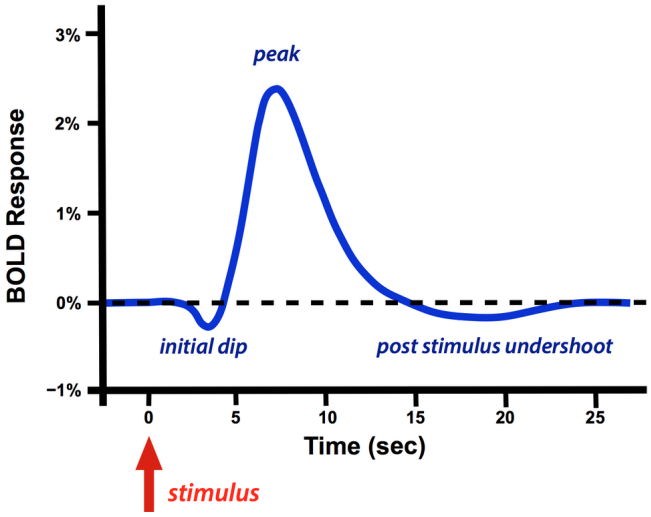

FIGURE 3.6: BOLD Hemodynamic Response Function (HRF) following a single brief stimulus.

3.3.2 Analysis of Task fMRI Data

The fMRI task has been widely used for the detection of brain activation and brain network analysis. The fMRI experiment uses sensory stimuli to induce the participant to perform a behavioral task while BOLD contrast images are acquired for a fixed duration of a few minutes. These stimuli can be visual, auditory or other forms depending on the desired behavioral manipulation. Then, the time-series data are compared against a hypothesized model of neural function based upon the cognitive task being performed. Through statistical inference, the hypothesis can be accepted or rejected for each voxel, in the end, a map of the brain regions that respond to the task is constructed [119], Figure 3.7.

Correlation Analysis

Correlation approach was one of the earliest techniques applied to task-based fMRI studies in the 1990s. Since we know that the BOLD response is mediated by blood flow, it is possible to improve the detection of activation by examining the temporal synchrony between each voxel's time series and the predicted response of the experiment derived by convolving the task control boxcar waveform with a canonical HRF [120]. The choice of an appropriate reference predicted is vital for the success of this technique in finding activation. The degree of temporal synchrony between two-time series **X** and **Y** can be expressed by the correlation coefficient (r) calculated as :

$$r = \frac{\sum(x_i - \bar{X})(y_i - \bar{Y})}{\sqrt{\sum(x_i - \bar{X})^2 \sum(y_i - \bar{Y})^2}} \tag{3.2}$$

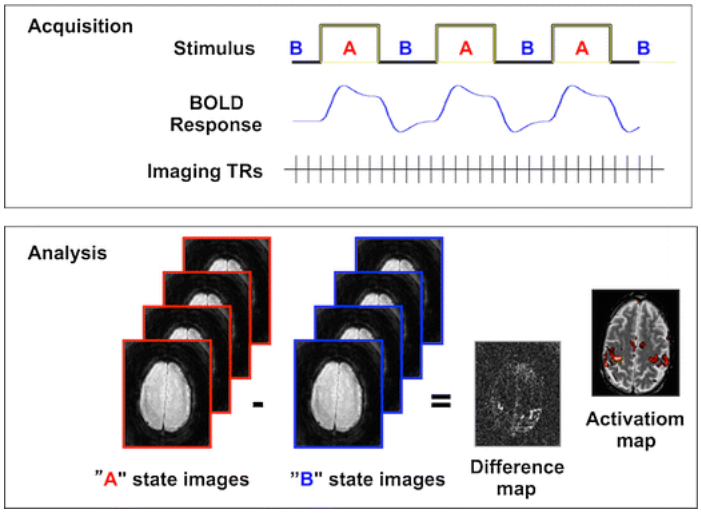

FIGURE 3.7: Task-based fMRI experiment acquires a time series of images while the participant performs cognitive manipulation that causes a change between brain states A and B. The functional map depicts those regions that were more metabolically activated in state A than B, using a statistical test to demonstrate significant signal differences in each voxel.

Where Y is the time course of the fMRI signal from a single voxel while X is the expected hemodynamic response to a task or stimulus. $\bar{X}$ and $\bar{Y}$ denote the means of X and Y. When r = 0 implies no correlation, r = 1 perfect correlation, and r = -1 perfect anti-correlation. Correlation analysis can be used for resting-state fMRI (rs-fMRI), where X and Y are the signals from two different voxels or brain regions, and the higher r-values reflect greater connectivity between pairs of areas and assist in neural network modeling, Figure [3] 3.8.

The General Linear Model GLM

The General Linear Model (GLM) has been classically used for statistical analysis of BOLD fMRI to examine the temporal synchrony between experimental observations and the predicted responses [121]. It makes use of the knowledge of the hemodynamic response function and linear time-invariant assumption to model the observed BOLD signal and at the end yields statistical parametric maps that are used to test for region-specific effects relative to a given hypothesis. Before going into further details about GLM, we define the design matrix X as the temporal effects that can be observed in the fMRI data. The columns in the design matrix consist of the convolution of the HRF by the occurrence of stimuli presentation in the experimental design, as well as confounding variables and filters (i.e. motion, respiratory cycle, cardiac rhythm fluctuations, and low-frequency signals). The relationship between each signal of a voxel

[3] www.mriquestions.com

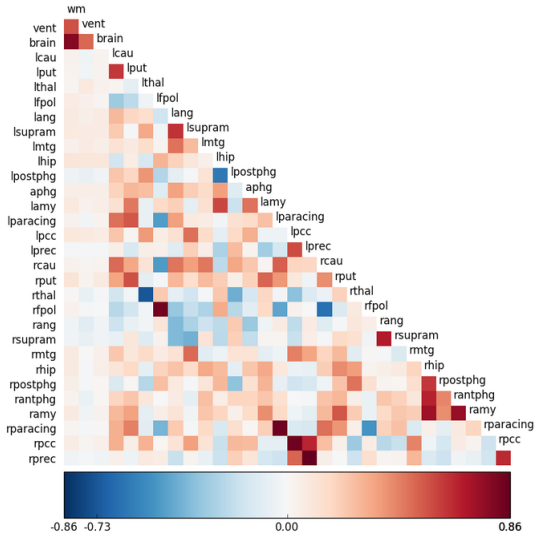

FIGURE 3.8: Correlation graph for pairs of 30 different brain regions in rs-fMRI experiment.

y_i and its predicted response for a stimulus can be written as a linear regression $y_i = x_i\beta + \varepsilon_i$, where β is the calculated slope of the line and ε_i is the calculated error (or residual) distance, and we have actually produced n separate equations, where n is the number of data points acquired for each time interval i. Matrix algebra allows us to condense this set of equations into a more manageable form. We do this by defining Y, X, and ε as column vectors, each containing a list of individual measured or calculated values, Figure 3.9 [122] [123] [119]. The GLM in its basic form can be expressed as:

$$Y = X\beta + \varepsilon \tag{3.3}$$

In short, the GLM is that Y (the fMRI signal measured by a single voxel as a function of time) can be expressed as the sum of one or more experimental design variables X, each multiplied by a weighting factor β, plus random error ε. The aim of any GLM experiment is to provide an estimate of the model parameter β and, most usually, to draw inference about these estimates.

Second Level Analysis

Analysis of fMRI datasets typically consists of a two-level model. The first-level analysis detects the activation of each individual subject for a contrast of interest while second-level analysis localizes common activation among multiple subjects [124]. Multiple subjects are studied to obtain second-level analysis, and common activation among these subjects specify a group map

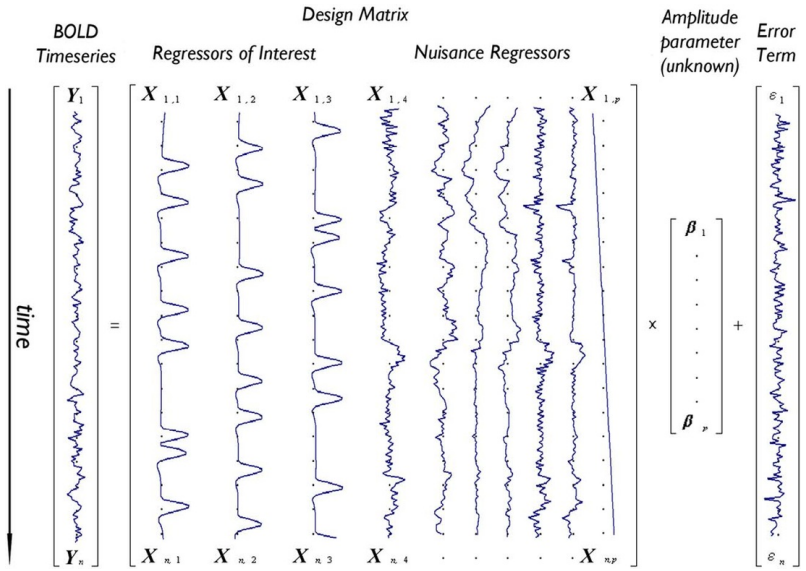

FIGURE 3.9: Depiction of the GLM model for an imaginary voxel with time-series Y predicted by a design matrix X including 10 effects (three regressors of interest – e.g., tasks A, B, C – and seven nuisance regressors – e.g., six motion parameters and one linear drift) of unknown amplitude β_i, and an error term.

[125]. One of the key issues in the second-level analysis is the scope of the inferences that can be validly drawn from aggregate statistics [122].

Hypothesis Testing

In cognitive neuroscience, researchers design experiments to test whether a brain region shows more activity for a particular condition than for others (e.g. it responds to a condition A and not B). When the subject is performing a specified motor or cognitive task or receiving a given sensory stimulus. The image series must then be analyzed in order to detect the voxels which show significant responses to the activation–baseline pattern. In this section, we take the two-condition blocked design (experimental vs. control) and we want to identify voxels actively involved in the imposed task, i.e., voxels whose temporal behaviors differ significantly between the experimental and control conditions. Specifically, we test the research hypothesis H_1: experimental condition $\neq$ control condition, against its null hypothesis H_0: experimental condition $=$ control condition. There are parametric and non-parametric tests. The parametric tests (t-test and F-test) assume a known probability distribution for the distribution parameter that is under consideration. Non-parametric tests (Wilcoxon signed-rank test) do not assume a known form of this probability distribution although they might require some regularity conditions on the distribution such as symmetry.

Let c be the linear combination of the experimental conditions that are of particular interest; it is also called a functional contrast, c is a vector $\in R^K$. For each voxel j, the noise can be

modeled as a Gaussian white noise with zero mean and variance δ_j^2 . Assuming the gaussian noise with variance δ_j^2 and full column rank of X, the best-unbiased estimator of β is :

$$\hat{\beta} = X^+ Y = \beta + X^+ \varepsilon \tag{3.4}$$

where X^+ denotes the moore-Penrose pseudo inverse of X, and $X^+\varepsilon$ is also Gaussian with zero mean. For each voxel $j \in [n]$, the null hypothesis $H_0 : c^T \beta_j = 0$, the difference is due to chance; the alternative hypothesis corresponds to $H_1 : c^T \beta_j \neq 0$. After fitting the GLM, we have:

$$c^T \beta_j = c^T \hat{\beta}_j - c^T X^+ \varepsilon_j \tag{3.5}$$

Then, we can use several statistical test, we often consider:

1. **z-test:**

$$z = \frac{c^T \beta}{\delta \sqrt{c^T (X^T X)^{-1} c}} \tag{3.6}$$

2. **t-test:**
   In general, we do not know the noise variance δ^2 that may vary from voxel to voxel. Therefore, z can not be computed, and we have to estimate it to $\hat{\delta}$. In t-test, assumes that the measured time-series at each voxel consists of a known activation signal in Gaussian white noise [126]. the t-test given as follows :

$$t = \frac{c^T \hat{\beta}}{\hat{\delta} \sqrt{c^T (X^T X)^{-1} c}} \tag{3.7}$$

3. **F-test:**
   F-test is the optimal solution when the measured data are modeled to consist of an unknown activation signal that lies in a known lower-dimensional subspace of the measurement space with added Gaussian white noise [126]. The F-test can be seen as a generalization of the one-sample t-test to several groups, instead of testing that a given contrast is significantly different from zero, we will test that a set of contrasts are all simultaneously different from zero. In this case, the contrast c is a matrix with k columns describing the possible linear combinations to be tested. For example, using a model with four parameters to test whether all of them are equal to 0, $H_0 : \beta_1 = \beta_2 = \beta_3 = \beta_4 = 0$, one would specify

a contrast of the form $c = I$, where I is the identity matrix of size 4×4. For an arbitrary contrast c, the F-test for this test is given by

$$F = \frac{Tr(c\beta\beta^T c^T)}{\delta^2 Tr(c^T(X^T X)^{-1}c)} \tag{3.8}$$

4. **p-value:**
   Colors on fMRI maps represent brain regions or voxels where statistically significant levels of activation or correlation are thought to have occurred. After the calculation of test statistic (t-, F- or z-test) for each voxel or brain region from the fMRI data. Under the null hypothesis (H_0) that no true activation has occurred, a p-value can be determined, representing the probability of observing samples at least as favorable to the alternative hypothesis as the current samples. We can set an arbitrary significance level (e.g. 5% or 1%), which controls the number of false positives, whenever the p-value is less than the arbitrary preselected level of significance, we conclude the measurement is unlikely to have occurred by chance and classify the voxel as activated or correlated, Figure 3.10 [127].

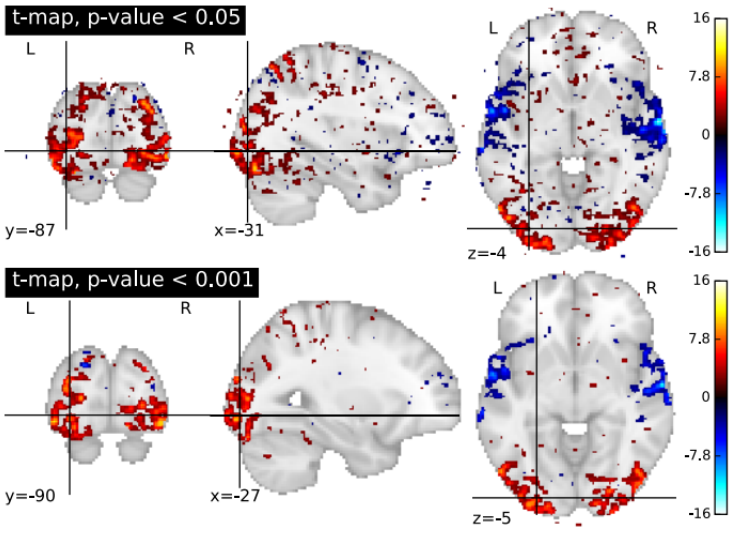

FIGURE 3.10: Visualization of the voxels selected by thresholding the p-values for the visual contrast at different thresholds (0.05 and 0.01).

5. **Wilcoxon signed-rank test:**
   The Wilcoxon signed-rank test can be used to asses whether two population means differ. That is, given the samples $\{x_1,..,x_2\}$ and $\{y_1,..,y_2\}$, we would like to test the following hypothesis $H_0 : \bar{x} = \bar{y}$, $H_1 : \bar{x} \neq \bar{y}$, where $\bar{x}$ and $\bar{y}$ are the samples mean.

Correction for Multiple Comparisons

Applying the previously explained statistical tests independently we get brain maps (statistical parametric maps or SPM), then if we attempt to identify active voxels for example across 100,000 voxels under the significance level $\alpha = 0.05$, ~ 5000 voxels may be falsely classified as active by random chance under the null hypothesis. We have to measure the false positive errors over the whole image and correct these false-positive errors, this problem is referred to as the multiple testing problem and it is a critical issue in fMRI data analysis, several approaches have been proposed, see [128] for a review. Basically, there are two measures of false-positive risk: the family-wise error rate and the false discovery rate.

1. **Family-Wise Error Rate (FWER):**
   FWER is the probability of considering active voxels that are truly inactive. We can apply different corrections of the significance level: Bonferroni correction assumes that all voxels are independent, and corrects the significance level by dividing it by the number of tests performed. This method becomes conservative when there is a strong correlation between tests. Due to the smoothness of fMRI data, Bonferroni is conservative and has little power to detect true effects. Random field theory considers that a smooth statistical map has a lower probability of exceeding a threshold by chance. This threshold is chosen to control the probability of maximum above a given threshold [129]. Resampling methods use the data to obtain empirical null distributions of interest [130]. The most common resampling techniques are permutation tests and bootstrap. They are accurate, but computationally demanding. A comparative review can be found in [131].

2. **False Discovery Rate (FDR):**
   It is the expected proportion of false positives among detected activation [131]. In [132] authors proposed a procedure consists of an adaptive Bonferroni correction that applies a different correction depending on the significance of the voxel.

Inter-subject Analysis

The previous approaches discussed focused on identifying task activation in a single subject. However, an fMRI study typically recruits several or many subjects in order to probe biodiversity and generalize across a population or disease state. Therefore, we need to combine results across subjects to better test the experimental hypothesis. There are a variety of statistical methods for combining results across sessions or subjects, to either create a single result for a group of subjects or to compare different groups of subjects. These methods include fixed-effect analysis and random-effect analysis [119].

The fixed-effect analysis is to combine the time points of all the examined subjects in a single time series and perform single-subject level analysis. The temporal combination of each subject's data can improve the detection power by either increasing the degrees of freedom or reducing intra-subject variations. However, due to this assumption, the result of the fixed-effect analysis is very sensitive to outliers within the recruited subjects (subjects with extreme task responses). Consequently, the conclusions are restricted to the specific subjects scanned within the study, and may not generalize to a larger population.

The random-effect analysis is more commonly applied in fMRI studies nowadays. This analysis assumes that each subject is drawn from a large population of subjects and that his response represents an independent sample from the overall distribution of task effects. The random-effect analysis is performed in two stages. In the first stage, summary statistics regarding task activation from each individual subject is analyzed independently. In the second stage, the distribution of summary statistics derived from the first stage is tested for significance. If intra-subject variations in the first stage are carried up to the second stage, this analysis can also be referred to as mixed-effect analysis [133].

3.3.3 Analysis of Resting State fMRI Data

The resting-state functional magnetic resonance imaging (rs-fMRI) technique has gained advantages over other functional magnetic resonance imaging (fMRI) techniques due to its ease in signal acquisition and does not require subjects to perform a task or respond to stimuli. Subjects merely lie in the scanner for 5-10 minutes with their eyes closed or staring at a fixed point while whole-brain BOLD data is collected [134]. It has permitted the discovery of at least 20 distinct patterns of brain connections called resting-state networks (RSNs), Figure 3.11 [135]. The most important include the default mode network (DMN) which is the most active at rest, involved with introspection and mind-wandering. Also networks for visual and auditory processing, executive control, dorsal attention, and salience (identification of unusual/remarkable events). These networks have provided significant insights into the cognitive organization of the brain in health and disease. In this section, we provide a discussion of rs-fMRI analysis techniques. The approaches of rs-fMRI can be broadly divided into 2 types: functional segregation and functional integration [136] [137].

Functional Segregation Methods for Identifying Neural Networks

Functional segregation divides the brain into regions according to their specific functions and is mainly used for brain mapping [136]. The Amplitude of Low-Frequency Fluctuations (ALFF)

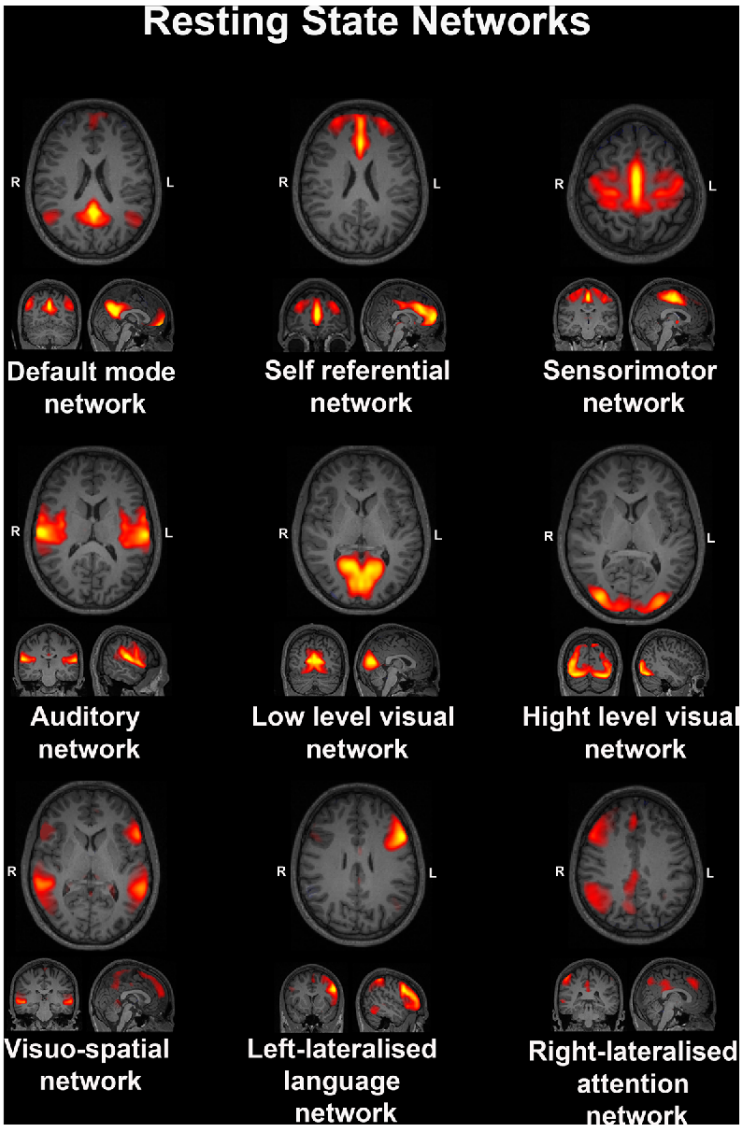

FIGURE 3.11: Some important resting-state networks (RSNs) and their corresponding node regions.

and regional homogeneity (ReHo) are methods commonly used in functional segregation assessments [34].

1. **ALFF Analysis:**
   The Amplitude of low-frequency fluctuation (ALFF) was introduced as a measure the total power within the frequency range between 0.01 and 0.1 Hz and considered as an effective approach to detect the regional intensity of spontaneous fluctuations and to reflect spontaneous brain activity of the brain in the BOLD signal of the rs-fMRI [138] [139], Figure 3.12 [34]. Fractional-ALFF is a variant that measures the power within the low-frequency range (0.01–0.1 Hz) divided by the total power in the entire detectable frequency range and represents the relative contribution of the low-frequency oscillations that can improve the sensitivity and specificity for the detection of spontaneous brain activities by surpassing the physiological noise, especially in perivascular, periventricular

and periaqueductal regions [140]. ALFF has already been applied to patient studies including attention deficit hyperactivity disorder [141] and early Alzheimer's disease [142] and its advantage lies in the simplicity of the analysis without any underlying hypothesis [143].

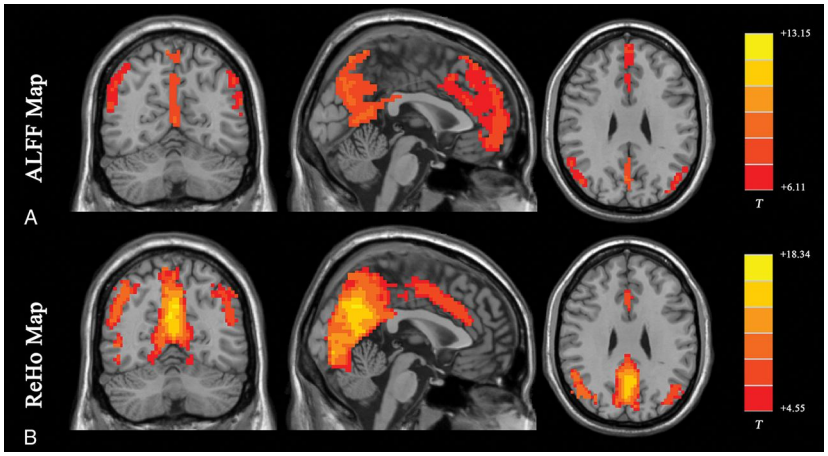

FIGURE 3.12: Results of ALFF and ReHo studies. Both ALFF and ReHo results reflect regional neural activities. ALFF is focused on measuring the strength of the activity, while ReHo is more specific for coherence and centrality of regional activity. T indicates peak intensity.

2. **Regional Homogeneity Analysis:**
   ReHo is a voxel-wise measure of the synchronization of the time-series of a given voxel and its adjacent neighboring voxels, Figure 3.12. This measure is calculated by the Kendall coefficient of concordance of the BOLD time-series [144]. The ReHo algorithm was based on the hypothesis that intrinsic brain activity is manifested by clusters of voxels rather than single voxels [145]. It requires no a priori definition of ROIs and can provide information about the local or regional activity of regions throughout the brain and has been applied to different diseases [146] [147]. ReHo is usually calculated within a low-frequency range, typically between 0.01 Hz and 0.1 Hz. It can be subdivided into different frequency bands. Lower frequency (0.01 – 0.04 Hz) ReHo is more sensitive to cortical activity [148].

Functional Integration Methods for Identifying Neural Networks

Recently, much research has focused on large-scale networks in the brain and investigating their functional significance. They are most commonly extracted by functional connectivity (FC) analyses of fMRI data which measures the degree of synchrony of the BOLD time-series between different brain regions using one of the functional integration Methods. The connectivity may result from a direct anatomical connection or an indirect path through a mediating region, or

may not have a known anatomical correlation [149]. Functional integration is the study of how brain regions work together to process information and affect responses. It is commonly used computational methods include functional connectivity density analysis, seed-based analysis, independent component analysis (ICA), principal component analysis (PCA) and clustering analysis.

1. **Functional Connectivity Density Analysis (FCD):**
   Functional connectivity density (FCD) analysis measures the BOLD time-series correlation between each voxel and all other voxels within the brain and attempts to identify the highly connected functional hubs [150]. The analysis of FCD does not require any model assumptions to be made and it may reveal the importance of functional brain connectivity hubs, but it does not indicate which regions are connected. The voxel with a higher FCD value indicates that it is functionally connected to numerous other brain voxels, and suggests that this voxel plays a more important role in brain information processing than those voxels with lower FCD values. Through functional connectivity density (FCD) mapping of voxels across the whole brain, short-range and long-range FCD can be measured separately, which leads to the measurement of all brain functional information. The short-range FCD may reflect the regional plasticity of functional connectivity around this voxel. The long-range FCD is the product of the global FCD minus [151] [152]. The exploration of abnormal changes in FCD has been widely used in several diseases, including Alzheimer's disease [153], Parkinson's disease [154] and depression [155].

2. **Seed Based Analysis:**
   One of the most common approaches to exploring functional connectivity in the brain is to analyze seed-based functional connectivity (ROI-based functional connectivity). This requires first creating seed regions (seed voxel) of the brain (voxel, cluster or region of interest), then depending on the time series of the seed regions, connectivity is calculated as the correlation of time series for all others voxels in the brain by one of these metrics (eg, the cross-correlation coefficient, partial correlations, multiple regressions, and synchronization likelihood) [156] [157]. Two regions are functionally connected if the time series of their activity is highly correlated, which means that they are likely to communicate and share information. The result of the seed-based functional connectivity analysis can be visualized using a connectivity matrix to show how well its time series correlates between seed regions within the brain. The main disadvantage of seed-based functional connectivity analysis is its dependence on the selection of seed regions, which makes it vulnerable to bias [34]. There is no golden standard method for seed regions selection.

3. **Independent Component Analysis (ICA):**
   ICA is a mathematical technique that maximizes statistical independence between its components, used to identify unknown independent source signals which have been linearly mixed together. For example, ICA methods could be used to extract the voice of singers

and musical instruments from recorded songs without prior knowledge of their sources or locations. For rs-fMRI data, ICA uses multivariate decomposition to separate the BOLD signal into several independent functional networks in the form of spatial maps, which are temporally correlated [158] [159]. These functional networks represent distinct RSNs, Figure [4] 3.13. ICA can be used for task-fMRI in combination with GLM approaches but has found its most common use for rs-fMRI data analysis. Compared with seed-based method, ICA can be performed without any prior assumptions (knowledge of the experimental task or shape of the hemodynamic response function), except the selection of the number of independent components to identify.

The basic of the ICA algorithm is to construct a matrix (Y) such that each column represents a single voxel time course, and each row represents an fMRI signal at a certain time point (observed data) [160]. That is Y is a $T \times N$ matrix where T is the number of time points, and N is the number of voxels, where we assume $T < N$. After some preprocessing to normalize means and variances, Y is decomposed into the product of two matrices (A and S):

$$Y = AS \tag{3.9}$$

Where A is a $T \times T$ matrix of time courses and S is a $T \times N$ matrix of spatial components. A function f (eg, Mutual information, Negentropy and a summary of a finite number of higher-order moments) should be chosen to be an empirical estimate of the statistical dependence between the rows of S. In practice, find the matrix A which minimizes $f(S)$. On an anatomic image, the resulting independent component signals can then be color-coded and overlaid.

4. **Principal Component Analysis (PCA):**
PCA is a technique for individualizing important modes of variation of high-dimensional data in the form of a set of orthogonal directions in space [161]. It is used to extract features and as a technique for data dimension reduction, widely used in the fields of image and signal processing, medical imaging and pattern recognition. PCA works by constructing a sequence of orthogonal linear combinations of the original variables, called the principal components (PC), that have maximum variance. The associated vectors of coefficients of the linear combinations are the PC loadings [162]. The dimensionality of the data is also most often reduced by discarding the principal components with the lowest variance [163]. The number of important principal components that must be preserved can be determined by studying their contribution to the explanation of the total variance or by using a model selection criterion [164] [165]. PCA as a linear statistical technique can not accurately describe non-linear structures, so kernel principal component analysis (KPCA) has been proposed as a non-linear extension of PCA [166].

[4] www.mriquestions.com

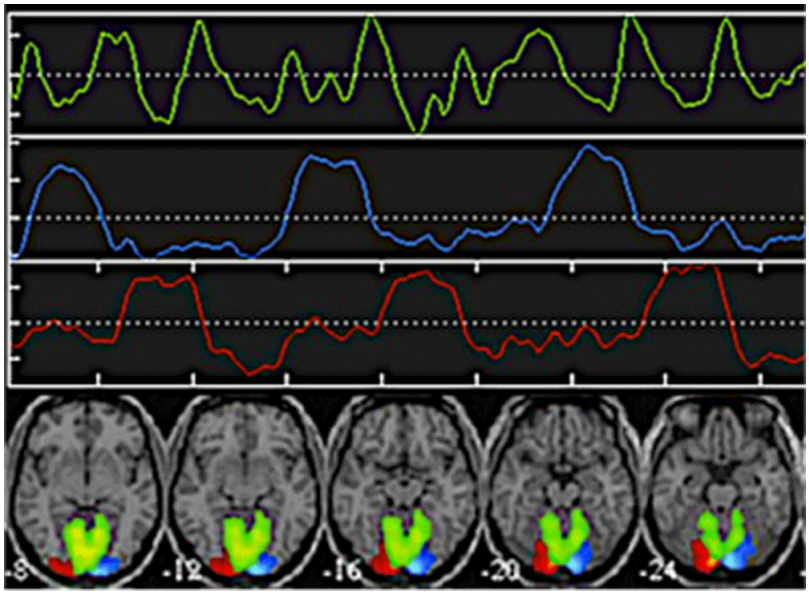

FIGURE 3.13: Spatial ICA separates signals from visual cortex into three components.

5. **Clustering Analysis:**
   Clustering analysis approach aims to parcellate the brain into different clusters on the basis of a collection of relevant features such that similarity within clusters is higher than the similarity between clusters. A distance metric is used to group a set of voxels or ROIs into the same cluster according to the similarity in their BOLD time courses. Obviously, if the cluster number is correctly chosen, voxels belonging to the same functional network will fall within the same cluster. Several approaches have been proposed in the literature for clustering analysis of rs-fMRI data, Figure 3.14 [167]: K-means [168], c-means [169], hierarchical clustering (Ward's clustering) [170] [171], spectral-based clustering [172], and graph-based clustering [173].

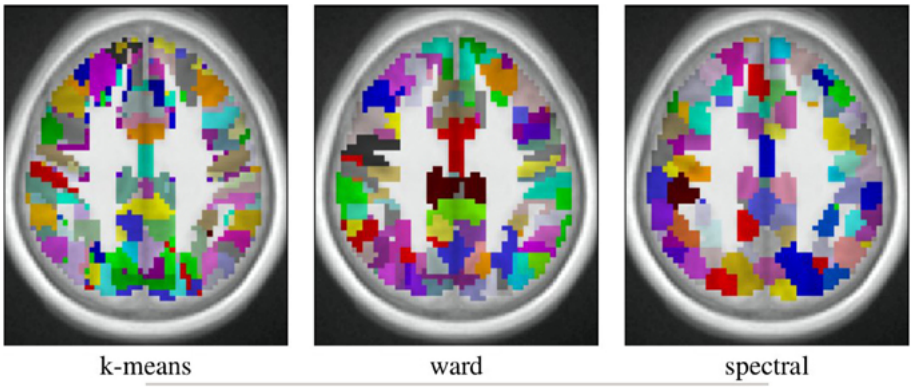

FIGURE 3.14: The result of three clustering algorithms (K-means, Ward, and spectral) that parcel the brain into 500 parcels.

3.3.4 Advanced fMRI Analyses

In this section, we review some advanced fMRI analyses approaches that have been computationally informed in this way.

Graph Analysis

Graph theoretical method has been used in the mathematical representation and study of complex networks such as the brain network, which is based on the description of a pairwise relation between nodes. In neuroimaging and neuroscience, graph theory is applied to establish mathematical models of complex network functions within the human brain. Graph theory provides a theoretic framework to represent the whole brain as a brain network and analyzing its topology [174]. This network has associations and connections between various regions and subregions in the brain and can be defined as a graph G (V, E) [175], where nodes (V) may represent voxels or ROIs. For example, the Automated Anatomical Labeling (AAL) atlas divides the whole brain into 116 distinct brain structures (90 cortical and subcortical regions and 26 cerebellar regions). It has been widely used for neuroanatomic labeling of brain structures in functional imaging [176]. For each region, the representative time course in each region was obtained by averaging the time series across all voxels in the region. Then, the weight of each edge ($e \in E$) in the brain network was computed based on the correlation coefficient between time series from all pairs of regions, Figure 3.14. Here are some of the key topological metrics for graph analysis: (1) Node degree, (2) Characteristic path length, (3) Centrality, (4) Clustering coefficient, (5) Modularity.

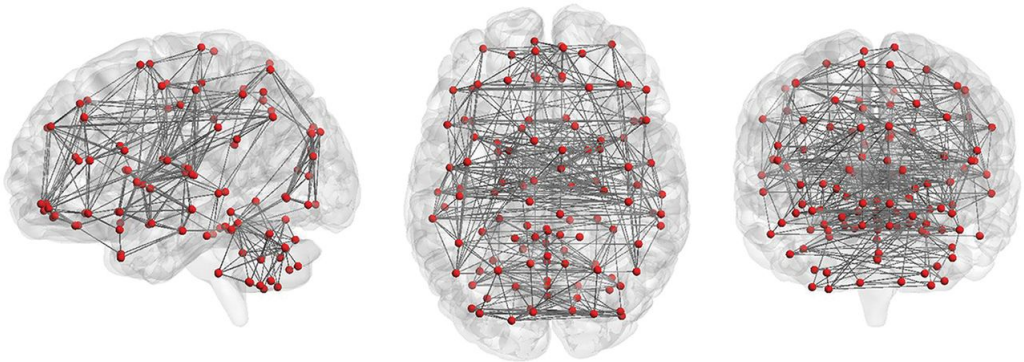

FIGURE 3.15: Representation of the brain as a graph where the regions are obtained on the basis of the anatomical parcellation defined by AAL, there are 116 regions (red dots). The lines represent the functional connections between these regions.

Multivariate Analysis

The most common approaches to analyze fMRI data are approaches that analyze each voxel's time series or region independently (univariate analysis) such as the standard GLM. Unlike univariate approaches, multivoxel pattern analysis (MVPA) considers spatial patterns of activity over ensembles of voxels to evaluate the correlation and recover what information they represent collectively, rather than proceeding on a voxel-by-voxel basis. Figure 3.16 provides a simple explanation of the difference between univariate and multivariate approaches [177]. MVPA has been used in fMRI to extract information from spatially distributed activation patterns, which could go undetected in conventional univariate analysis. Generally, MVPA has two distinct methods. The first method uses classifiers from machine learning to learn a mapping between multi-voxel brain states and cognitive state information. Classifier-based MVPA is the most common method of interpreting internal cognitive states trial-by-trial steps, such as what participant is attending to, thinking about or remembering. The second method examines the similarity structure of multi-voxel patterns and uses information from this similarity structure to draw conclusions about which information is expressed in these patterns [178][179].

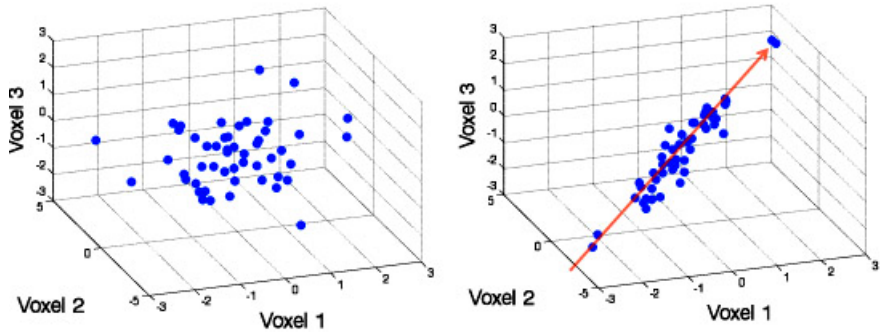

FIGURE 3.16: This simple figure describes the difference between univariate and multivariate analytic strategies: a hypothetical 3-dimensional data set is displayed in this illustration. On the left side, there is no correlation between the 3 variables plotted. On the right side in contrast, one can see a major source of variance indicating a positive correlation between all three voxels. A univariate analysis that just considered mean values on a voxel-by-voxel basis could not tell any difference between these two scenarios. Multivariate analysis, in contrast, identifies the major sources of variance in the data (red arrow) before proceeding to construct neural activation patterns form these sources.

Real-Time Analysis

In the standard fMRI analysis approach, fMRI data are collected first after the experiment then preprocessed and analyzed offline over hours, days, weeks or months. Recent progress

in computer hardware and software makes it possible to perform an analysis of fMRI data and to access results while the subject is inside the scanner, which has led to an interest in the real-time analysis of fMRI data. Real-time fMRI analysis involves the online measurement of a subject's neural activity, indirectly, through the measurement of the BOLD signal. It is performed by reading, analyzing and visualizing the hemodynamic brain signals in real-time during a continuous experiment [180]. One of the most common uses is to try to influence the participant through feedback on their brain activity (neurofeedback). Neurofeedback is a type of biofeedback in which neural activity is measured, and a visual, an auditory or another representation of this activity is presented to the participant in real-time to train him to increase or decrease activity in a region of the brain underlying some cognitive process or disorder, Figure [5] 3.17 [181]. Neurofeedback experiments showing that humans could self-control electroencephalographic signals in real-time [182]. Such findings led to the development of the field of brain-machine interfaces, also known as brain-computer interfaces [183], in which individuals aim to control external devices directly instead of neural substrates.

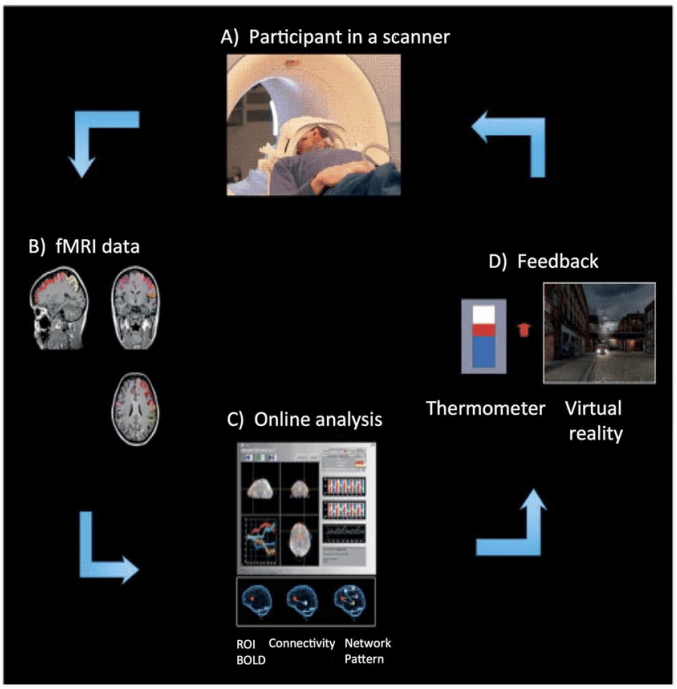

FIGURE 3.17: Overview of a real-time fMRI based neurofeedback system that comprises the following subsystems. (A) Participant in the MRI scanner. (B) Signal acquisition (fMRI data). (C) Online analysis and computation of the neurofeedback based on the BOLD response. (D) Visual feedback via the scanner projection system.

[5]The real-time fMRI system presented in this figure was developed at the Institute of Medical Psychology and Behavioral Neurobiology, University of Tübingen, Germany.

Model-Based Analysis

In model-based fMRI analysis, a model describing the hypothesized cognitive processes underlying the behavior concerned is generated. After that, the information coming from that model which simulates the process of interest is compared with fMRI data, showing which brain areas show activation patterns that are consistent with the process of interest [184]. Typically, the generated model has one or more parameters. These parameters must be adjusted to fully define the model, which is generally achieved by fitting them to the observed behavior [185]. Models for adjusting these parameters (e.g, reinforcement learning, decision theory, Bayesian inference and game theory) have seen increasing use as tools to develop precise hypotheses about the underlying computations [178]. This approach has proved to be very successful in fMRI analysis and allows researchers to go beyond localizing model variables in the brain. When their localize is known, these signals can be interpreted in later experiments and used to estimate parameters independently of behavior.

3.4 Functional Connectivity Analysis

The human brain is a complex network of a large number of different brain regions that each have their own task and function, but are functionally and structurally interconnected regions. Brain function is not only the result of activity in different specialized and isolated brain regions but also the result of interactions between brain regions [186]. Interactions between brain regions are likely to play a key role in complex cognitive processes, making the examination of functional connectivity in the human brain very important and providing important new information on the core organization of the human brain. Functional connectivity (FC) is defined as the temporal correlation between the time series of different brain regions, reflecting the level of functional communication between regions. More generally, functional connectivity between two given regions is considered in terms of the temporal coherence or correlation between the oscillatory firing rate of neuronal assemblies [187]. Analysis of functional connectivity can be carried out at the level of the individual voxels or at the level of regions of interest (ROIs). Methods for functional connectivity analysis are always based on some measure related to the correlation between two or more fMRI time series. The results of functional connectivity are usually represented by a matrix called the connectivity matrix, which is typically estimated using the correlation between time series, where each cell in the connectivity matrix contains a correlation coefficient that crosses the correlation between two regions of the brain, Figure 3.18. Functional connectivity studies have been extensively applied to analyze the pathophysiology of neurodegenerative disorders [188], such as Alzheimer's Disease [189], Parkinson's disease [190], Dementia [191], Schizophrenia [192], and Autism [193].

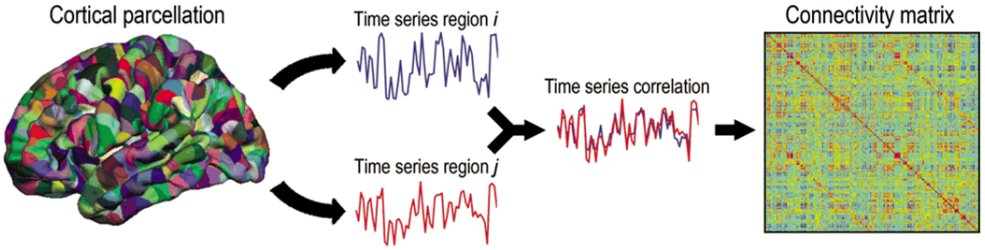

FIGURE 3.18: Construction of the functional connectivity matrix by the correlation between time series was extracted from brain regions [1].

3.5 Classification and Prediction in fMRI Analysis

Brain functional imaging data, especially fMRI data, have been using to reflect functional integration of the brain by detecting changes associated with blood flow. Cerebral blood flow and neuronal activation were coupled and when an area of the brain was in use, blood flow to that region increases. The identification of the active regions allowed us to understand how the healthy brain functions, and in an increasing number of studies, it was applied to understand which brain function was affected by a particular disease [194]. In the last few years, there has been growing interest in the use of machine learning and deep learning for analyzing fMRI data in order to classify or predict diseases, behaviors, diagnosis of cognitive disorders and mapping of functional brain regions [195] [196] [197]. A growing number of studies have shown that both machine learning and deep learning can be used to extract exciting new information from neuroimaging data [198].

FMRI data analysis is highly interdisciplinary, majorly influenced by fields such as machine learning, signal processing, and theory of graphs. Machine learning approaches provide a rich characterization of fMRI data, often in a data-driven manner. It is widely used neuroimaging studies, the study of functional connectivity with rs-fMRI is a major focus in this area which has been applied in many fields, Figure 3.19 [199]. Deep learning approaches are successful when there are large amounts of data available for training. Under controlled conditions, most typical studies of neuroimaging have collected data from only tens to hundreds of subjects to identify slight differences between different states, for example in [196], the authors proposed a deep neural network to analyze t-fMRI, Figure 3.20.

There are many different classifiers that have been used for prediction, whether linear or non-linear, sparse or non-sparse, require or do not require prior selection of features (supervised learning or unsupervised learning). Supervised learning methods in fMRI focus on classifying patients versus controls, or predicting diseases and guiding treatments, on the other hand, unsupervised learning methods are mainly focused on understanding the functional organization of the healthy brain and its dynamics. A taxonomy of supervised learning and unsupervised learning methods used for rs-fMRI analysis was listed by [199] as shown in Figure 3.21. For deep learning

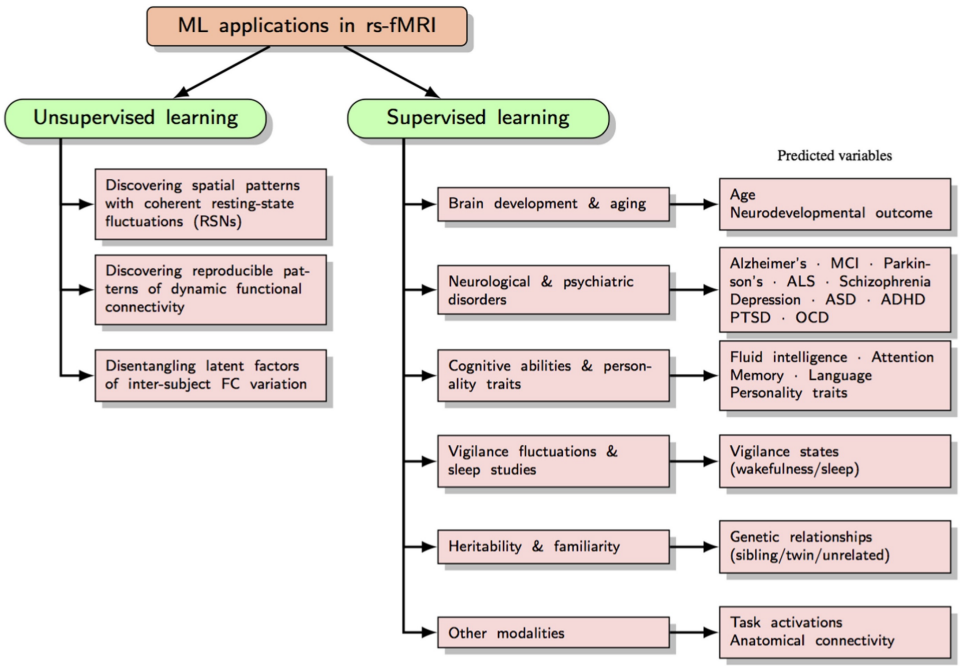

FIGURE 3.19: Applications of machine learning methods in rs-fMRI.

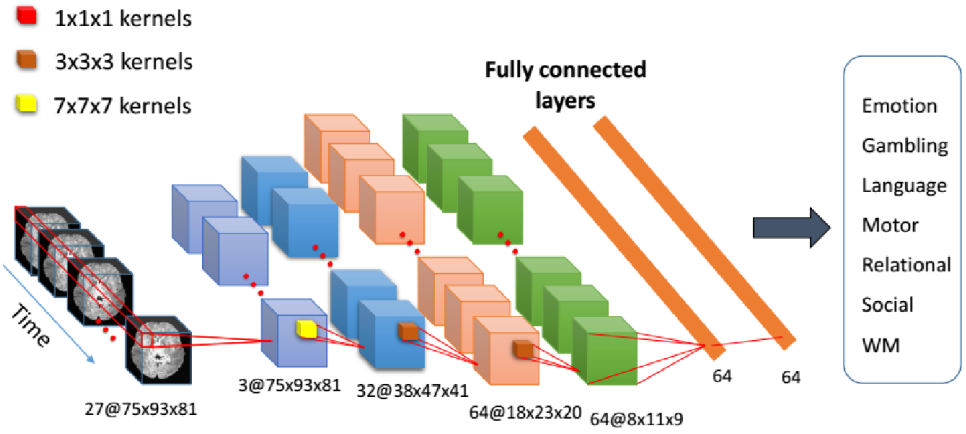

FIGURE 3.20: A proposed deep neural network for analyzing t-fMRI where the model t-fMRI scans as input and provides labeled task classes as output.

methods that have been widely used in the study of neuroscience, a brief overview of deep learning methods to process fMRI data can be found in [197].

Feature selection is the process of reducing the number of input variables, removing noisy, redundant or irrelevant features that contribute most to your prediction variable or output that interests you. Having irrelevant features in your data can decrease the accuracy of the models and make your model learn based on irrelevant features. Methods of feature selection in t-fMRI are generally not suited for rs-fMRI, for this reason, we must choose the appropriate method according to the type of fMRI and the purpose of the process.

Functional connectivity is the most common feature representation of rs-fMRI analysis. It is assumed to be stationary over the scanning time (usually several minutes), and static

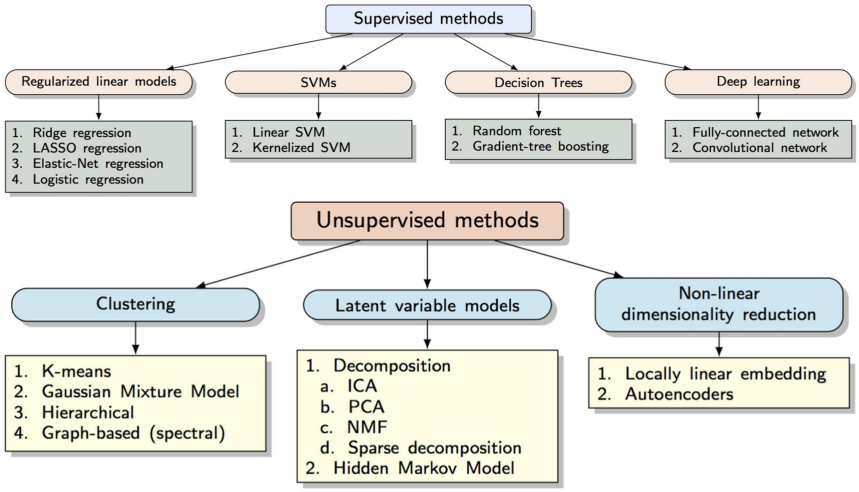

FIGURE 3.21: A taxonomy of supervised learning and unsupervised learning methods used for rs-fMRI analysis.

functional connectivity approaches were used in most previous fMRI studies. Until recently, researches have shown that brain functional connectivity as dynamic over time can be effective in uncovering disorders of normal human brain disease [200]. The main functional connectivity analysis methods and possible connectivity features used for classification/prediction problems were summarized in Figure 3.22 [198]. Figure 3.23 shows a general illustration of the pipeline used in rs-fMRI functional connectivity-based predictive models [201].

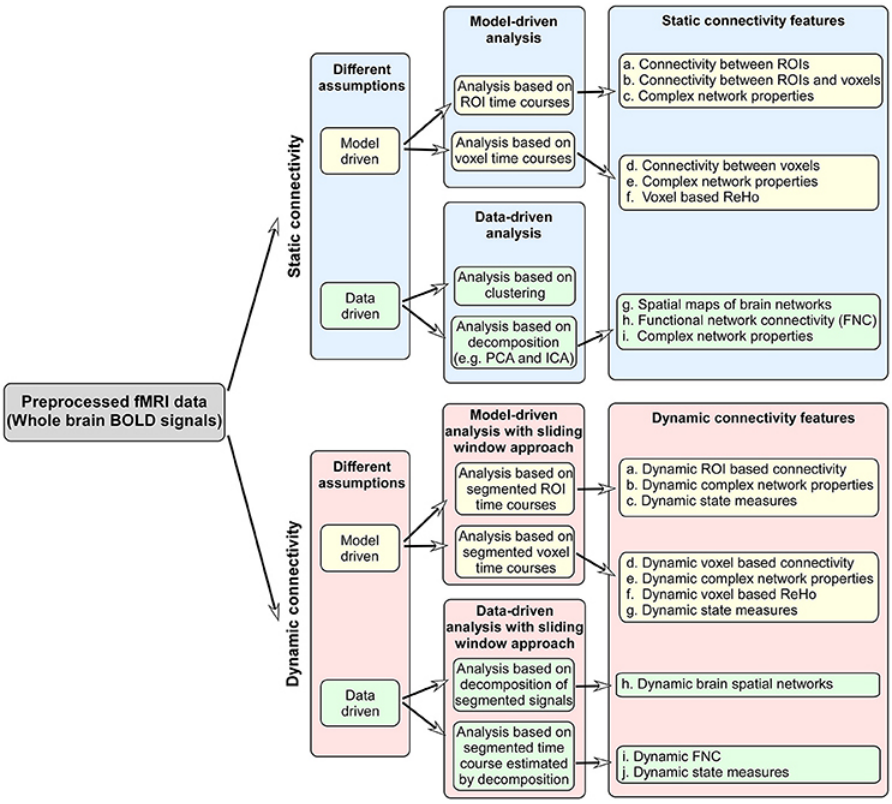

FIGURE 3.22: The key methods for functional connectivity analysis and possible connectivity features used for classification/prediction problems.

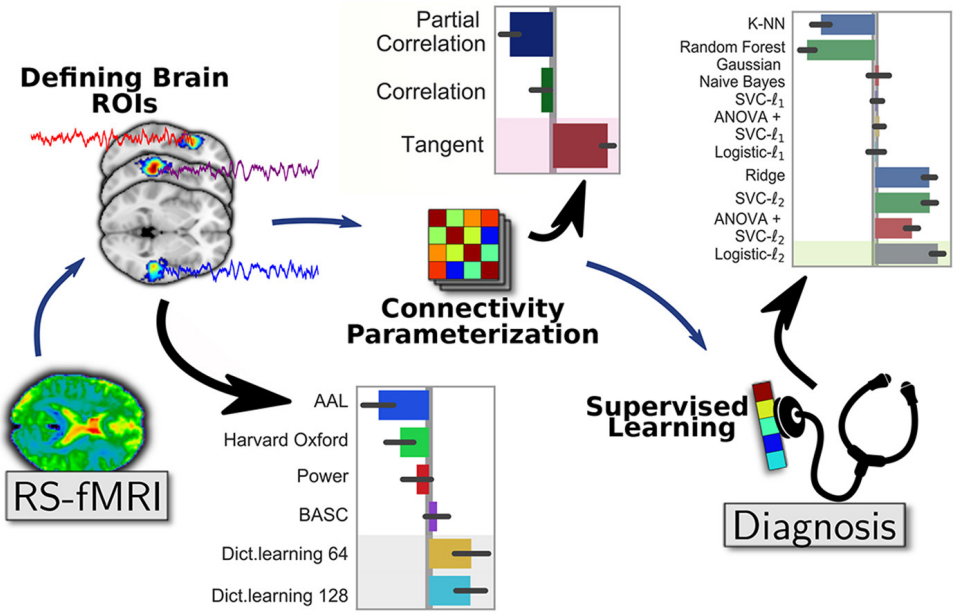

FIGURE 3.23: A general pipeline for rs-fMRI functional connectivity-based prediction with three main steps: 1) Definition of brain regions (ROIs) from rest-fMRI images or using already defined reference atlases, 2) building the functional connectivity matrix from time-series signals extracted from these ROIs for every subject and 3) comparisons of functional connectivity matrices across subjects using machine learning algorithms.

3.6 Conclusion

In recent years, functional magnetic resonance imaging (fMRI) has become a hot topic within the fields of neuroscience and neuroimaging, as its spatial resolution makes it suitable to study the functional structure of the brain, map different sensor, motor and cognitive functions to specific regions in the brain. To get information from the brain by fMRI, researchers design experiments to test whether or not there is a difference in a hypothesized brain region. Usually, this consists of fitting a model followed by statistical inference. In this chapter, we have reviewed the essential steps for working on fMRI. Where we presented the preprocessing steps to prepare the data for the analysis step, then the main statistical analysis methods for both t-fMRI and rs-fMRI, we then presented a complete overview of the current state of the art of advanced methods of fMRI analysis, functional connectivity analysis and machine learning in fMRI analysis. The different methods of analysis are complementary and the application of several methods to the same dataset may produce better results compared to the application of a single method alone.

Chapter 4

Graph Matching for Brain MRI and fMRI Analysis

4.1 Introduction

Graphs are a powerful and universal tool widely used in information processing. Numerous methods for graph analysis have been developed. In particular, graph representations are extremely useful in image processing and understanding. In this chapter, we provide an overview of graph matching, we focused on three main components. Firstly, an introduction to graph theory, we mainly concentrate on the fundamental concepts. Secondly, an overview of graph matching and the most important methods used. Thirdly, we provide some methods based on graph matching techniques that may be successfully applied to neuroimaging data for understanding the brain structure or its structural and functional connectivity.

4.2 Graph Theory Basics

Graph theory is originated with the problem of Königsberg Bridge, in 1735. This problem leads to the Eulerian Graph concept. Euler studied the problem of Königsberg Bridge and established a structure to resolve the problem called the Eulerian graph. The paper written by Leonhard Euler on Königsberg's Seven Bridges, and published in 1736, is considered to be the first paper in graph theory history. The field has exploded since Euler resolved this very first problem in Graph Theory, becoming one of the most important areas of applied mathematics we are currently studying. Graph Theory is generally a branch of Combinatorics but is closely related to Applied Mathematics, Optimization Theory, and Computer Science. In this section, we will discuss some basic definitions of graph theory.

Graph: a graph (G) is a mathematical abstraction that is useful for solving many kinds of problems. Fundamentally, a graph consists of a set of vertices (V), and a set of edges or links (E), where an edge is something that connects two vertices (u,v $\in$ V) in the graph. Therefore G =(V,E). $|V|$ and $|E|$ are the number of vertices and edges of the graph respectively.

We call a graph G an undirected graph when edges have no orientation. The edge (u,v) is identical to the edge (v,u), i.e., they are not ordered pairs. In directed graphs, elements of E are ordered pairs, means (u,v) distinct from (v,u). Directed edges are called arcs. Directed graphs often called digraphs.

For a graph G=(V, E), we have the following terminologies[1] [202]:

1. Edges that have the same end vertices are parallel.
2. An edge of the form (v,v) is a loop.
3. A graph is simple if it has no parallel edges or loops.
4. A graph with no edges (i.e. E is empty) is empty.
5. A graph with no vertices (i.e. V and E are empty) is a null graph.
6. A graph with only one vertex is trivial.
7. Edges are adjacent if they share a common end vertex.
8. Two vertices u and v are adjacent if they are connected by an edge, in other words, (u,v) is an edge.
9. The degree of the vertex v, written as d(v), is the number of edges with v as an end vertex. By convention, we count a loop twice and parallel edges contribute separately.
10. A pendant vertex is a vertex whose degree is 1.
11. An edge that has a pendant vertex as an end vertex is a pendant edge.
12. An isolated vertex is a vertex whose degree is 0.
13. **Connected graph and Disconnected Graph:** A graph G =(V, E) is said to be connected if there exists at least one path between every pair of vertices in G. Otherwise, G is disconnected.
14. **Regular graph:** In a graph if all vertices have same degree (incident edges) k than it is called a regular graph.

[1] GRAPH THEORY: by Keijo Ruohonen

15. **Complete graph:** A simple graph G =(V, E) with n mutually adjacent vertices is called a complete graph G and it is denoted by K_n or a simple graph G =(V, E) in which every vertex in mutually adjacent to all other vertices is called a complete graph G.

16. **Cycle graph:** A simple graph G =(V, E) with n vertices ($n \geq 3$) called a cycle graph where vertices connected in a closed chain.

17. **Wheel graph:** A wheel graph G =(V, E) with n vertices ($n \geq 4$), is a simple graph which can be obtained from the cycle graph C_{n-1} by adding a new vertex (as a hub), which is adjacent to all vertices of C_{n-1}.

18. **Cyclic and acyclic graph:** A graph G =(V, E) has at least one Cycle is called cyclic graph and a graph has no cycle is called Acyclic graph.

19. **Bipartite graph:** A simple graph G =(V, E) is Bipartite if we may partition its vertex set V to disjoining sets U and V such that there are no edges between U and V. We say that (U, V) is a Bipartition of G.

20. **Complete bipartite graph:** A bipartite graph G =(V, E) with vertex partition U, V is known as a complete bipartite graph if every vertex in U is adjacent to every vertex in V.

21. **Weighted Graph:** A weighted graph is a graph where its vertices, edges or both are given a numerical weight.

22. **Path:** A path is a simple graph whose vertices can be ordered so that two vertices are adjacent if and only if they are consecutive in the list.

23. **Simple path:** Simple path is a path in which all the vertices are distinct.

24. **Tree**: An undirected connected graph T is called tree if there are no cycles in it. There is exactly one simple path between any vertices u and v.

25. **Vertex coloring:** An assignment of colors to the vertices of a graph G so that no two adjacent vertices of G have the same color is called vertex coloring of a graph G.

26. **Eulerian Path, Eulerian cycle, and Euler graph:** An Eulerian path is a path in a graph that visits every edge exactly once. An Eulerian cycle is an Eulerian path that starts and ends on the same vertex. An Eulerian graph is a graph containing an Eulerian cycle that contains all edge of the graph. i.e if we can draw the graph on a plain paper without repeating any edge or letting the pen.

27. **Hamiltonian path, hamiltonian cycle, and Hamiltonian graph:** A Hamiltonian path is a path that visits each vertex of the graph exactly once. A hamiltonian cycle is a cycle that visits each vertex exactly once. A graph called Hamiltonian graph if there exists a Hamiltonian cycle which contains all vertices of the graph.

4.2.1 Graph Representations

Graph representation is a technique used to store graphs in a computer memory. To represent a graph, we just need a set of vertices, and for each vertex, the neighbors of the vertex. If the graph is weighted, the weight will be assigned to each edge. There are different ways to optimally represent a graph, depending on the density of its edges, type of operations to be performed and ease of use.

Adjacency Matrix

Adjacency Matrix A is a binary matrix of size $V \times V$ where V is the number of vertices in a graph. If there is an edge from a vertex i to vertex j, then the corresponding element of A, $a_{ij} = 1$, otherwise $a_{ij} = 0$, Figure 4.1. If there is a weighted graph then instead of 1s and 0s, we can store the weight of the edge.

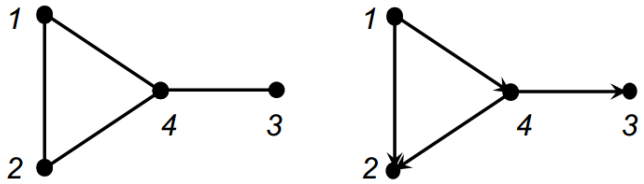

$$\mathbf{A}_u = \begin{pmatrix} 0 & 1 & 0 & 1 \\ 1 & 0 & 0 & 1 \\ 0 & 0 & 0 & 1 \\ 1 & 1 & 1 & 0 \end{pmatrix}, \quad \mathbf{A}_d = \begin{pmatrix} 0 & 1 & 0 & 1 \\ 0 & 0 & 0 & 0 \\ 0 & 0 & 0 & 0 \\ 0 & 1 & 1 & 0 \end{pmatrix}$$

FIGURE 4.1: Adjacency matrix example. left: Undirected graph. Right: Directed graph.

Incidence Matrix

Incidence matrix B is a matrix of size $|V| \times |E|$. For undirected graphs, the entries of B are: $b_{ij} = 1$, if vertex i incident to edge j otherwise 0. For directed graphs: $b_{ij} = 1$, if edge j is (k, i). $b_{ij} = -1$, if edge j is (i,k) otherwise 0, Figure 4.2.

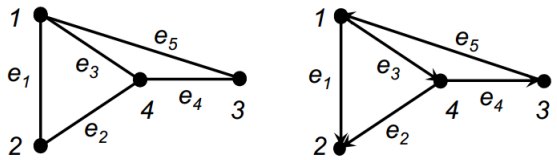

$$\mathbf{B}_u = \begin{pmatrix} 1 & 0 & 1 & 0 & 1 \\ 1 & 1 & 0 & 0 & 0 \\ 0 & 0 & 0 & 1 & 1 \\ 0 & 1 & 1 & 1 & 0 \end{pmatrix}, \quad \mathbf{B}_d = \begin{pmatrix} -1 & 0 & -1 & 0 & 1 \\ 1 & 1 & 0 & 0 & 0 \\ 0 & 0 & 0 & 1 & -1 \\ 0 & -1 & 1 & -1 & 0 \end{pmatrix}$$

FIGURE 4.2: Examples of incidence matrix for undirected graphs and directed graphs.

Adjacency List

Adjacency list is an array of size $|V|$ where for each vertex in the graph, we maintain the list of its neighbors. It means, every vertex of the graph contains a list of its adjacent vertices (The i-th array element is a list of the vertices adjacent to i), Figure 4.3. Similarly, an edge list stores the vertex pairs incident to each edge.

$$\begin{aligned} L_a[1] &= \{2,4\} \\ L_a[2] &= \{1,4\} \\ L_a[3] &= \{4\} \\ L_a[4] &= \{1,2,3\} \end{aligned}$$

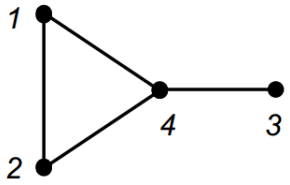

FIGURE 4.3: Example of an adjacency list.

4.3 Graph Matching

Graph matching is the process of finding a correspondence between the nodes and the edges of two or more graphs that satisfies some (more or less stringent) constraints ensuring that similar substructures in one graph are mapped to similar substructures in the others. In realistic applications, the matching is done by comparing the model graph which is stored in a file and an input graph that is given at the run time. Computing the similarity of two graphs is typically exponential in the number of nodes of the two graphs involved. In this section, we will present an overview of the algorithms that have been proposed and used for the graph matching problem.

4.3.1 Problem Statement

We can state the graph matching problem as follows: Given two graphs $G1 = (V_1, E_1)$ and $G2 = (V_2, E_2)$, generally, the task of correspondence matching is to find a mapping $f : V_1 \longrightarrow V_2$ such that $(u, v) \in E_1$ iff $(f(u), f(v)) \in E_2$. When such a mapping f exists and $|V1| = |V2|$, this is called an isomorphism, and G_2 is said to be isomorphic to G_1. This type of problems is said to be the exact graph matching. When the number of vertices is different in both the two graphs $|V1| \neq |V2|$, this means that it is not possible to find an isomorphism between the two graphs to be matched, so this type of problems is said to be the inexact graph matching.

Graph matching computations can be broadly classified into two groups. In the first group of methods, the outcome of the computation is a single similarity score between two graphs G_1 and G_2, typically normalized in the range $[0, 1]$. This similarity score indicates how similar two graphs G_1 and G_2 are in their entirety. In this group, the methods are based on the principle that two graphs are similar if they share many vertices and/or edges. In nodes ranking, the similarity of two graphs is based on the similarity of the ranking of their nodes, as quantified by a rank correlation method. In the second group of methods, the outcome of the computations is a set of numbers x_{ij}, representing the similarity of each vertex i in the first graph to every vertex j in the second graph. This notion of node wise similarity can be extended to edge-wise similarity, or to similarity of small subgraphs in the two graphs. This second class of methods reflects a finer-grained notion of graph similarity. Also, we have divided the matching methods into two broad categories: the first contains exact matching methods that require a strict correspondence among the two graphs being matched or at least among their subparts. The second category defines inexact matching methods, where a matching can occur even if the two graphs being compared are structurally different to some extent.

4.3.2 Exact Graph Matching

In exact graph matching, the objective is to determine the mapping between the nodes of two graphs must be edge-preserving in the sense that if two nodes in the first graph are linked by an edge, they are mapped to two nodes in the second graph that is linked by an edge as well, the mapping must be bijective [203]. That is, a one-to-one correspondence must be found between each node of the first graph and each node of the second graph. The identical between the two graphs in terms of nodes and edges leads to the graph isomorphism problem. Two graphs, $G1$ and $G2$, are isomorphic if there is a one-to-one correspondence between the vertices of $G1$ and those of $G2$ with the property that the number of edges joining any two vertices of $G1$ is equal to the number of edges joining the corresponding vertices of $G2$, Figure 4.4.

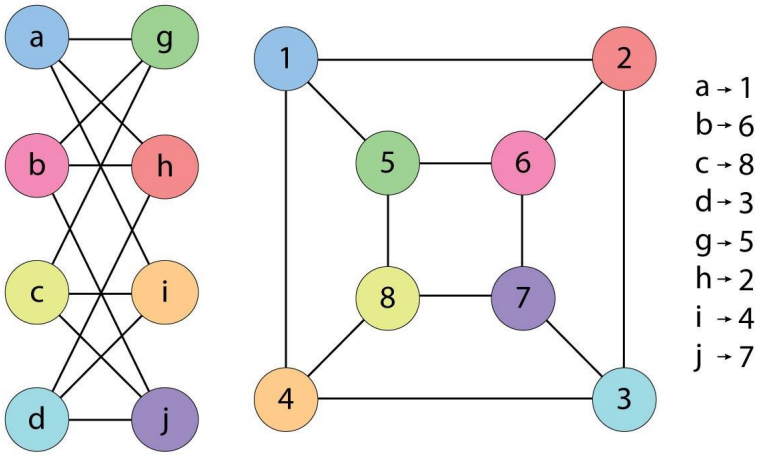

FIGURE 4.4: Example of isomorphic graphs.

The graph isomorphism problem is of considerable practical importance and also of theoretical interest because it lies in the complexity class NP, but it is not known whether it lies in P or NP-complete. See [204] for more details. Checking whether two Graphs are isomorphic or not is an old and interesting computational problem. The simplest, but the inefficient approach for checking two graphs $G1$ and $G2$, each with vertices v is making all the permutation of the nodes and see if it is edge-preserving bijection or not. Obviously, this solution takes $O(v^2v!)$ time, where v is the number of vertices of the graph. Even for smaller values of v the problem becomes intractable because of this enormous time complexity.

The graph isomorphism problem for a general case is a hard problem, many works have been done for special families of graphs or by imposing certain restrictions on the underlying graphs where it is possible to derive algorithms of polynomial-time complexity. Polynomial-time algorithms were found for trees in [205] [206], low-order polynomial-time methods [207] [208], polynomially bounded method for the isomorphism detection of graphs with bounded valence [209], planar graphs [208], graphs with bounded genus [210], graphs with bounded eigenvalue multiplicity [211], graphs with bounded degree [209], graphs with bounded color class size [212], permutation graphs [213], quadratic-time algorithms [214].

An extended method of graph isomorphism is the subgraph isomorphism where we have to detect if a smaller graph is present in a larger graph. A subgraph isomorphism from $G1$ to $G2$ exists if there exists a subgraph $G \subseteq G2$ such that there is a graph isomorphism between $G1$ and G. Subgraph isomorphism can also be determined by the graph isomorphism method mentioned above. Subgraph isomorphism is considered to belong to the class of NP-complete problems.

4.3.3 Inexact Graph Matching

In graph representations of real-world problems, it is often the case that graphs from the same class differ due to several causes: Intrinsic pattern variability, noise in the acquisition phase, the existence of non-deterministic elements in the processing steps leading to the graph representation, are among the possible reasons for having actual graphs that differ somewhat from their ideal models. Hence, the graph matching process needs to take structural errors into account and must be tolerant. It must accommodate the differences by relaxing, to some extent, the constraints that define the matching type. Even when no deformation is expected, this can be useful. Several methods of achieving this goal will be discussed in this section.

Graph Edit Distance

Graph edit distance (GED) is one of the most flexible graph matching approaches since it can compare any kind of labeled graph given an appropriate cost function. It is defined as the minimum cost of an edit path transforming one graph into another, where an edit path is a sequence of edit operations. Generally, these edit operations are substitutions, deletions, and insertions of nodes and edges [215]. A cost function assigns a cost to each of these edit operations, Figure 4.5.

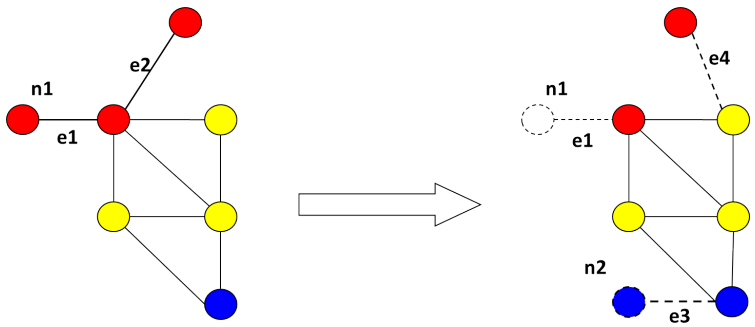

FIGURE 4.5: Graph edit distance example. Transforming graph $G1$ (right) into graph $G2$ (left) where: 1- delete edge $e1$ delete node $n1$. 2- delete edge $e2$ insert edge $e4$. 3- insert node $n2$ insert edge $e3$. We suppose that the cost of edit operations: Deletion and insertion of both edges and nodes = 1. Substitution of both edges and nodes = 0. We have 6 operations so the cost of $GED(G_1, G_2) = 6$.

The problem of measuring the dissimilarity of two graphs is then equivalent to the problem of finding the edit path that models the structural difference of two graphs in the least costly way. Consequently, the graph edit distance of two graphs is defined by the minimum cost edit

path from the first to the second graph. Given two graphs $G1$ and $G2$, let c(f) denote the cost of edit path f. The edit distance of $G1$ and $G2$ can be defined by

$$GED(G_1, G_2) = min_{all\ edit\ paths\ f\ from\ G_1\ to\ G_2}\ c(f) \tag{4.1}$$

If the two graphs under consideration are very similar, it can be assumed that only minor edit operations are required to transform the first into the second graph, which results in a low-cost optimal edit path. In this case, the resulting edit distance will be small. Conversely, if the two graphs differ significantly, every edit path will necessarily include strong modifications and hence result in high costs [216].

Graphs are flexible and can be large and complex, in the case of modeling complex patterns and objects, the exact computing of GED becomes difficult and intractable in practice due to its exponential time complexity. Computing graph edit distance is known to be an NP-hard problem [217], research has mainly focused on heuristics. In the literature, both exact and heuristics methods can be found. In the exact methods, the GED problem was addressed by exact methods based on mathematical programming, and more specifically by Mixed Integer Linear Program formulations. In [218], the authors have proposed two Mixed Integer Linear Program formulations (F1 and F2) to solve the GED problem. F1 simply minimizes the cost of assigning the vertices plus the cost of assigning the edges. F2 is a reformulation of F1 with a reduced number of variables and constraints, another method that ignored the attributes of edges in [219]. Regarding heuristics methods, researchers have designed fast heuristics to solve the problem and provide good quality solutions. Methods proposed were particularly triggered by the algorithms of the bipartite graph edit distance that present in [220] and [217]. The main advantage of these algorithms is that it is fast and can solve large and hard instances in a short amount of time. The problem turned into the linear sum assignment problem with error correction (LSAPE), by computing a special cost assignment matrix for the vertices sets of the two graphs. In [221], the authors proposed an innovative approach to deal with the GED problem. It introduces a new heuristic called Local Branching (LocBra), which is an adapted version of the general local branching metaheuristic originally proposed by [222]. Two other heuristics Integer Projected Fixed Point (IPFP) and Graduate Non-Convexity and Concavity Procedure (GNCCP) have proposed by [223]. Both are adapted to operate over a Quadratic Assignment Problem that models the GED problem. The heuristics aim at approximating the quadratic objective function to compute a solution and then improve it by applying projection methods.

Graph Distance Based on mcs and MCS

A common subgraph of G_1 and G_2, $cs(G_1, G2)$, is a graph G, such that there exist subgraph isomorphisms from G to G_1 and from G to G_2. We call G a maximum common subgraph of

G_1 and G_2, $mcs(G_1,G_2)$, if there exists no other common subgraph of G_1 and G_2 that has more nodes than G. A maximum common subgraph of two graphs represents the maximal part of both graphs that is identical. Note that, in general, the maximum common subgraph is not uniquely defined, that is, there may be more than one common subgraph with a maximal number of nodes.

A popular metric for the similarity of two graphs is the size of their mcs, which is most frequently defined as the largest graph isomorphic to some induced subgraph in each of them. Detection of the maximum common subgraph of two given graphs is a well-known problem and it is NP-complete problems. A significant number of mcs detection algorithms have been proposed in the literature, but still are not clear how the behavior of these algorithms varies as the type and the size of the graphs to be matched changes from an application to another. Clique-based methods are the most widely used in the literature. These depend on finding a maximum clique in the association graph [224] [225]. Intuitively speaking, the larger a maximum common subgraph of two graphs is, the more similar are the two graphs. This observation leads to graph dissimilarity measures that are able to cope with structural errors. In [226], the authors have introduced such a distance measure:

$$d_{mcs}(G_1,G_2) = 1 - \frac{|mcs(G_1,G_2)|}{max\{|G_1|,|G_2|\}} \tag{4.2}$$

As shown, d_{mcs} produces a value in $[0,1]$. Also, as we mentioned earlier, the mcs of two graphs is not uniquely defined, which means the d_{mcs} distance too. If two graphs are isomorphic, their d_{mcs} distance is 0; if two graphs have no part in common, their d_{mcs} distance is 1.

A second distance measure which has been proposed in [227], based on the idea of graph union, where we dived the size of mcs by the size of the union of the two graphs minus the size of mcs. This distance measure behaves similarly to d_{mcs}. The motivation of using graph union in the denominator is to allow for changes in the smaller graph to exert some influence over the distance measure, which does not happen with d_{mcs}. This measure was also demonstrated to be a metric and creates distance values in [0, 1], [216].

$$d_{UG}(G_1,G_2) = 1 - \frac{|mcs(G_1,G_2)|}{|G_1| + |G_2| - |mcs(G_1,G_2)|} \tag{4.3}$$

A similar distance measure [228] which is not normalized to the interval [0, 1] is

$$d_{mcs1}(G_1,G_2) = |G_1| + |G_2| - 2|mcs(G_1,G_2)| \tag{4.4}$$

A common supergraph of G_1 and G_2, $cs(G_1,G2)$, is a graph G, such that there exist subgraph isomorphisms from G to G_1 and from G to G_2. We call G a minimum common supergraph of G_1 and G_2, $MCS(G_1,G_2)$, if there exists no other common supergraph of G_1 and G_2 that has less nodes than G. The minimum common supergraph of two graphs, G_1 and G_2 , is defined as the smallest graph that includes, as subgraphs, both G_1 and G_2. It is shown that minimum common supergraph computation can be solved by means of maximum common subgraph computation.

Algorithms known from the literature show that for a certain class of cost functions, the concept of graph edit distance is closely related to the minimum common supergraph.

In [229], the authors have proposed a distance measure based on both the maximum common subgraph and the minimum common supergraph

$$d_{MCSmcs}(G_1, G_2) = |MCS(G_1, G_2)| - |mcs(G_1, G_2)| \tag{4.5}$$

We can also create a version of this distance measure which is normalized to [0, 1] as follows:

$$d_{MCSmcsN}(G_1, G_2) = 1 - \frac{|mcs(G_1, G_2)|}{|MCS(G_1, G_2)|} \tag{4.6}$$

If two graphs are identical, then both their maximum common subgraph and minimum common supergraph are the same as the original graphs and $|G_1| = |G_2| = |MCS(G_1, G_2)| = |mcs(G_1, G_2)|$, which leads to $d_{MCSmcs}(G_1, G_2) = 0$. As the graphs become more dissimilar, the size of the maximum common subgraph decreases, while the size of the minimum supergraph increases. This in turn leads to increasing values of $d_{MCSmcs}(G_1, G_2)$.

4.3.4 Similarity Scores Between Nodes

In this approach, we construct a similarity matrix M to indicate the compatibility of nodes in the two graphs being matched, where element M_{ij} denotes the similarity of node i in the first graph to node j in the second graph, depends on the specific measure of node similarity that differ along many dimensions, for example, the topological scope of the measure. The goal is to identify one or multiple possible mappings between the nodes of the input graphs and, for each mapping, the corresponding set of conserved edges, this problem is also known as graph alignment problem. Corresponding to these conserved edges, there exists a mapping between the nodes of the graphs. Constraints can be imposed on M so that each node from the first graph must be mapped to a single node in the second graph. Such a representation and the algorithms applied to it for determining graph matching are straightforward; however, they can require generating all the permutations of possible node matchings over the matrix. To improve time complexity, we can instead attempt to approximate the optimal solution by finding good suboptimal solutions. This problem can be formulated in various ways, depending on the kind of input (pairwise vs multiple matching) and the scope of node mapping desired. Local measures define similarity on the basis of the neighborhood of nodes. Global measures define similarity based on network connectivity patterns over the entire graph.

IsoRank Algorithm

The key problem that IsoRank algorithm targets is identifying the node mappings between two graphs; the input consists of a similarity measure between the nodes of the two graphs. These similarity scores (e.g., BLAST similarity scores, synteny-based scoring, functional similarity) may be defined only for some node-pairs. Given the inputs, we construct an eigenvalue problem whose solution leads to a mapping between the nodes. From this mapping, the set of conserved edges can be easily computed.

The algorithm works in two stages. It first associates a score with each possible match between nodes of the two graphs. Let R_{ij} be the score for the nodes pair *(i, j)* where i is from graph G_1 and j is from graph G_2. Given graph and sequence data, we construct an eigenvalue problem and solve it to compute R (the vector of all R_{ij}). The eigenvalue problem explicitly models the trade-off between the twin objectives of high graph overlap and high sequence similarity between mapped node-pairs. The second stage constructs the mapping for the global measures by extracting from R high scoring, pairwise, mutually-consistent matches. To compute the functional similarity score R_{ij}, we pursue the intuition that *(i, j)* is a good match if i and j's respective neighbors also match well with each other. The intuition is to set up a system of constraints, where we compute the neighborhood scores in a recursive fashion. The equations needed to compute R can be found in [230] and [231].

Hyperlink-Induced Topic Search (HITS) Algorithm

HITS algorithm is also known as hubs and authorities, it is a link analysis algorithm that rates web pages, developed by Jon Kleinberg [232]. In [233], the authors proposed a new algorithm inspired by HITS, where they construct a matrix X of dimensions $|V_B| \times |V_A|$ between two graphs G_A and G_B, which is initialized to all 1's. The following iterative procedure is then applied:

$$X \leftarrow BXA^T + B^T XA \tag{4.7}$$

Where x_{ij} expresses how similar vertex j in G_A is to vertex i in G_B, we say that x_{ij} is their similarity score. A and B are adjacency matrices of the graphs. After a number of iterations, the matrix X is converged to a new matrix different from the initial matrix.

PageRank Inspired Algorithm

Singh et al. [231] propose an iterative procedure of the form:

$$X \leftarrow \alpha \tilde{B} X \tilde{A}^T + (1-\alpha)H \tag{4.8}$$

Where H is the matrix corresponding to the elemental similarity score between node $i \in V_B$ and $j \in V_A$. Successive iterates scale topological similarity and elemental similarity of nodes by factors $\alpha \leq 1$ and $1-\alpha$, respectively. Matrix $\tilde{A}$ is the normalized version of the matrix A^T; We get it by the following equation :

$$\tilde{A}_{ij} = \frac{a_{ji}}{\sum_{i=1}^{N} a_{ji}} \tag{4.9}$$

The topological similarity component in this equation $\alpha \tilde{B} X \tilde{A}^T$ has an interesting interpretation along the lines of the score transport metaphor, see Figure 4.6 .

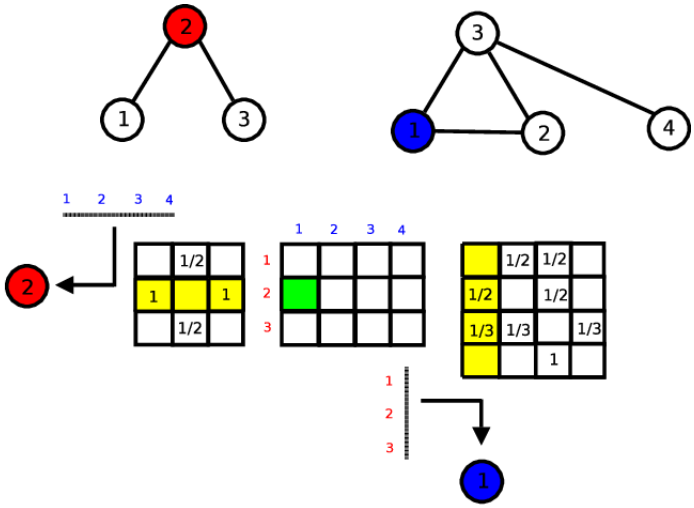

FIGURE 4.6: An example 3×4 similarity matrix X (bottom center) between $\tilde{B}$ and $\tilde{A}^T$ under their respective graphs G_B and G_A (at top left and top right respectively) exactly as in $\tilde{B} X \tilde{A}^T$. Node 2 "pulls" the total score of its two neighbors; however there are 4 ways of doing this (2nd row of $\tilde{B}$ multiplied with each of the 4 columns in X gives a row vector y() with 4 elements). This corresponds to the fact that node 2's neighbors are implicitly linked with each of the 4 nodes in the other graph (i.e., for possible matchings). However, the X_{21} entry will finally be updated only by y(2) and y(3) weighted contributions, because only nodes 2 and 3 happen to be neighbors of node $1 \in V_A$ ("pushing" their contributions to it). The weights will are $\frac{1}{2}$ and $\frac{1}{3}$, because in turn nodes 2 and 3 have 2 and 3 neighbors, respectively.

Network Similarity Decomposition (NSD)

Network Similarity Decomposition (NSD) is a highly efficient algorithm for Page-Rank-based topological similarity computations. It works by un-coupling and decomposing similarity computations. In addition to significant improvements in computational cost (orders of magnitude), NSD supports a rich-query set efficiently, generates execution traces that can be used to identify patterns that contribute significantly to topological similarity scores and is highly amenable to

parallel implementation. It also supports parameters that can be tuned for the desired model, as well as performance requirements [234]. NSD adopts the approach proposed in [231]. It dramatically reduces the cost of these computations. Furthermore, it provides execution traces that can be used to interpret topological similarity scores by identifying link patterns that significantly contribute to topological similarity.

NSD starts by expanding The equation 4.8, and without loss of generality, we use H as the initial condition $X^{(0)}$, and after t iterations, $X^{(t)}$ takes the form:

$$X^{(t)} = (1-\alpha)\sum_{k=0}^{t-1}\alpha^k \tilde{B}^k H(\tilde{A}^T)^k + \alpha^t \tilde{B}^t H(\tilde{A}^T)^t \tag{4.10}$$

The fact is that Singular Value Decomposition (SVD) is only one of the alternatives for decomposing H into a sum of outer products for a given number, s, of vector pairs. Such a decomposition can generally be expressed as:

$$H = \sum_{i=1}^{s} w_i z_i^T \tag{4.11}$$

After substituting equation 4.11 in equation 4.10 we get the following :

$$X_i^{(t)} = (1-\alpha)\sum_{k=0}^{t-1}\alpha^k w_i^{(k)} z_i^{(k)^T} + \alpha^t w_i^{(t)} z_i^{(t)^T} \tag{4.12}$$

and:

$$X^{(t)} = \sum_{i=1}^{s} X_i^{(t)} \tag{4.13}$$

Note that the decomposition happens along sets of paths of successively larger length k. However, their contributions are damped because of the $(1-\alpha)\alpha^k$ factor with $\alpha \in [0,1]$. In this context, $w_i^{(k)} = \tilde{B}^k w_i$, and $z_i^{(k)} = \tilde{A}^k z_i$. Here, s is simply the number of components used. The process mentioned above is outlined in Algorithm 1. The second step of the algorithm uses a maximum weight bipartite matching algorithm to find the best matching pairs of vertices in graphs G_A and G_B based on the similarity scores X computed in the first step.

Algorithm 1 NSD: Calculate $X^{(n)}$

given $A, B, \{w_i, z_i | i = 1, ..., s\}, \alpha$ and n;
compute $\tilde{A}, \tilde{B}$;
for i = *1 To* s **do**
  $w_i^{(0)} \leftarrow w_i$;
  $z_i^{(0)} \leftarrow z_i$;
  for k = *1 To* n **do**
    $w_i^{(k)} \leftarrow \tilde{B} w_i^{(k-1)}$;
    $z_i^{(k)} \leftarrow \tilde{A} z_i^{(k-1)}$;
  end
  zero $X_i^{(n)}$;
  for k = *1 To* n *-1* **do**
    $X_i^{(n)} \leftarrow X_i^{(n)} + \alpha^k w_i^{(k)} z_i^{(k)^T}$;
  end
  $X_i^{(n)} \leftarrow (1-\alpha) X_i^{(n)} + \alpha^n w_i^{(n)} z_i^{(n)^T}$;
end
$X^{(n)} \leftarrow \sum_{i=1}^{s} X_i^{(n)}$;

4.3.5 Parallel Algorithms for Graph Matching

Parallel computing has been successfully used to handle time-consuming operations. In the graph matching, the computation methods mainly focused on the combinatorial methods aimed at identifying subgraph isomorphisms or maximum cliques by used different parallel platforms.

In [235], The authors proposed a highly efficient and scalable parallel formulation based on the network similarity decomposition where the new formulation accelerates the computing of NSD. This acceleration has been shown to yield orders of magnitude improvement in serial runtime, depending on the size of the networks. We provide an overview of NSD acceleration in chapter 5, Section 5.3.

In [236], a parallel algorithm for exact graph edit distance (GED) computation is proposed. This method based on a branch-and-bound algorithm coupled with a load balancing strategy. Parallel threads run a branch-and-bound algorithm to explore the solution space and to discard misleading partial solutions. The key idea of this algorithm is that a parallel execution can help to converge faster to the optimal solution. This method is very generic and can be applied to directed or undirected fully attributed graphs (i.e., with attributes on both vertices and edges). By limiting the run time, this exact method provides (sub)optimal solutions and becomes an efficient upper bound approximation of GED. The authors provided a complete comparative study where 6 exact and approximate GED algorithms were compared on a set of 4 graph datasets. By

considering both the quality of the proposed solutions and the speed of the algorithm, they show that their proposal is a good choice when a fast decision is required as in a classification context or when the time is less a matter but a precise solution is required as in image registration.

GPUs with massively parallel processing architectures have been successfully leveraged for fundamental graph operations on large graphs, among them are graph matching. In [237], the authors proposed a GPU-efficient subgraph isomorphism algorithm using the Gunrock graph analytic framework, GSM (Gunrock Subgraph Matching), to compute graph matching on GPUs. In this algorithm, they make the following contributions: They designed a subgraph matching approach using breadth-first search as the core operation. They focused on the problem of memory capacity, optimizing their algorithm to generate as few intermediate results as possible by limiting the memory usage linear to matched subgraphs; and they achieved best-of-class performance on a variety of datasets and scenarios when compared to prior CPU and GPU algorithms. Another algorithm based on GPU is proposed in [238], where authors proposed a fine-grained shared-memory parallel algorithm for generating greedy matchings of undirected graphs. This algorithm was inspired by the parallel graph coarsening algorithm discussed in [239] and follows a paradigm similar to that of the auction algorithm for bipartite graphs, but applying to general greedy matchings in arbitrary undirected graphs.

There are some other efforts aimed at parallel graph matching. In [240], the authors computed histograms of the spectra of the weighted Laplacians of the subgraphs induced around each vertex up to a number of shortest path lengths. These serve as vertex signatures that can drive matching at the next stage implementing a seed-and-extend strategy that is sequential; however, computing signatures is parallelizable. In [241], two methods, Matching Relaxation (MR) and Belief Propagation (BP) are used to compute the similarity matrix, followed by 1/2-approximate matching, are parallelized for a shared memory platform.

4.4 Graph Matching for Brain MRI/FMRI Analysis

Neuroimaging techniques have recently become one of the most influential tools to detect structural and functional brain abnormalities. The brain can be regarded as a network Figure 4.7, where nodes represent brain regions, and edges represent the anatomical or functional connections between brain regions [174] [175]. Recent research has shown that graph-theory based complex network analysis provides a powerful framework for examining the topological properties of brain networks [242]. In this section, we presented two main points. The first: how to represent MRI and fMRI data by a graph. The second: how to use graph matching for brain MRI and fMRI analysis.

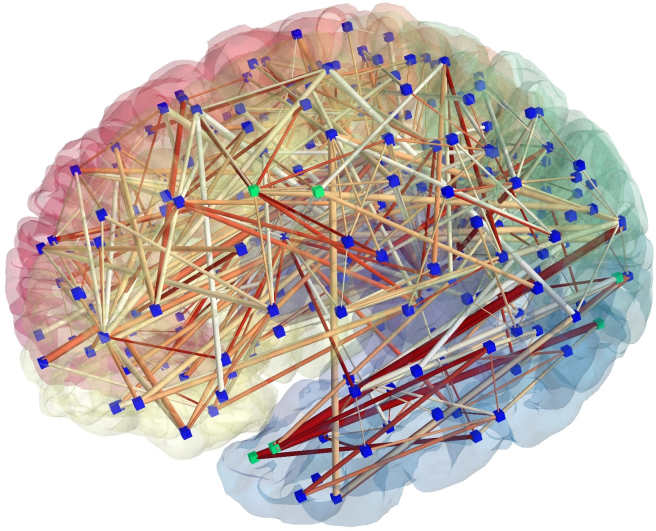

FIGURE 4.7: The brain represented as a network: image obtained from MR connectomics. (Provided by Patric Hagmann, CHUV-UNIL, Lausanne, Switzerland).

4.4.1 Representing Brain MRI/FMRI Data by Graphs

MRI Data

- **Nodes:** (vertices) denoting neural elements (neurons or brain regions). Parcellation of the cerebral cortex is the widely used approach for defining nodes for brain graphs [102].
- **Edges:** are defined by the inter-regional correlations of the cortical thickness or volume MRI measurements estimated in groups of subjects and characterized by properties related to the white matter pathways (indicate the presence of an anatomical path between those regions).

fMRI Data

- **Nodes:** stand for different brain regions (e.g. parcellated areas or recording sites), there are several approaches to define brain nodes in fMRI data. The most commonly used approach is to use a fixed anatomical atlas [243]. Using single voxels directly as brain nodes was the earliest approach for graph analysis [244]. Approaches to aggregate voxels into nodes as voxel-based modalities [245] and independent component analysis (ICA)[246].
- **Edges:** In fMRI, the links of a brain graph are given by evaluating the similarity between two brain signals, through FC measures. Several approaches have been developed in the last decade to measure FC based on various concepts from signal processing to autoregressive

modeling and information theory. Each method has its own specifications but essentially they all apply to a set of signals $X_1(t)...X_N(t)$ recorded from N different brain nodes, where $N \geq 2$, and give, for each pair of nodes i and j, the magnitude of the statistical interaction between their activities. These magnitudes represent the weighted links w_{ij} of the brain graph [175].

Topological Metrics

The comparison of brain graphs in terms of topological metrics is often achieved by comparing theoretical reference graphs produced by simulation models or by comparing the collection of brain graphs, either between specific experimental conditions or different populations. Recently, several empirical studies on structural and functional brain networks have contained small-world architectures. Discovering that brain networks are small-world networks is only the first step towards a comprehensive understanding of how these networks are structurally organized and how they generate complex dynamics.

Topological properties of brain networks can be derived at the large scale of the whole brain, at the intermediate-scale of several regions of the brain, or locally, at the small-scale of single regions, i.e. metrics on single nodes. A vast number of graph metrics do exist to extract topological properties [103] [247]. In practice, graph metrics (or indices) such as clustering coefficient, path length and efficiency measures are often used to characterize the 'small-world' properties of brain networks [248] [249]. Centrality metrics such as degree, betweenness, closeness and eigenvector centrality are used to identify the crucial areas within the network. Community structure analysis, which detects the groups of regions more densely connected between themselves than expected by chance, is also essential for understanding brain network organization and topology [103].

Graph Matching in Application

Graph theory has drawn a lot of attention in the field of Neuroimaging and Neuroscience during the last decade, mainly due to the abundance of tools that provides to explore the interactions of elements in a complex graph like the brain. In these fields, the construction of a representative brain graph for each individual is critical for further analysis. Additionally, graph matching is an essential step for inference and classification analyses on brain graphs.

Among the researches which used the graph matching with the brain MRI, there is the labeling of the brain sulci. In [250], the authors proposed a quantitative method for automatically comparing and analyzing the sulcal pattern between individuals twin using a graph matching approach, where the sulcal pattern was represented as a graph structure with sulcal pits as

nodes. The similarity between graphs was computed with a spectral-based matching algorithm by using the geometric features of nodes (3D position, depth, and area) and their relationship. In particular, they exploited the feature of graph topology (the number of edges and the paths between nodes) to highlight the interrelated arrangement and patterning of sulcal folds. In [251], the authors put forward two optimization methods for graph matching and compare them in the context of brain sulcus identification. The first approach is based on a constraint search in a neighborhood; the second uses a genetic algorithm for optimization. In [252], the authors introduced a sulcus identification algorithm based on a genetic algorithm for solving the problem of graph matching using shape, orientation, location, and neighborhood information. In [253], the authors proposed a multi-view framework to identify the correspondence of 3-hinge cortical landmarks across subjects, in which all gyral hinges within a subject are taken as a system and its structural and functional connective networks are used as inputs. The effectiveness of this framework is demonstrated by cross-subject consistency of anatomical, structural connective and functional metrics. In [254], the authors proposed a novel group-wise graph matching framework, to which they fed structural connective matrices among gyral hinges from all subjects. The correspondence estimated by this framework is demonstrated by cross-subject consistency of both structural connective and functional profiles.

Recent years have seen the evolution of connectomics, the study of brain connectivity, in which structural and functional connectivity of the brain are modeled as graphs of interconnected regions with weighted edges representing the strength of connectivity. The problem of finding (dis)similarities between structural and functional connectomes can be considered as an instance of the graph matching problem [203]. In [255], the authors proposed a multimodal connectomics paradigm using graph matching to measure similarity between structural and functional connectomes. They investigated the traffic pattern that best describes the structure-function relationship in the brain, and how structure-function relationships determine the interactions among large-scale functional systems. In [256], A novel method is proposed to match functional connectivity patterns represented by graphs for spatial registration of fMRI data. The proposed method adopts a graph representation to characterize functional connectivity information among all voxels in fMRI data of each subject, then detects spatial correspondence between subjects using graph matching. To integrate information of both functional connectivity strength and spatial relations, the graph representation of functional connectivity information of fMRI data models each voxel as one graph node and connects each pair of graph nodes with an edge-weighted by their functional connectivity strength measure, estimated as correlation coefficient between their functional signals. To make the graph matching computationally feasible, an iterative matching strategy with stochastic resampling is proposed to match graphs of spatially distributed local functional connectivity patterns and subsequently to drive the image registration iteratively. In [257], based on a graph matching based approach, the authors proposed a measure to quantify how dissimilar a traumatic brain injury patient is relative to healthy subjects using their structural and functional connectomes.

4.5 Conclusion

In this chapter, we have given an overview of graph matching, we started by describing the base concepts of graph theory, then we talked about both exact and inexact graph matching methods. Particularly, the concept of inexact graph matching provides us a means of measuring the similarity of graphs and thus lays the foundation of using the versatile and flexible tool of graphs in case-based reasoning in dealing with complex networks as brain networks. Next, we discussed the methods used for representing brain MRI/fMRI data by graphs and some works that used these types of data with graph matching approaches. To conclude, we should keep in mind that the human brain is a complex system that can represent it by a complex network, and graph matching has successfully been applied to various problems in neuroimaging and neuroscience.

Chapter 5

Graph Matching Approach and Generalized Median Graph for Automatic Labeling of Cortical Sulci with Parallel and Distributed Algorithms

5.1 Introduction

Recently, there has been a major progress in the use of medical imaging techniques such as magnetic resonance imaging (MRI) in the study and treatment of many diseases, especially in neuroimaging has contributed a lot both in the medical domain and in neurology field. The external surface of the brain is a thin layer composed of gray matter called cerebral cortex, it is highly convoluted and consists of many convoluted folds called gyri separated by spaces called sulci. The sulcus is very important where we are allowed to distinguish different functional areas of the brain [62].

Recognition of cortical sulci in MRI images is a hard problem which requires anatomical expertise and it is a time consuming because these structures have very complex geometry and variation in their shape from an individual to another. This difficulty is related to several things, including the difference in the location, extent, orientation, and morphology of the sulci, sometimes the sulci are intertwined [252]. Various approaches have been proposed to tackle this challenging problem. Each approach is based on some a priori knowledge generally low level descriptors about cortical sulci and recognition strategy.

Graph is a powerful tool for pattern representation and recognition in various fields. The primary advantage of graph-based representation is that it can represent patterns and relationships among data easily. The graph matching techniques have been successfully applied to many areas, such as biology and biomedicine, biometric identification [258] [259] [260], document

processing [261], 2D and 3D image analysis [262][263] [264] [265], and video analysis [266] [267] [268]. The concepts of generalized median graphs have a great potential for applications, e.g. in clustering or classification , chemistry, molecular biology, and handwriting recognition [269] [270] [271].

In this work, we proposed an approach based on a graph representation with graph matching framework and generalized median graph for automatic labeling of cortical sulci with parallel algorithms.

In the following sections, we introduce: In Section 2, we have presented a state of the art on the labeling of cortical sulci. In Section 3, we have presented our approach: characteristics of the sulcal segments, representation of cortical sulci by a graph, distance between the graphs, generalized median graphs and graph matching problem. In Section 4, we have presented our experiments. At the end, we terminate with some conclusions and possible future research lines.

5.2 Overview of Recognition and Labeling of Cortical Sulci Approaches

In this section, we have presented an overview on the approaches of automatic image annotation.

5.2.1 Morphometric Based Approach

This approach based on recalibration of deformable atlases, its principle consists in the recalibration of a deformable atlas where all the anatomical structures have been labeled manually by an expert [272], [273].

These approaches are simple and they have demonstrated a successful identification of some major sulci but modeling the variability of structures are limited, convergence not guaranteed [274].

5.2.2 Statistical Based Approach

Several alternative approaches have been proposed in which the sulci are matched with models from a training database based on characteristics such as the shape, the location or structure. We present below a few approaches based on this paradigm.

In [275], the authors have based on a nearest neighbor algorithm to define the classes of the sulcal region using anatomical landmarks such as gyri as a features. In [276], the authors

proposed a markovian framework to recognize sulci in which they have used the probabilistic Statistical Parametric Anatomy Map (SPAM) model as the prior information about sulci locations that returns the probability of presence of each sulcus at a given 3D location and the SVR algorithm to learn shapes and local sulci scheme. In [277], the authors proposed a method to automatically label sulcal basins that employs a model contains both a volumetric description of the mean shape and possible variations in the location of each sulcal basin obtained from the set of training images. In [278], a technique has been proposed for automatically assigning a neuroanatomical label to both sulci and gyri. In this procedure, they have used probabilistic information about their spatial distribution estimated from a manually labeled training set.

Statistical model-based approaches are frequently used in this context because it is simple to implement and they rely on strong mathematical theories that allow to well represent the interindividual variability [274].

5.2.3 Graph Based Approach

These approaches are very powerful for anatomical structures presenting high interindividual variability where the sulci are represented by nodes and the edges represent the relationships between them and they contain all the necessary information to identify the cortical structures.

In [279], the authors presented an approach to associate labels of sulci from a brain atlas to individual brains. All information related to topologically and geometry of the cortical sulci is saved in a topology graph, so that each node contains the location and size of the associated sulcus and the associated edges contain connectivity information between the sulci. The mapping is performed by matching between the topology graphs for both atlas brain and individual brain candidate. In [280], the authors presented an approach for joint sulci identification on cortical surfaces by using graphs models and boosting techniques incorporate shape priors of major sulci and their Markovian relations, where the sulci are represented by nodes in the graph model and detect the sulci jointly via the solution of an inference problem on graph models. In [252], the authors proposed a graph-based approach for the automatic identification of major sulci where each subject is represented by a graph describing the sulci by their shape, orientation and location. The identification is formulated as a graph matching problem between a model graph describing the sulcal characteristics and their neighborhood relations and a candidate graph composed of sulcal segments obtained from the test subject. In [274], the authors proposed a hybrid approach based on a graph representation coupling high-level knowledge with low level knowledge in graph matching framework based on local search algorithm and followed by a paradigm of ontology for representation high level knowledge about sulci and their spatial relations, where as low-level knowledge consists of graph model.

The advantage of this approach is its rich structural context representation of sulcal segments including location, orientation and shape because the relative position of sulci is highly invariant and using neighborhood relationships is very advantageous for identification [252].

5.3 Method

The objective is automatic labeling the cortical sulci localized in any MRI examination therefore we followed a general approach which several steps according to Figure 5.1, that was proposed in [2]. The steps begin by reconstruction of cortical surface and segmenting sulcal segments from cortical surface until sulcus recognition.

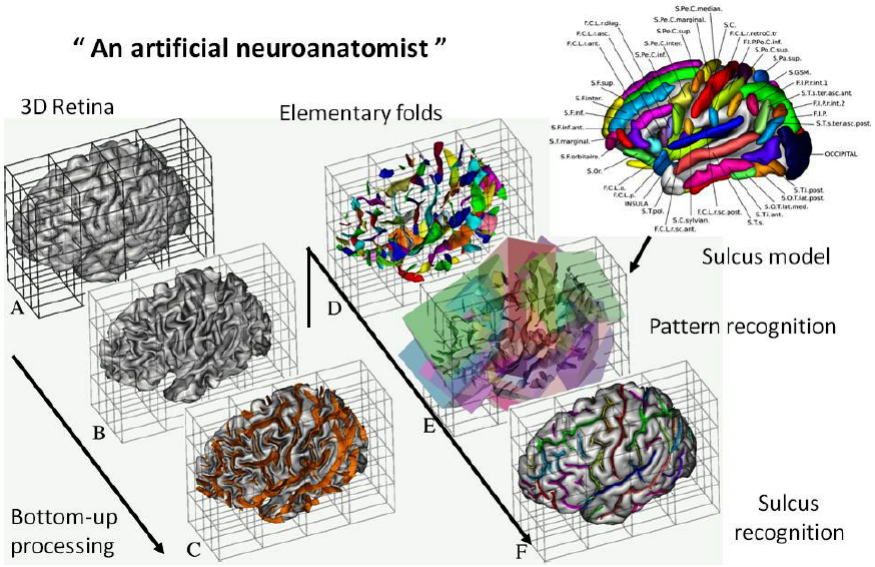

FIGURE 5.1: The general approach proposed for sulci recognition. After detection of the building blocks of the folding pattern from a negative mold of the brain, the sulci of the standard nomenclature are reassembled according to a model inferred from a learning database [2].

We proposed a new approach of automatic labeling of cortical sulci that consists of several steps, Figure 5.2. The first, a model graph representation was constructed from a training dataset of MRI brain images where a neuroanatomist manually labeled sulci in the training cases that were obtained automatically from surface segmentation. The second, the relationships between neighboring sulci were also extracted from the training set. The third, all information is represented as a model graph in which each node contains the attribute descriptors of a sulcus and edges indicate neighborhood relationships between sulci. The fourth, from the previous results of manual annotation, we build a similar graph from the candidate subject, sulcal segments, and their neighborhood relationships. Finally, a graph matching algorithm is applied to determine the labels of graph candidate from the modal graph.

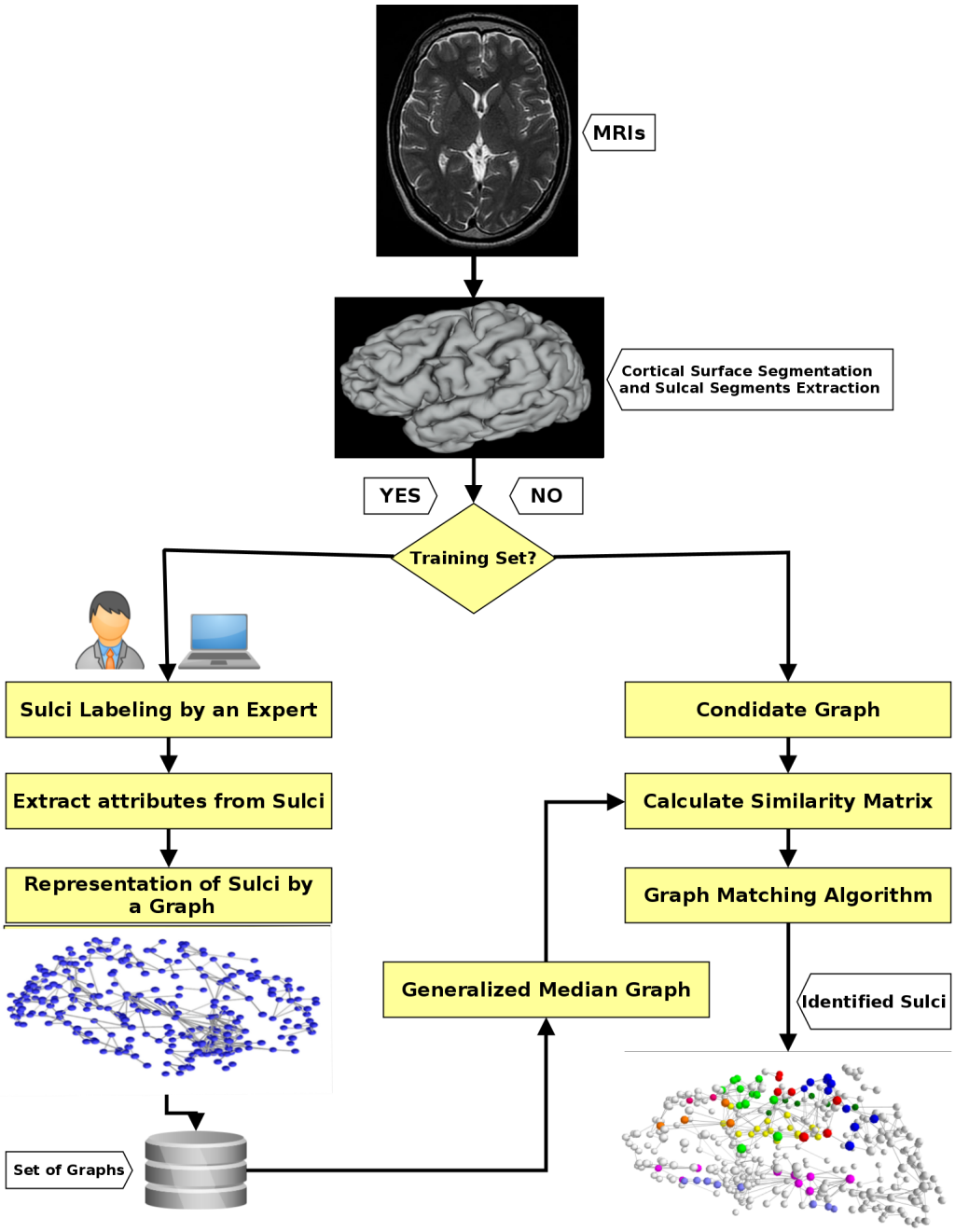

FIGURE 5.2: Our approach for automatic labeling of cortical sulci.

5.3.1 Characteristics of the sulcal segments

We used the methods implemented in the Brainvisa software (`http://www.brainvisa.info`), with this tool, all of the cortical folds are represented as a sets of voxels. Thus we get a very detailed description of the sulci incorporating all the folds and tertiary the more variable, Figure 5.3 [2].

We chosen the location, orientation, and shape as the characteristics that describe a sulcal segment [251]. The sulcus is found in a relatively constant region of the cortical surface, so location is critical for the identification task. Location with orientation information are reliable

for each sulcus [281] [282]. In order to describe the characteristics of the shape that is also an important factor in the description of the sulcal segments, we used the geometric moment to describe the sulcus shape [283], then we put all these characteristics in a characteristic vector as follow $V = (v_1,v_2,...,v_n)$.

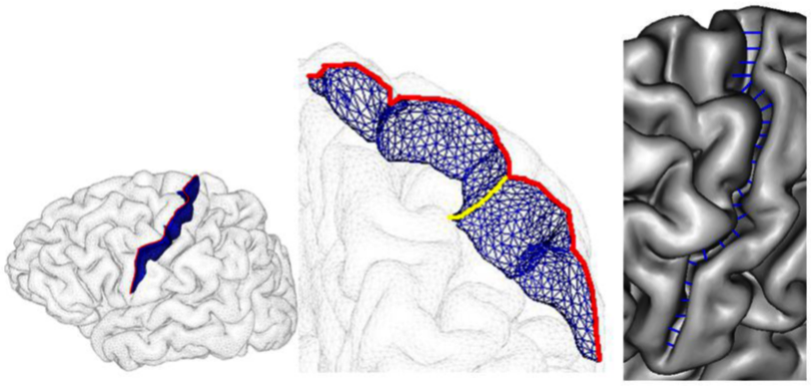

FIGURE 5.3: Characteristics that describe a sulcal segment like length (red), depth (yellow), surface area (blue) or average span between its walls (right).

5.3.2 Graph Representation

Several pre-processing steps are necessary before creating a graphical representation, tissue segmentation [284], extraction of cerebral hemispheres [285], reconstruction of cortical surfaces [285] [286] [287], sulci segmentation [287] [288]. The procedure briefly described and illustrated in Figure 5.4. The sulcal segments are represented by nodes in the graph and the edges represent the relationships between them and include all the information necessary to identify the cortical structures, Figure 5.5. This higher level representation leads to more efficiency in the annotation process and is very powerful for anatomical structures with high inter-individual variability.

5.3.3 Definitions and Notation

Let L be a finite alphabet of labels for nodes and edges respectively (L_V and L_E). A graph G is defined by $G = (V,E,\mu,\xi)$, where (V) is the set of nodes, ($E \subseteq V \times V$) is the set of edges, ($\mu : V \longrightarrow L_V$) is the node labelling function, ($\xi : E \longrightarrow L_E$) is the edge labelling function. The number of nodes of a graph G is denoted by $|G|$. If $V = \varnothing$, then G is called the empty graph.

A common supergraph G of two graphs G_1 and G_2 is minimum $MCS(G_1,G_2)$ if all other common supergraphs of G_1 and G_2 have at least $|G|$ vertices.

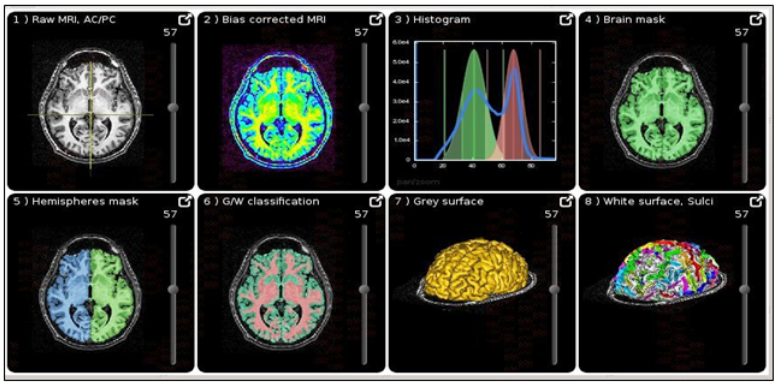

FIGURE 5.4: The cortical sulci extraction procedure. (1) Preparation of the subject (manual positioning of the anterior and posterior commissures). (2) Bias corrected. (3) Analysis of the histogram. (4) Brain segmentation. (5) Separation of hemispheres. (6) G/w classification. (7,8) Reconstruction of cortical surfaces.

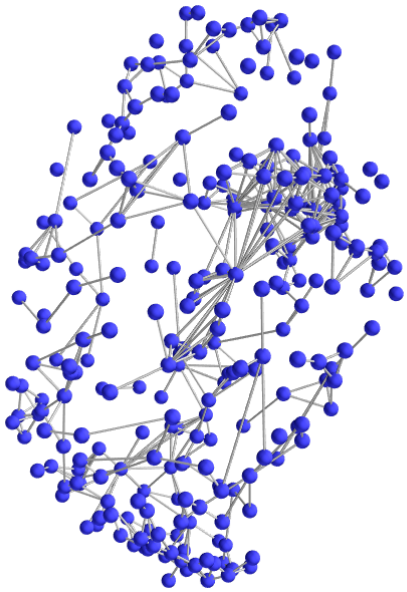

FIGURE 5.5: Representation of the left hemisphere of the brain by a graph where the nodes represent the descriptors of each sulcus and the edges represent the relations between them.

A common subgraph G of two graphs G_1 and G_2 is maximum $mcs(G_1,G_2)$ if all other common subgraphs of G_1 and G_2 have at most $|G|$ vertices.

Distance between the graphs

When we use graph-based representations in applications to represent objects, we need a measure of the dissimilarity between graphs to identify the objects that belong to the same class but have a different graphical representation. Several exact and approximate algorithms have been presented in the past related to the computation of the distance between two graphs, one of them

the graph edit distance [228] [289] [290]. Other distance between graphs in [229] [291] [292]. In this work, we have used one of these distances based on the maximum common subgraph and minimum common supergraph given in [293], the distance between two graphs that we have used is :

$$\begin{aligned} d(G_1,G_2) &= (|G_1|+|G_2|) - (2\times|mcs(G_1,G_2)|) \\ &= (2\times|MCS(G_1,G_2)|) - (|G_1|+|G_2|) \\ &= |MCS(G_1,G_2)| - |mcs(G_1,G_2)| \end{aligned} \tag{5.1}$$

The proof of validation and the application of this equation is given in [293]. In the rest of the chapter we will use this equation to measure the distance between two graphs.

5.3.4 Generalized Median Graph

The generalized median graph is a very useful tool to represent a set of graphs by a single graph. Let U be the set of all graphs defined over the alphabet L. Given S a set of graphs, $S = \{ G_1; G_2, \ldots, G_n \} \subseteq U$. We can define the generalized median graph $\bar{G}$ of a set of graphs S such that $G \in U$ by :

$$\bar{G} = argmin_{G\in U} \sum_{i=1}^{n} d(G,G_i) \tag{5.2}$$

Notice that $\bar{G}$ minimizes the sum of its distances to all graphs in S and $\bar{G}$ is not necessarily a member of S, as there can be more than one $\bar{G}$, [294],[271].

The computation of the generalized median graph is related to the complexity of the distance function and the size of the search space U. As a consequence, in real applications, we need to use approximate methods to solve the generalized median graph problem in a reasonable time because the exact algorithms can not treat the large graphs. The exact algorithms are limited to small problems. On the contrary, approximate methods have usually used some types of heuristics in order to reduce the complexity of the calculation of the distance between graphs and the size of the search space, respectively. Some exact algorithms and approximate for the calculation of the generalized median graph have been developed up to now include greedy [295] and genetic algorithms [294]. An exact algorithm with 25 nodes [296] [297]. Other approaches based on graph embeddings [298] [299] [300].

We used a heuristic to solve the generalized median graph problem. The heuristic that we used is obtained by removing the nodes *(v)* of the minimum common supergraph *MCS(S)* one by one in the decreasing order of the estimates $d(MCS(S)^{(-v)},S)$. The heuristic relies on removing a node whenever that can improve the current solution.

A heuristic algorithm called *greedy adaptive* proposed by [271], can be derived from this algorithm. The principle of this algorithm is every time we remove a node from the current solution and we recalculate all estimates each time, the next node we will delete should improve the current solution after removing it. The algorithm stops when we examine all the candidate nodes or when there is no improvement in the current solution. The pseudo-code for this algorithm is presented in Algorithm.2.

Algorithm 2 Greedy-Adaptive

```
Set CurrentSolution ← MinSup(S);
Set CurrentSOD ← SOD(MinSup(S),S);
Let Candidates be the vertex set of CurrentSolution;
Compute the estimate SOD ( MinSup(S)^(−v),S) for each vertex v of MinSup(S);
while Candidates ≠ ∅ do
  u ← argmin(SOD(CurrentSolution^(−v),S) : v ∈ Candidates;
  Let Solution be the graph obtained by removing vertex u from CurrentSolution;
  if SOD(Solution,S) < SOD(CurrentSolution,S) then
    CurrentSOD ← SOD(Solution,S);
    CurrentSolution ← Solution;
  end
  Candidates ← Candidates \ {u};
  Update SOD(CurrentSolution^(−v),S), for each vertex v of CurrentSolution;
end
Return CurrentSolution;
```

5.3.5 Graph Matching Problem

Graph matching is a technique to identify related nodes between two distinct graphs. The result is a matching between the nodes of each graph such that a node can only be matched to a single node in the opposite graph.

The graph matching problem between two graphs can be formulated as an NP-hard computational [301], and it can be broadly classified into local or global measures of cost. In local graph matching the result is a single similarity score. This similarity score indicates how similar two graphs G_A, G_B are in their entirety [302] [303] [304] [231]. In contrast, global graph matching relies on a matrix of elements X_{ij}, representing the similarity of each node i in the first graph to every node j in the second graph. This second class of methods reflects a more accurate concept of graph matching [305] [306] [231]. The methodology of graph matching has its roots in the domains of ontology alignment [307]. Protein-protein network analysis [308] [231]. Object recognition [203]. PageRank [309] [310]. IsoRank algorithm [231]. Graph kernel approach

[311]. Determining molecular similarity [312]. Anomaly detection [313]. Social network de-anonymization [314]. Multimodal network alignment [315]. Large-Scale graph [240] [316] [317].

There have been some recent efforts aimed at parallel graph matching [318] [241] [319] [238] [320] [321]

In [231], the authors proposed IsoRank approach which consists of two steps. The first step, a similarity score matrix X is constructed between two graphs G_B and G_A, where element x_{ij} denotes the similarity of node i in the first graph to node j in the second graph. The number of nodes per graph is m and n, respectively ($m \leq n$). Step two, based on the similarity matrix X, we apply a node matching algorithm selects pairs of nodes, one from each graph, optimizing an aggregate similarity score measure.

Terminologies

We represent a graph by $G_A = (V_A, E_A)$. V_A and E_A denote the set of nodes and the set of edges of G_A respectively and A its adjacency matrix, where $a_{ij} = 1$ if node i has a connection with node j and zero otherwise. Matrix $\tilde{A}$ is the normalized version of the matrix A^T; We get it by the following equation :

$$\tilde{A}_{ij} = \frac{a_{ji}}{\sum_{i=1}^{N} a_{ji}} \tag{5.3}$$

wher $N = \mid V_A \mid$ for nonzero rows j of A and zero otherwise. According to [231] , we can transform the similarity matrix X into a bipartite graph $G = (V_A, V_B, E)$, where $E \subseteq V_A \times V_B$. Each row i represents a vertex in V_A, and each column j a vertex in V_B. A non-zero entry x_{ij} in the matrix represents a weight of the edge $(i, j) \in E$. A subset $M \subseteq E$ in a bipartite graph is called a matching if no pair of edges of M are incident to the same vertex, [235].

5.3.6 Network Similarity Decomposition (NSD)

We used Network Similarity Decomposition (NSD) in the case of parallel that has proposed in [235] for the construction of the similarity matrix. According to [231] the IsoRank iteration kernel is the form :

$$X \leftarrow \alpha \tilde{B} X \tilde{A}^T + (1 - \alpha) H \tag{5.4}$$

Where H is the matrix of distances between nodes of two graphs, these distances are calculated from the characteristics that we extracted in section 3.1, where the focus is on the topological connectivity because it does not appear in the first part of The equation 5.4. The factor $\alpha \in [0, 1]$ is a coefficient that indicates the contribution of the topological component in the process of calculating the similarity matrix X.

We used the Euclidean distance between the nodes characteristics vectors to construct the matrix H, where each element :

$$h_{ij} = d(node_i, node_j) = \frac{1}{\sqrt{\sum_{k=1}^{n}(Vnode_{ik} - Vnode_{jk})^2}} \tag{5.5}$$

$Vnode_{ik}, Vnode_{jk}$: are the vectors of characteristics of node i and node j, n : is the number of characteristics, If the two vectors are corresponding then $h_{ij} = 1$.

In [235], they proposed an acceleration technique called Network Similarity Decomposition (NSD), NSD adopts the approach of IsoRank to reduce the temporal and spatial complexity resulting from triple matrix product in equation 5.4. Steps to calculate the similarity matrix by (NSD) is briefly described as follows where we use H as the initial condition $X^{(0)}$, and after t iterations, $X^{(t)}$ takes the form :

$$X^{(t)} = (1-\alpha)\sum_{k=0}^{t-1} \alpha^k \tilde{B}^k H(\tilde{A}^T)^k + \alpha^t \tilde{B}^t H(\tilde{A}^T)^t \tag{5.6}$$

Using Singular Value Decomposition *(SVD)* or Non-negative Matrix Factorization *(NMF)* [322], we can decompose matrix H into a set of s vector, that can be expressed as:

$$H = \sum_{i=1}^{s} w_i z_i^T \tag{5.7}$$

After substituting equation 5.7 in equation 5.6 we get the following :

$$X^{(t)} = \sum_{i=1}^{s} X_i^{(t)} \tag{5.8}$$

Where :

$$X_i^{(t)} = (1-\alpha)\sum_{k=0}^{t-1} \alpha^k w_i^{(k)} z_i^{(k)^T} + \alpha^t w_i^{(t)} z_i^{(t)^T} \tag{5.9}$$

and $w_i{}^{(k)} = \tilde{B}^k w_i$, $z_i{}^{(k)} = \tilde{A}^k z_i$. This formulation provides the basis for the NSD method. For more details on NSD, including the derivation of the associated expressions, see [319].

We used a generic approach for NSD parallelization proposed by [235]. The pseudo-code for the parallel NSD algorithm is presented in Algorithm 3.

Algorithm 3 Parallel NSD

1: Root (lines 2 - 11) and (r,u) worker process in the p×q grid(lines 12 - 18)
2: compute $\tilde{A}$,$\tilde{B}$;
3: **for** *i = 1 To s* **do**
4: $w_i^{(0)} \leftarrow w_i$, $z_i^{(0)} \leftarrow z_i$;
5: **for** *k = 1 To n* **do**
6: $w_i^{(k)} \leftarrow \tilde{B}\ w_i^{(k-1)}$;
7: $z_i^{(k)} \leftarrow \tilde{A}\ z_i^{(k-1)}$;
end
end
8: **for** *i = 1 To s, k = 0 To n* **do**
9: Partition $w_i^{(k)}$ in p fragments, $w_{i,1}^{(k)}$, ... ,$w_{i,p}^{(k)}$;
10: Partition $z_i^{(k)}$ in q fragments, $z_{i,1}^{(k)}$, ... ,$z_{i,q}^{(k)}$;
end
11: Send to every process (r,u) in the process grid p×q its corresponding $w_{i,r}^{(k)}$, $z_{i,u}^{(k)}$ fragments, ∀i = 1, ... ,s, k = 0, ... ,n (r = 1, ... ,p, u = 1, ... ,q);
12: Receive corresponding $w_{i,r}^{(k)}$, $z_{i,u}^{(k)}$, ∀i = 1, ... ,s, k = 0, ... ,n from the root process;
13: **for** *i = 1 To s* **do**
14: zero $X_{i,ru}^{(n)}$;
15: **for** *k = 0 To n-1* **do**
16: $X_{i,ru}^{(n)} \leftarrow X_{i,ru}^{(n)} + \alpha^k\ w_{i,r}^{(k)}\ z_{i,u}^{(k)T}$;
end
17: $X_{i,ru}^{(n)} \leftarrow (1 - \alpha)\ X_{i,ru}^{(n)} + \alpha^n\ w_{i,r}^{(n)}\ z_{i,u}^{(n)T}$;
end
18: $X_{ru}^{(n)} \leftarrow \sum_{i=1}^{s} X_{i,ru}^{(n)}$;

5.3.7 Graph Matching Algorithm

Graph Matching Algorithm

We proposed an algorithm based on the similarity matrix X, such that for each node of graph G_A, we choose the best similar node from graph G_B. This means that we will choose the highest possible value in each row and column of the similarity matrix, such that a node can only be matched to a single node in the opposite graph. Where a node i of graph G_A matched to a node j of graph G_B, the node i get the label of the node j. In practice, we choose a value of the similarity matrix which is the maximum value in the row and it is the maximum value in the column at the

same time for each two nodes matched together, then we change the values of the corresponding column and the corresponding row to zero and so with the rest, Algorithm 4.

Algorithm 4 Graph Matching Algorithm

Input : X_n : similarity matrix , L : list of all nodes;
Output: Matching M;
$M = \varnothing$;
$C \leftarrow copy(X_n)$;
while $L \neq \varnothing$ **do**
  $i, j \leftarrow$ choose index of the maximum value in the rows and columns of C;
  $M[i, j] \leftarrow 1$;
  $C[i,] \leftarrow 0$;
  $C[, j] \leftarrow 0$;
  L $\leftarrow$ L/ {node i};
end
Return M;

Parallel Graph Matching Algorithm

To parallelize the calculations, we proposed an algorithm for the parallel computation of a matching M (M is initially empty) between two graphs $G_A = (V_A, E_A)$ and $G_B = (V_B, E_B)$ is based on the concept of the similarity matrix, Figure 5.6. The algorithm starts with the similarity matrix entry distributed among the processors and for each row i there is one dedicated owner of that row. Each processor then operates in synchronized rounds where first performs a local version of the sequential algorithm followed by communication.

$$M_{ij} = \begin{cases} 1 & \text{if } i \in V_A \text{ and } j \in V_B \,/\, X_{ij} = max(X_{ik}), k = 1...|G_B| \\ 0 & \text{otherwise.} \end{cases}$$

Where X is the similarity matrix.

The general principle is for each node of graph G_A we choose the best similar node of graph G_B, this means that we choose the highest possible value in each row and column of the similarity matrix, as a mapping of each node of graph G_A to a unique node of graph G_B, see Algorithm 5.

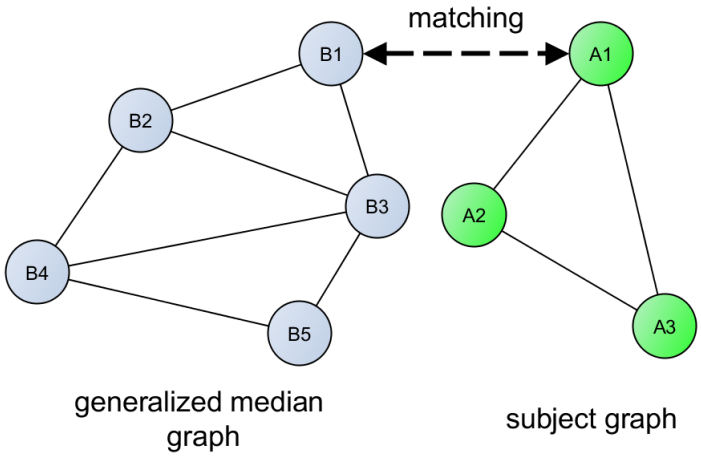

FIGURE 5.6: Example explains the graph matching between two graphs, each node has its own characteristics, B1 ($label_{B1}$, $location_{B1}$, $orientation_{B1}$, $momentInvariants_{B1}$), A1 ($location_{A1}$, $orientation_{A1}$, $momentInvariants_{A1}$), the node A1 corresponds to the node B1 therefore the node A1 takes the node label B1.

Algorithm 5 Parallel Graph Matching

Input : X_n : similarity matrix , L : list of all nodes, P : number of processes;
Output: Matching M;
$M = \varnothing$;
$C \leftarrow \text{copy}(X_n)$;
distribute the list of nodes L on P processes;
for *each processes* P_k **do**
while $L_k \neq \varnothing$ **do**
  $i, j \leftarrow$ choose index of the maximum value in the rows and columns of C;
  lock
  $M[i, j] \leftarrow 1$;
  $C[i,] \leftarrow -1$;
  $C[, j] \leftarrow -1$;
  endlock
  $L_k \leftarrow L_k / \{\text{node i}\}$;
  end
  end
Return M

5.4 Experimental Results

We used a dataset of MRI images weighted in T1 and with voxel dimensions of $1\times1\times1$ mm^3. The dataset is available online (http://jerlab.psych.sc.edu/NeurodevelopmentalMRIDatabase/). A fuller description of the rationale and characteristics of the dataset may be found in [323]. This dataset contains healthy subjects of adults to evaluate our method. Our dataset is grouped into two sets, the first one is the training set used for the construction of the generalized median graph, and the second set is used for the evaluation of the performance of the proposed approach. In this work, we focus on the recognition of the insula (INS), the central (CS), postcentral (PTS), precentral (PCS), superior temporal (STS), callosal (CLS), cingulate (CIs), superior frontal (SFS) and inferior frontal sulcus (IFS). These nine sulci are well-defined and comprise the major sulci on the lateral and medial cortical surfaces [252]. A neuroanatomist manually labeled these sulci to build the generalized median graph. We used estimation measures to evaluate the automatic labeling accuracy for each sulcus by each test subject that are the true positive rate (TPR), false positive rate (FPR) and the similarity index (SI) such that :

$$TPR = \frac{TP}{TP+FN} \tag{5.10}$$

$$FPR = \frac{FP}{FP+TN} \tag{5.11}$$

$$SI = \frac{2TP}{2TP+FP+FN} \tag{5.12}$$

Where TP corresponds to the number of vertices of a specific sulcus that were correctly labeled by our algorithm. FN is the number of vertices that belong to this sulcus but were unlabeled. FP is the number of vertices falsely labeled as this sulcus and TN is the number of vertices that do not belong to this sulcus and are unlabeled. We chose the parameter α used in similarity matrix construction is set to 0.85 (recall that α is the fraction of the similarity score that comes from the topological similarity; the rest comes from the elemental similarity), the number of iterations n = 200 and s = 10.

A quantitative comparison with other sulcus identification methods is highly desirable but not easily accomplished. Sulci were represented by very different representations that lead to different quality measures [252]. We compared our recognition results for those sulci (9 sulci) that were studied with some methods. Behnke et al [275], the probabilistic atlas method as proposed by [324] and a graph-based approach proposed by [252]. Behnke et al studied only five sulci, so we have compared the five common sulci with our method. The results of the

three methods were obtained in [252]. The average TPR, FPR, and SI using features (location, orientation and moment invariants) are tabulated in Table.1 (NGMA = Normal graph match algorithm) and (PGMA = Parallel graph match algorithm) for each sulcus. Our method achieves an average SI = 0.796 for the normal graph match algorithm and SI = 0.802 for the parallel graph match algorithm compared to other methods.

TABLE 5.1: Recognition results for our method (NGMA = Graph match algorithm, PGMA = Parallel graph match algorithm), Behnke 's method, Probabilistic atlas and Graph-based approach : central sulcus (CS), insula (INS), superior temporal sulcus (STS), superior frontal sulcus (SFS), cingulate sulcus (CIS), postcentral sulcus (PTS), precentral sulcus (PCS), callosal sulcus(CLS) and inferior frontal sulcus (IFS).

-	NGMA			PGMA			Behnke 's method			Probabilistic atlas			graph-based approach		
sulci	TPR	FPR	SI	TPR	FPR	SI	TPR	FPR	SI	TPR	FPR	SI	TPR	FPR	SI
CS	86	22	0.83	89.7	61.3	0.81	100	05.8	/	94.1	0.2	0.94	94.5	02	0.94
INS	83	28	0.76	90	65.3	0.78	92.0	06.0	/	88.9	0.6	0.89	90.0	0.6	0.90
STS	84	25	0.79	90	62.6	0.80	83.6	12.9	/	85.0	0.6	0.85	88.9	0.5	0.87
SFS	83.5	23	0.81	90.3	62.3	0.80	72.8	29.7	/	59.4	0.4	0.61	85.0	0.4	0.80
CIS	82	26	0.78	90.4	63.3	0.79	74.7	02.1	/	85.1	0.6	0.85	91.5	0.7	0.88
PTS	81	28	0.74	89.3	62.3	0.79	/	/	/	71.0	0.4	0.72	87.3	0.7	0.81
PCS	83	31	0.73	91	62.3	0.81	/	/	/	47.9	0.6	0.52	79.9	0.5	0.80
CLS	84.5	29	0.77	90.4	60.3	0.81	/	/	/	54.0	0.02	0.55	93.7	0.1	0.95
IFS	98	08	0.95	90.4	61	0.82	/	/	/	56.7	0.4	0.56	74.5	0.7	0.7
Avg	85	24	0.796	90.16	62.3	0.802	86.6	11.3	/	71.3	0.4	0.72	87.2	0.5	0.85

In Figure 5.7, we examined a comparison between the various estimated measurement values that we used (TP, FP, TN, FN, TPR, FPR, SI) for the central sulcus (CS). To further provide a visual impression of the identification results, we include identification results for a subject in Figure 5.8, and Figure 5.9, which are selected randomly from the subjects of the test.

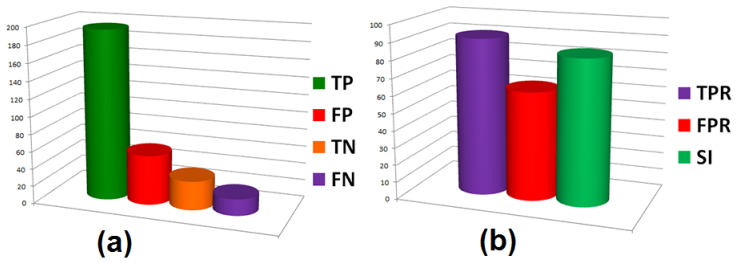

FIGURE 5.7: A random subject from the subjects of the test by parallel graph match algorithm (PGMA). (a) the values (TP,FP,TN,FN), (b) the values (TPR,FPR,SI), for central sulcus (CS).

In this work, we used several computer tools necessary to implement and test our approach. The Brainvisa tool is an open-source framework so that it allows to use of all the libraries implemented and to deploy new processing easily (segmentation and reconstruction of the mesh of the cortical surface). Anatomist (open source) offers tools to visualize the volumes of the

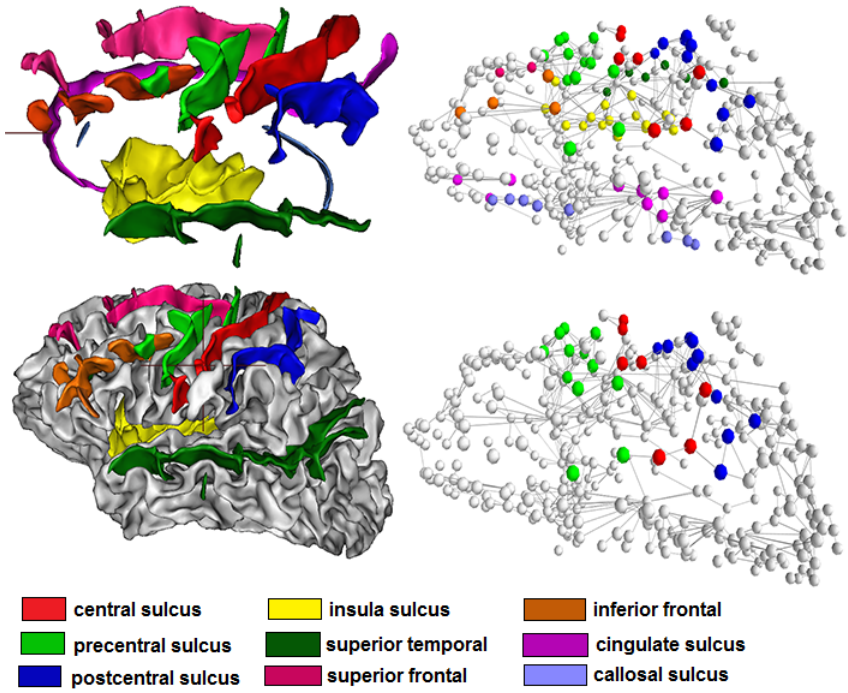

FIGURE 5.8: Automatic identification result for a subject by parallel graph matching algorithm (PGMA) (a).

brain from all angles of 3D images and manual annotation of cortical sulci (http://www.brainvisa.info). Mayavi package (http://mayavi.sourceforge.net/) for 3-dimensional visualization. The algorithms are implemented using Python Language and simulated by multithreaded programming.

5.5 Conclusion

We introduced the generalized median graph and graph matching strategy for automatic labeling of brain sulci with parallel and distributed solutions that uses prior statistical information about location, orientation, shape and neighborhood structure. These features are verified as effective for characterizing sulci. Labeling is recast as a graph matching problem between a model graph of sulcal features and their neighborhood relationships and a candidate graph composed of sulcal segments obtained in a specific dataset. The problem is solved using the generalized median graph (model graph) to represent the graphs of the training set and the graph matching to match the model graph and the candidate graph. To validate our method we used the similarity index that represents how well the automatically recognized region matches with expert identified sulci to guarantee an objective validation, manual labeling and segment splitting were performed independently and without referencing automatically splitting results.

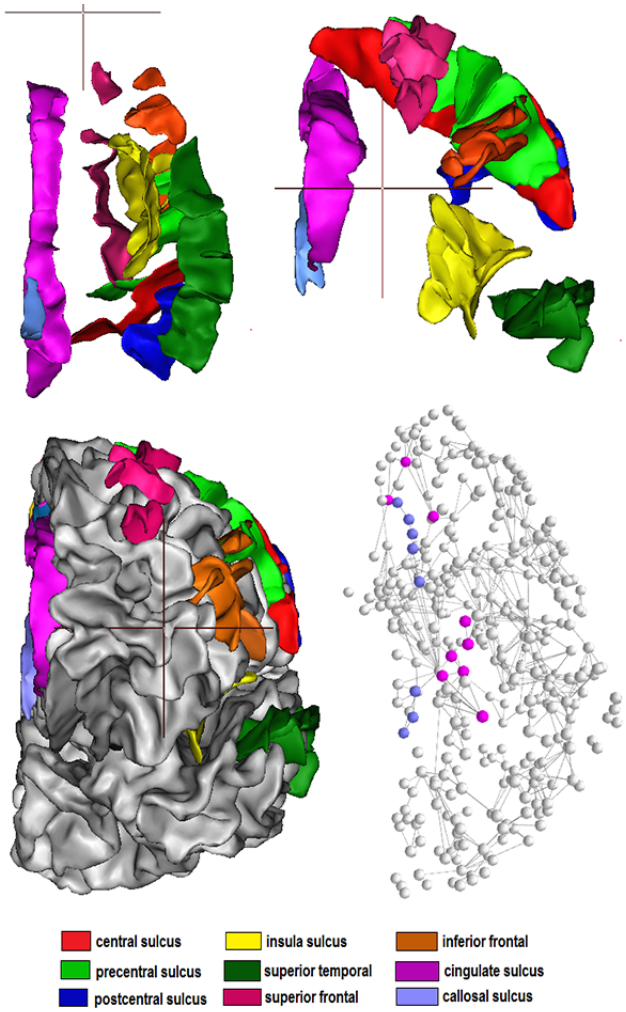

FIGURE 5.9: Automatic identification result for a subject by parallel graph matching algorithm (PGMA) (b).

Our approach is an initial attempt to combine these approaches and a resulting average similarity index of (SI = 0.802) is very encouraging. Our aim is to develop a system of automatic labeling of cortical sulci to improve the understanding of the structural organization of the human brain to help neuroscientists in their work.

Chapter 6

Graph Convolutional Networks and Functional Connectivity for Identification of Autism Spectrum Disorder

6.1 Introduction

Autism Spectrum Disorder (ASD) is a neurodevelopmental disorder of the brain characterized by socio-communicative impairments, social skills, imagination, stereotypic behaviors, and altered sensory processing [325], it affects 2.24% of children aged 3 to 17 years in the United States [326]. Early diagnosis of autistic individuals is considered very important and has been shown to improve the quality of life for children with ASD and their families [327]. In any case, it is not always easy to make a diagnosis of ASD. There is no lab test for it, so specialists depend on the behaviors of young children and listening to the concerns of their parents. There are many symptoms for ASD, some people with ASD have severe mental disabilities, others are exceptionally intelligent and ready to live independently.

The combination of machine learning (ML) algorithms and neuroimaging techniques have recently become one of the most influential tools in the detection of structural and functional brain abnormalities, and machine learning algorithms can be trained to aid in ASD diagnosis [328]. The aim of our study was to classify individuals with ASD and control individuals based on functional connectivity using resting-state functional magnetic resonance imaging (rs-fMRI) data. We used a large brain imaging collection data, the Autism Brain Imaging Data Exchange I (ABIDE I) and one of the graphs deep learning methods: graph convolutional networks (GCNs). Recent researches have demonstrated that graph-theory based complex network analysis provides a powerful framework for examining the topological properties of brain networks, where nodes represent brain regions and edges represent the functional connections between brain regions [329] [174].

The challenge of this study was to demonstrate the effectiveness of using graph convolutional networks (GCNs) and functional connectivity with a large multi-site dataset, such as ABIDE I, for discrimination of autism patients and healthy controls.

The rest of the chapter is organized as follows: we overview the related work in Section 2. Section 3 presents our approach; a brief description of the dataset we have used, graph convolutional networks, and the method used to classify subjects. In Section 4, we present the results and experiments that we have obtained. Concluding remarks, discussion, and avenues for future work are presented in Section 5.

6.2 Neuroimaging and Machine-learning for Disease Prediction

Machine learning in Neuroimaging using fMRI has been the subject of many studies in recent years and has achieved great success in diagnosing many structural or psychological brain diseases which makes it an important domain in the study of the human brain and understanding its behavior. With the availability of data sources, researchers have been encouraged to use deep learning methods in their research and the automatic diagnosis of brain diseases now provides many encouraging results for a realistic application to diagnose patients. The classification of patients with Alzheimer's disease [330] [331] [332] [333], Schizophrenia [334] [335] [336], Major Depression [337] [338], Borderline personality disorder [339], Social anxiety disorder [340], Antisocial personality disorder [341].

The related studies with our study which applied machine learning algorithms to autism spectrum disorder (ASD) and used ABIDE dataset also achieved very good results in the classification process of patients with ASD and healthy control subjects. We can refer to the following papers.

In [342], the authors presented a thorough evaluation of a generic framework that leverages both imaging and non-imaging information and can be used for brain analysis in large populations. This framework exploits Graph Convolutional Networks (GCNs) and involves representing populations as a sparse graph, where its nodes are associated with imaging-based feature vectors, while phenotypic information is integrated as edge weights. In [4], the authors proposed a novel 3D convolutional neural networks (CNN) approach which takes advantage of the full-resolution 3D spatial structure of rs-fMRI data and fits non-linear predictive models to overcome the limitations of traditional machine learning models for connectomes that often rely on region-based summary statistics and/or linear models. In [343], they applied deep learning algorithms to identify autism spectrum disorder (ASD) patients from a large brain imaging dataset, based solely on the patient's brain activation patterns. In [344], the authors

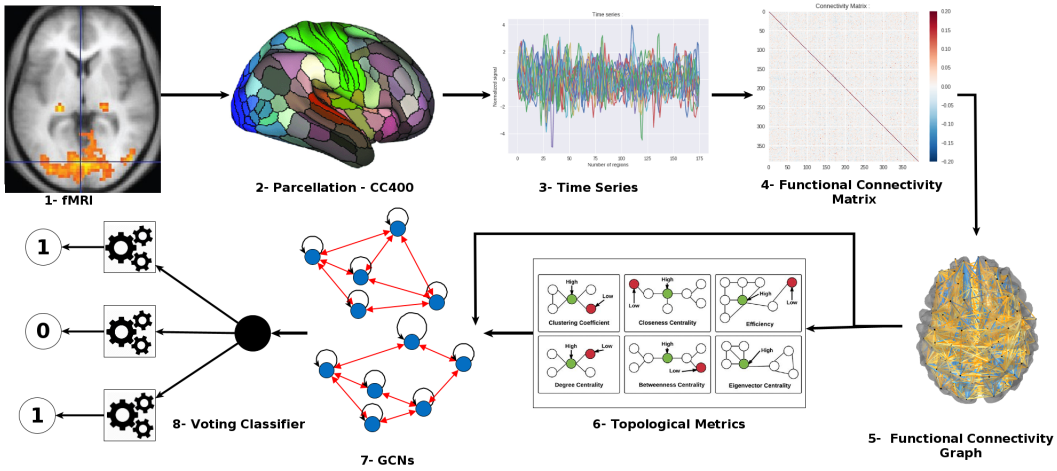

FIGURE 6.1: Our proposed approach where: 1- We used rs-fMRI data. 2- Parcellation of rs-fMRI data by CC400 atlas. 3- Extract the time series from brain regions. 4- Construction of the functional connectivity matrix. 5- build the functional connectivity graph. 6- Extract the topological metrics from the graph. 7- Using GCNs with topological metrics to create new relevant features. 8- using a voting classifier model to classify patients with ASD.

investigated pipelines that extract the most predictive biomarkers from the data, these pipelines build participant-specific connectomes from functionally-defined brain areas. Other articles use a limited number of subjects or focus on a specific age group or region, as in [345] where conditional random forest and random forest were used. In [346], they introduce a new biomarker extraction pipeline for ASD that relies on the use of graph theoretical metrics of fMRI-based functional connectivity to inform a support vector machine (SVM). In [347], they used machine learning to model the functional connectivity entropy relationship across cortical and subcortical resting-state networks (RSNs). In [348], they developed a deep transfer learning neural network (DTL-NN) framework for enhancing the classification of whole brain functional connectivity patterns. In [349], they utilized deep belief networks (DBNs), they used only 185 individuals ranging in age from 5 to 10 years.

6.3 Materials and Methods

We proposed a new approach to classify patients with autism spectrum disorder (ASD) that contain several steps, Fig.6.1. In the following subsections, we described each step in detail.

6.3.1 Dataset

Our study was accomplished using rs-fMRI data from the Autism Brain Imaging Data Exchange (ABIDE I) (http://fcon_1000.projects.nitrc.org/indi/abide/). ABIDE I is a multi-site consortium collected from 17 international sites. It is available for the scientific community and sharing resting state functional magnetic resonance imaging (rs-fMRI), anatomical and phenotypic information for each patient. The database consists of 539 from individuals with ASD (Autism Spectrum Disorder) and 573 from typical controls (ages 7-64 years, median 14.7 years across groups), for more information [343].

6.3.2 Data Preprocessing

The Preprocessed Connectomes Project (PCP) was used for getting preprocessed rs-fMRI data (DPARSF) which released preprocessed versions of ABIDE-I using several pipelines [350]. The pipeline of preprocessed rs-fMRI data performs slice time corrected, motion corrected, spatial smoothing, normalization and registration to a template space (MNI152). The signal noise was removed by motion parameters, CompCor with 5 components, applied a global signal regression and band pass filtering (0.01–0.1 Hz). In our experiments, we used ABIDE I multiple sites and the subject data that passed the quality assessment for all raters. The final size of the dataset we used is 774 subjects, comprising 379 subjects with ASD and 395 typical controls.

6.3.3 Extracting ROIs Time Series and Connectivity Matrix from an Atlas

ROIs (Region Of Interest) were extracted by using Craddock 400 (CC400) atlas which has (392) regions, then we extracted the mean time series for each region per each subject. From the time series that were extracted previously, we construct the functional connectivity matrix. The functional connectivity matrix is typically estimated using the correlation between time series, where each cell in the connectivity matrix contains a correlation coefficient which crosses of the correlation between two regions of the brain. We used Nilearn module for extracting ROIs, time series, and construction of the functional connectivity matrix. Nilearn is a Python module for fast and easy statistical learning on NeuroImaging data (https://nilearn.github.io/). The functional connectivity matrix is always fully connected and thus most probably contain spurious connections (i.e. false positives) that do not have a true neurobiological origin. Therefore, we had to use proportional thresholding of the functional connectivity matrix to reduce the number of edges and select only the significant edges using PyNets module. PyNets is a Fully-Automated Workflow for Reproducible Ensemble Graph Analysis of Functional and Structural Connectomes (https://pynets.readthedocs.io/).

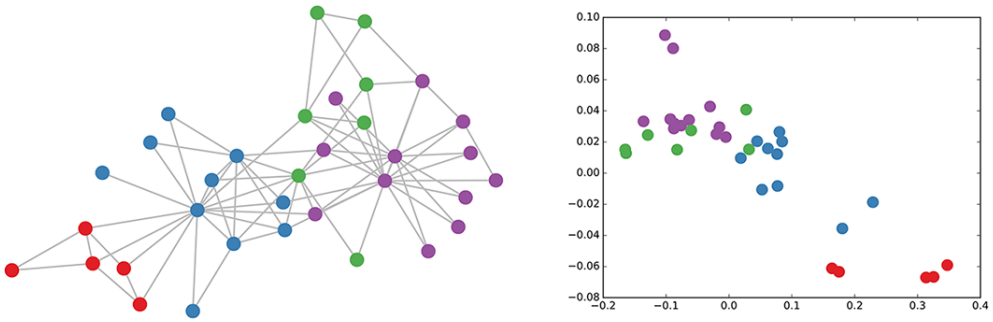

FIGURE 6.2: Left: Zachary's karate club network, colors denote communities obtained via modularity-based clustering. Right: Embeddings obtained from an untrained 3-layer GCN model with random weights applied to the karate club network. more details in [3].

Functional connectomes are commonly analyzed as sparse graphs, constructed by thresholding cross-correlations between regional neurophysiological signals. Thresholding generally retains the strongest edges (correlations), either by retaining edges surpassing a given absolute weight or by constraining the edge density [351] [352].

6.3.4 Graph Convolutional Networks

In the real world, there are several important datasets come in the form of graphs or networks like the World Wide Web, citation network, social networks, knowledge graphs, protein-interaction networks, bioinformatics, urban computing, and cyber-security, ... etc, so graph classification is an important problem in these fields but the problem with that is that graphs have a very complex structure which makes using machine learning or deep learning a challenging problem.

Graph convolutional networks (GCNs) are a powerful tool for machine learning on graphs when the data represented in the form of graphs. A good example of this is Zachary's karate club network which contains 34 nodes, connected by 154 (undirected and unweighted) edges [353]. Every node is labeled by one of four classes, obtained via modularity-based clustering [354], as illustrated in Fig.6.2. This simple example of GCNs provides insights into how the GCNs model can make use of the graph structure to learn embeddings that are useful for a classification task. Many papers have recently been published on the use of (GCNs) in many fields. Some papers focus to use specialized architectures for specific problems [355] [356] [357] [358] [359] [360] [361] [362] [363]. Some other papers tried to generalizing convolutional neural networks (CNNs) on graphs [364] [365] [366] [367]. A general graph representation learning framework for learning deep node and edge representations from large graphs [368]. In [3], the authors proposed a scalable approach for semi-supervised learning on graph structured data that is based on an efficient variant of convolutional neural networks which operate directly on graphs.

classification with graph convolutional networks

Before we go deeper into machine learning on (GCNs) let us define some notations used throughout this chapter. We represent a graph by $G = (V, E)$, V and E denote the set of nodes and the set of edges of G respectively and A its adjacency matrix, as a note we consider undirected graphs. Denote by D the diagonal node degree matrix and $X_{N\times M}$ is the feature matrix of the nodes (N is the number of nodes and M is the number of input features).

The graph convolutional networks classifier takes as input a set of graphs, then perform several operations as feature extraction, re-representation and in the end, gives us the class of each graph.

A naive approach to graph convolutional networks classification is to take the adjacency matrix A and feature matrix X, then concatenate them and feed them into deep neural networks. But the problem with that is that a huge number of parameters and needs to be re-trained if the number of nodes changes.

The model for learning a (GCNs) in each hidden layer can be written as :

$$H^{(l+1)} = f(H^{(l)}, A) \tag{6.1}$$

where $H^{(l)}$ denotes the $l^{(th)}$ layer in the network and $H^{(0)} = X$, f is a propagation rule.

In [3], they proposed a simplification of this model so that the convolution becomes :

$$H^{(l+1)} = \delta(\tilde{D}^{-\frac{1}{2}}\tilde{A}\tilde{D}^{-\frac{1}{2}}H^{(l)}W^{(l)}) \tag{6.2}$$

where $\tilde{A} = A + I_N$ is a re-normalization trick of adjacency matrix in which we add a self-connection to each node of the graph and I_N is the identity matrix. $\tilde{D}$ is the diagonal node degree matrix of $\tilde{A}$. $W^{(l)}$ is a weight matrix for the $l^{(th)}$ neural network layer. We will use this equation in the rest of this chapter.

6.3.5 Functional Connectivity Graph and Feature Selection

According to the functional connectivity matrix previously, we construct a functional connectivity graph, where the regions extracted from the cerebral atlas are represented by nodes in the graph and the correlation coefficient between two regions representing the weight of the edge that connects them.

Recent research has shown that graph theory based complex network analysis provides a powerful framework for examining the topological properties of brain networks, where nodes represent brain regions, and edges represent the functional connections between brain regions

[242] [174] [103] [369] [339]. Topological properties of brain networks can be derived at the large-scale of the whole brain, i.e. metrics on the entire graph; at the intermediate scale of several regions of the brain. It follows that the selection of the topological metrics is an important step that requires great attention. Depending on the nature of the neuroimaging experiment, the functional connections, and the thresholding method, some graph indices can result in being more appropriate than other ones [175].

In this study, we selected only six features for nodes (Betweenness Centrality, Clustering Coefficient, Squares Clustering Coefficient, Closeness Centrality, Eigenvector Centrality, Degree Centrality). The feature matrix for each subject becomes $X_{392\times6}$, where each column contains one of the features we have chosen. We also chose one kind of features for edges (Edge Betweenness Centrality) and we represent it in the form of a matrix $EBC_{392\times392}$ where $ebc_{ij} \neq 0$ if node *(i)* has a connection with node *(j)* and zero otherwise. In the end, we got the feature matrix $C_{392\times6}$ of each subject that was calculated using our proposed equation :

$$C = \tilde{D}^{-1} \times \tilde{A} \times FCM \times EBC \times X \tag{6.3}$$

where $FCM_{392\times392}$ is the functional connectivity matrix.

There may be significant differences in the mean functional connectivity between groups, as this can lead to differences that do not necessarily relate to topological reorganization but are due to underlying differences in connectivity strength [352] [351]. In Fig.6.3, we kept the five relevant features of the matrix C, and then showed them. where the x-axis represents the five feature categories per subject (the number of columns in the C matrix), the y-axis represents the 392-regions features for the five feature categories (C-matrix height), and the z-axis represents the functional connectivity values for every region in each of the feature categories. It also showed how our method can clearly separate two individuals, one is with ASD and the other is healthy. But the problem is that the subjects still intertwined. Some subjects with ASD have a high value of the feature matrix C, and others have less value as well as healthy subjects. This makes the classification process complex and therefore we will need an assistant classifier to complete the process.

6.3.6 Classification Method

In this study, we proposed a new method to classify our subjects. The graph convolutional networks approach was used for feature extraction but for the final classification we have to combine it with another classifier. We noted that the graph convolutional networks are a helpful method for feature extraction, Fig.6.3, which helped us in the classification process, and on the

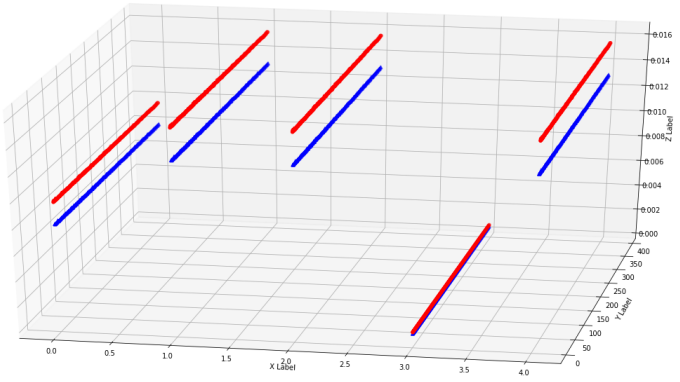

FIGURE 6.3: The features of matrix C which calculated by equation.3 of two subjects, where the red color indicates the individual with ASD and the blue color indicates the typical control. We note that the subjects are differentiated two by two but the problem with that is that it is difficult to separate them into two groups because of the overlap.

basis of this differentiation between the features of the studied subjects, we chose the voting classifier as a classifier in this study.

The voting classifier model combines multiple different models (multi-classifiers) into a single model, which is stronger than any of the individual models alone. It has demonstrated significant performance in enhancing the accuracy of predictions, It has been applied to a number of areas and impressive results have been achieved. In this paper, we used the voting classifier based on majority voting [370], which has been used majorly for prediction as the output of the classifier is the label with the highest number of votes from the base classifiers[370] [371]. The collection of basic classifiers we used in this study are: support vector machine (SVM), random forest and logistic regression classifier. We used python language and Scikit-learn library (`https://scikit-learn.org`) to implement this classifier.

We noticed that the extracted features (matrix C, Fig.6.3) were in the form of separate lines and each line containing N (number of nodes, here N = 392) points, so we had (392×5) features at last, to reduce the dimensionality of the output features representations we used the average of each line (5 features), then we generated a new feature matrix consisting of all polynomial combinations of the features. In the end, we got 21 features that we used with the majority voting classifier.

6.3.7 Parallel Method

Parallel programming is one of the common methods of intensive computing, big data, and complex problems to accelerate up calculations. One of the advantages of this method lies in our ability to perform parallel calculations. We calculated the matrix C of each subject

TABLE 6.1: Performance of different classifiers for classification of Autism Spectrum Disorder (ASD). Ridge Regression (Ridge), Support Vector Machine (SVM), Fully Connected Architecture (FCN), BrainNet Convolutional Neural Networks (BrainNet), 3D convolutional neural networks (3D-CNN) [4], and Graph Convolutional Networks (GCN).

-	Ridge	SVM	FCN	BrainNet	3D-CNN	**GCN**
accuracy %	70.2	69.4	71.0	71.3	71.7	**70.0**

independently and in parallel with other subjects before the start of the final classification process.

6.4 Results

In this study, we carried out two kinds of analysis based on the functional connectivity graph. Firstly, a graph convolutional networks approach was performed to extract the features of the healthy control group and patients with ASD. Secondly, a machine learning classifier was performed to classify subjects. We used the voting classifier and the best results we got after the multi-step training were (accuracy 70%, sensitivity 60%, specificity 80%). A comparison was effected between our approach and other approaches using (CC400) atlas and (ABIDE I) dataset as us, to validate the results we obtained and show that the method we have proposed by relying on graph convolutional networks is valid to be a competitive method for other methods in this area. The results are shown in Table.6.1. The results of other approaches can be obtained in [4]. The approaches that we compared our approach with them are: (Ridge Regression, Support Vector Machine, Fully Connected Architecture, BrainNet Convolutional Neural Networks, 3D convolutional neural networks) for more information about them see [4]. It has also been implemented the 3D convolution neural networks approach for CC200 atlas and it achieved an accuracy of 71.2%, [4]. In [343], they used the CC200 atlas too with deep learning (autoencoders) and they achieved a mean accuracy of 70%. In [342], the authors used an approach based on graph convolutional networks and they achieved an accuracy of 70.4%. In [344], the authors used an approach based on deriving reproducible biomarkers and they achieved an accuracy of 67%.

Experiments presented in this work were carried out using the High Performance Computing Platform IBNBADIS (`http://www.ibnbadis.cerist.dz`) provided by the Research Center on Scientific and Technical Information - CERIST (Algeria).

6.5 Discussion

In this study, we analyzed functional connectivity to identify autism spectrum disorders (ASD) using graph convolutional networks. In addition, we used a complex network analysis based on graph theory to characterize the global and regional topology in the networks of brain connectivity, which showed its ability to make a clear distinction between patients with ASD and healthy control subjects. The novelty of this study is using topological metrics and GCNs to create new relevant features of graphs that are helpful in the classification tasks.

This method can be executed in parallel and using all methods and tools of intensive computing or GPU and allows using many features to describe different brain regions and their connectivity or to describe the nodes and edges in the functional connectivity graph.

Although this is an efficient method, the calculation of the C matrix takes a long time (approximately 20 minutes for one subject). Its weakness lies in the complex calculations required for feature extraction as well as the complex network of functional connectivity graph that contains a large number of nodes and edges.

We used the Networkx package that does not deal with GPU, this has slowed down calculations and can be improved by using an efficient tool for graph theory calculations that allows manipulation of the GPU and using parallel algorithms.

6.6 Conclusion

In this study, we applied the graph convolutional networks (GCNs) and complex network measures on the resting-state fMRI data, where we used functional connectivity to classify patients with autism spectrum disorder (ASD) from the normal subjects. The dataset that was used by us in this study was (ABIDE I) with multi-site subjects. The results showed that graph convolutional networks are significantly more robust and accurate for classifying brain diseases as (ASD). The proposed approach in this study classified patients with ASD and normal subjects with accuracy of 70%. In addition, our experiments support and encourage us to generalize our proposed approach in this study to other brain diseases and develop this approach where we can adapt it with deep learning classifiers.

Chapter 7

Conclusion and Perspectives

MRI and fMRI are one of the most important medical imaging modalities. The main advantages of MRI and fMRI are high image quality, various tissue-contrast mechanisms, and the fact that are noninvasive and do not produce any harmful radiation. Analyzing the brain MRI and fMRI data is crucial to better understand the pathological mechanisms of complex brain diseases. In this context, graph theory is a powerful approach for the analysis of the brain network. Using the graph matching techniques, combined with powerful parallel and distributed algorithms, open new perspectives for the neuroimaging field.

In Chapters 1 to 4, we introduced an overview of brain anatomy, the main classical methods for preprocessing and analyzing both structural/functional magnetic resonance imaging of the brain and an overview of graph matching for analyzing brain network.

In this thesis, we developed two new approaches (chapters 5 and 6) for both MRI/fMRI analysis, which open new perspectives for taking advantage of the amount of data that is now available.

In the first approach (chapter 5), we introduced the generalized median graph and graph matching strategy for automatic labeling of brain sulci with parallel and distributed solutions that uses prior statistical information about location, orientation, shape, and neighborhood structure. Labeling is recast as a graph matching problem between a model graph of sulcal features and their neighborhood relationships and a candidate graph composed of sulcal. This approach was an initial attempt to combine these approaches and the result was very encouraging. In general, this work shows the path to future study that might try various topologies of structural brain networks, and to combine different modalities.

In the second approach (chapter 6), we applied the graph convolutional networks (GCNs) and complex network measures on the resting-state fMRI data, where we based on functional connectivity to classify patients with autism spectrum disorder (ASD) from the normal subjects. The results showed that graph convolutional networks are significantly more robust and accurate for classifying brain diseases as (ASD). In addition, our experiments support and encourage us to generalize our proposed approach in this study to other brain diseases and develop this approach where we can adapt it with deep learning classifiers.

A number of software contributions have been performed within the context of this thesis. All produced code was written in Python, using a combination of Brainvisa, Anatomist, Mayavi, Scikit-learn, Nilearn, PyNets for experiment design, efficient routine writing and model design, respectively. Software references are provided in the main section of this thesis.

Chapter 8

Bibliography

[1] Michael G Hart, Rolf JF Ypma, Rafael Romero-Garcia, Stephen J Price, and John Suckling. Graph theory analysis of complex brain networks: new concepts in brain mapping applied to neurosurgery. *Journal of neurosurgery*, 124(6):1665–1678, 2016.

[2] Jean-François Mangin, Matthieu Perrot, Grégory Operto, Arnaud Cachia, Clara Fischer, Julien Lefèvre, Denis Rivière, and CEA Neurospin. Sulcus identification and labeling. *Brain mapping: an encyclopedic reference. Academic Press: Elsevier, New York*, pages 365–371, 2015.

[3] Thomas N Kipf and Max Welling. Semi-supervised classification with graph convolutional networks. *arXiv preprint arXiv:1609.02907*, 2016.

[4] Meenakshi Khosla, Keith Jamison, Amy Kuceyeski, and Mert R Sabuncu. Ensemble learning with 3d convolutional neural networks for connectome-based prediction. *arXiv preprint arXiv:1809.06219*, 2018.

[5] Hichem Felouat and Saliha Oukid-Khouas. Graph matching and generalized median graph for automatic annotation of cortical sulci. In *2018 International Conference on Electrical Sciences and Technologies in Maghreb (CISTEM)*, pages 1–6. IEEE, 2018.

[6] Hichem Felouat and Saliha Oukid-Khouas. Graph matching approach and generalized median graph for automatic labeling of cortical sulci with parallel and distributed algorithms. *Cognitive Systems Research*, 54:62–73, 2019.

[7] Hichem Felouat and Saliha Oukid-Khouas. Graph convolutional networks and functional connectivity for identification of autism spectrum disorder. In *2020 Second International Conference on Embedded & Distributed Systems (EDiS)*, pages 27–32. IEEE, 2020.

[8] Fo Bloch, WW Hansen, and Martin Packard. Physics nobel price 1952. *Phys. Rev*, 69:127, 1946.

[9] Edward M Purcell, H Co Torrey, and Robert V Pound. Resonance absorption by nuclear magnetic moments in a solid. *Physical review*, 69(1-2):37, 1946.

[10] Jan Petr. Parallel magnetic resonance imaging reconstruction. *Prague: Czech Technical University*, 2005.

[11] Mark A Brown, Richard C Semelka, and Brian M Dale. *MRI: basic principles and applications*. John Wiley & Sons, 2015.

[12] Paul C Lauterbur et al. Image formation by induced local interactions: examples employing nuclear magnetic resonance. 1973.

[13] Anil Kumar, Dieter Welti, and Richard R Ernst. Nmr fourier zeugmatography. *Journal of Magnetic Resonance (1969)*, 18(1):69–83, 1975.

[14] DR Dance, S Christofides, ADA Maidment, ID McLean, and KH Ng. Diagnostic radiology physics: A handbook for teachers and students. endorsed by: American association of physicists in medicine, asia-oceania federation of organizations for medical physics, european federation of organisations for medical physics. 2014.

[15] David Moratal, A Valles-Luch, Luis Martí-Bonmatí, and Marijn E Brummer. k-space tutorial: an mri educational tool for a better understanding of k-space. *Biomedical imaging and intervention journal*, 4(1), 2008.

[16] Mahmood Qureshi, Muhammad Kaleem, and Hammad Omer. Journey through k-space: an interactive educational tool. 2017.

[17] Stig Ljunggren. Imaging methods. *Journal of Magnetic Resonance*, 54:338–343, 1983.

[18] Qing-San Xiang and R Mark Henkelman. K-space description for mr imaging of dynamic objects. *Magnetic resonance in medicine*, 29(3):422–428, 1993.

[19] J Hennig. K-space sampling strategies. *European radiology*, 9(6):1020–1031, 1999.

[20] Cynthia B Paschal and H Douglas Morris. K-space in the clinic. *Journal of Magnetic Resonance Imaging: An Official Journal of the International Society for Magnetic Resonance in Medicine*, 19(2):145–159, 2004.

[21] Martin J Graves and Donald G Mitchell. Body mri artifacts in clinical practice: a physicist's and radiologist's perspective. *Journal of Magnetic Resonance Imaging*, 38(2):269–287, 2013.

[22] Srinivasan Kathiravan and Jagannathan Kanakaraj. A review on potential issues and challenges in mr imaging. *The Scientific World Journal*, 2013, 2013.

[23] LJ Erasmus, D Hurter, M Naudé, HG Kritzinger, and S Acho. A short overview of mri artefacts. *SA Journal of Radiology*, 8(2), 2004.

[24] Mehdi Poustchi-Amin, Scott A Mirowitz, Jeffrey J Brown, Robert C McKinstry, and Tao Li. Principles and applications of echo-planar imaging: a review for the general radiologist. *Radiographics*, 21(3):767–779, 2001.

[25] Katarzyna Krupa and Monika Bekiesińska-Figatowska. Artifacts in magnetic resonance imaging. *Polish journal of radiology*, 80:93, 2015.

[26] Seiji Ogawa, Tso-Ming Lee, Alan R Kay, and David W Tank. Brain magnetic resonance imaging with contrast dependent on blood oxygenation. *proceedings of the National Academy of Sciences*, 87(24):9868–9872, 1990.

[27] Seiji Ogawa, Tso-Ming Lee, Asha S Nayak, and Paul Glynn. Oxygenation-sensitive contrast in magnetic resonance image of rodent brain at high magnetic fields. *Magnetic resonance in medicine*, 14(1):68–78, 1990.

[28] Frank G Hillary and John DeLuca. *Functional neuroimaging in clinical populations*. Guilford Press, 2007.

[29] Andres Hoyos Idrobo. Ensembles of models in fmri : stable learning in large-scale settings. (ensembles des modeles en fmri : l'apprentissage stable à grande échelle). 2017.

[30] Richard B Buxton. *Introduction to functional magnetic resonance imaging: principles and techniques*. Cambridge university press, 2009.

[31] Seiji Ogawa, David W Tank, Ravi Menon, Jutta M Ellermann, Seong G Kim, Helmut Merkle, and Kamil Ugurbil. Intrinsic signal changes accompanying sensory stimulation: functional brain mapping with magnetic resonance imaging. *Proceedings of the National Academy of Sciences*, 89(13):5951–5955, 1992.

[32] Jaime Arias, Philippe Ciuciu, Michel Dojat, Florence Forbes, Aina Frau-Pascual, Thomas Perret, and Jan Warnking. Pyhrf: A python library for the analysis of fmri data based on local estimation of the hemodynamic response function. 2017.

[33] Bharat Biswal, F Zerrin Yetkin, Victor M Haughton, and James S Hyde. Functional connectivity in the motor cortex of resting human brain using echo-planar mri. *Magnetic resonance in medicine*, 34(4):537–541, 1995.

[34] H Lv, Zhenchang Wang, E Tong, LM Williams, G Zaharchuk, M Zeineh, AN Goldstein-Piekarski, TM Ball, C Liao, and M Wintermark. Resting-state functional mri: everything that nonexperts have always wanted to know. *American Journal of Neuroradiology*, 39(8):1390–1399, 2018.

[35] Kalina Christoff, Alan M Gordon, Jonathan Smallwood, Rachelle Smith, and Jonathan W Schooler. Experience sampling during fmri reveals default network and executive system contributions to mind wandering. *Proceedings of the National Academy of Sciences*, 106(21):8719–8724, 2009.

[36] Michael G. Hart, Stephen J. Price, and John Suckling. Functional connectivity networks for preoperative brain mapping in neurosurgery. *Journal of Neurosurgery JNS*, 126(6), 2016.

[37] Audrey Vanhaudenhuyse, Quentin Noirhomme, Luaba J-F Tshibanda, Marie-Aurelie Bruno, Pierre Boveroux, Caroline Schnakers, Andrea Soddu, Vincent Perlbarg, Didier Ledoux, Jean-François Brichant, et al. Default network connectivity reflects the level of consciousness in non-communicative brain-damaged patients. *Brain*, 133(1):161–171, 2009.

[38] Heng Huang, Xintao Hu, Yu Zhao, Milad Makkie, Qinglin Dong, Shijie Zhao, Lei Guo, and Tianming Liu. Modeling task fmri data via deep convolutional autoencoder. *IEEE transactions on medical imaging*, 37(7):1551–1561, 2017.

[39] Robert Cox, John Ashburner, Hester Breman, Kate Fissell, Christian Haselgrove, Colin Holmes, Jack Lancaster, David Rex, Stephen Smith, Jeffrey Woodward, et al. A (sort of) new image data format standard: Nifti-1: We 150. *Neuroimage*, 22, 2004.

[40] J Mohan, V Krishnaveni, and Yanhui Guo. A survey on the magnetic resonance image denoising methods. *Biomedical signal processing and control*, 9:56–69, 2014.

[41] José V Manjón. Mri preprocessing. In *Imaging Biomarkers*, pages 53–63. Springer, 2017.

[42] Arno Klein and Jason Tourville. 101 labeled brain images and a consistent human cortical labeling protocol. *Frontiers in neuroscience*, 6:171, 2012.

[43] Hannu Huhdanpaa, Darryl H Hwang, Gregory G Gasparian, Michael T Booker, Yong Cen, Alexander Lerner, Orest B Boyko, John L Go, Paul E Kim, Anandh Rajamohan, et al. Image coregistration: Quantitative processing framework for the assessment of brain lesions. *Journal of digital imaging*, 27(3):369–379, 2014.

[44] Kaihua Zhang, Lei Zhang, Kin-Man Lam, and David Zhang. A local active contour model for image segmentation with intensity inhomogeneity. *arXiv preprint arXiv:1305.7053*, 2013.

[45] Chunming Li, Chenyang Xu, Adam W Anderson, and John C Gore. Mri tissue classification and bias field estimation based on coherent local intensity clustering: A unified energy minimization framework. In *International conference on information processing in medical imaging*, pages 288–299. Springer, 2009.

[46] Florent Ségonne, Anders M Dale, Evelina Busa, Maureen Glessner, David Salat, Horst K Hahn, and Bruce Fischl. A hybrid approach to the skull stripping problem in mri. *Neuroimage*, 22(3):1060–1075, 2004.

[47] Russell T Shinohara, Elizabeth M Sweeney, Jeff Goldsmith, Navid Shiee, Farrah J Mateen, Peter A Calabresi, Samson Jarso, Dzung L Pham, Daniel S Reich, Ciprian M Crainiceanu, et al. Statistical normalization techniques for magnetic resonance imaging. *NeuroImage: Clinical*, 6:9–19, 2014.

[48] Xiaofei Sun, Lin Shi, Yishan Luo, Wei Yang, Hongpeng Li, Peipeng Liang, Kuncheng Li, Vincent CT Mok, Winnie CW Chu, and Defeng Wang. Histogram-based normalization technique on human brain magnetic resonance images from different acquisitions. *Biomedical engineering online*, 14(1):73, 2015.

[49] Richard Nordenskjöld, Elna-Marie Larsson, Håkan Ahlström, Lars Johansson, and Joel Kullberg. Automated interhemispheric surface extraction in t1-weighted mri using intensity and symmetry information. *Journal of neuroscience methods*, 222:97–105, 2014.

[50] Ivana Despotović, Bart Goossens, and Wilfried Philips. Mri segmentation of the human brain: challenges, methods, and applications. *Computational and mathematical methods in medicine*, 2015, 2015.

[51] Xiao Han, Dzung L Pham, Duygu Tosun, Maryam E Rettmann, Chenyang Xu, and Jerry L Prince. Cruise: cortical reconstruction using implicit surface evolution. *NeuroImage*, 23(3):997–1012, 2004.

[52] Tianming Liu, Jingxin Nie, Ashley Tarokh, Lei Guo, and Stephen TC Wong. Reconstruction of central cortical surface from brain mri images: method and application. *NeuroImage*, 40(3):991–1002, 2008.

[53] Andrés Larroza, Vicente Bodí, David Moratal, et al. Texture analysis in magnetic resonance imaging: review and considerations for future applications. *Assessment of cellular and organ function and dysfunction using direct and derived MRI methodologies*, pages 75–106, 2016.

[54] R Cameron Craddock, G Andrew James, Paul E Holtzheimer III, Xiaoping P Hu, and Helen S Mayberg. A whole brain fmri atlas generated via spatially constrained spectral clustering. *Human brain mapping*, 33(8):1914–1928, 2012.

[55] Matthew F Glasser, Timothy S Coalson, Emma C Robinson, Carl D Hacker, John Harwell, Essa Yacoub, Kamil Ugurbil, Jesper Andersson, Christian F Beckmann, Mark Jenkinson, et al. A multi-modal parcellation of human cerebral cortex. *Nature*, 536(7615):171, 2016.

[56] Guillaume Auzias, Lucile Brun, Christine Deruelle, and Olivier Coulon. Deep sulcal landmarks: Algorithmic and conceptual improvements in the definition and extraction of sulcal pits. *Neuroimage*, 111:12–25, 2015.

[57] Nicholas J Tustison, Philip A Cook, Arno Klein, Gang Song, Sandhitsu R Das, Jeffrey T Duda, Benjamin M Kandel, Niels van Strien, James R Stone, James C Gee, et al. Large-scale evaluation of ants and freesurfer cortical thickness measurements. *Neuroimage*, 99:166–179, 2014.

[58] Kiho Im, Michael J Paldino, Annapurna Poduri, Olaf Sporns, and P Ellen Grant. Altered white matter connectivity and network organization in polymicrogyria revealed by individual gyral topology-based analysis. *Neuroimage*, 86:182–193, 2014.

[59] Syoji Kobashi, Shingo Sueyoshi, Katsuya Kondo, and Yutaka Hata. Automated gyrus labeling using knowledge-based fuzzy inference systems. In *2007 IEEE International Conference on System of Systems Engineering*, pages 1–6. IEEE, 2007.

[60] Maxime Boucher, Alan Evans, and Kaleem Siddiqi. Oriented morphometry of folds on surfaces. In *International Conference on Information Processing in Medical Imaging*, pages 614–625. Springer, 2009.

[61] Peter Kochunov, Paul M Thompson, Thomas R Coyle, Jack L Lancaster, Valeria Kochunov, Donal Royall, Jean-Fransçois Mangin, Denis Riviere, and Peter T Fox. Relationship among neuroimaging indices of cerebral health during normal aging. *Human brain mapping*, 29(1):36–45, 2008.

[62] Kamel Aloui, Amine Naït-Ali, and Mohamed Saber Naceur. Characterization of a human brain cortical surface mesh using discrete curvature classification and digital elevation model. *Journal of Biomedical Science and Engineering*, 5(03):133, 2012.

[63] VP Rathi and S Palani. Brain tumor mri image classification with feature selection and extraction using linear discriminant analysis. *arXiv preprint arXiv:1208.2128*, 2012.

[64] Brijesha D Rao and Mukesh M Goswami. A comprehensive study of features used for brian tumor detection and segmentation from mr images. In *2017 Innovations in Power and Advanced Computing Technologies (i-PACT)*, pages 1–6. IEEE, 2017.

[65] Nilesh Bhaskarrao Bahadure, Arun Kumar Ray, and Har Pal Thethi. Image analysis for mri based brain tumor detection and feature extraction using biologically inspired bwt and svm. *International journal of biomedical imaging*, 2017, 2017.

[66] Jose Bernal, Kaisar Kushibar, Daniel S Asfaw, Sergi Valverde, Arnau Oliver, Robert Martí, and Xavier Lladó. Deep convolutional neural networks for brain image analysis

on magnetic resonance imaging: a review. *Artificial intelligence in medicine*, 95:64–81, 2019.

[67] Yong-Ku Kim and Kyoung-Sae Na. Application of machine learning classification for structural brain mri in mood disorders: Critical review from a clinical perspective. *Progress in Neuro-Psychopharmacology and Biological Psychiatry*, 80:71–80, 2018.

[68] Talha Khan Burki. Predicting lung cancer prognosis using machine learning. *The Lancet Oncology*, 17(10):e421, 2016.

[69] Evanthia E Tripoliti, Theofilos G Papadopoulos, Georgia S Karanasiou, Katerina K Naka, and Dimitrios I Fotiadis. Heart failure: diagnosis, severity estimation and prediction of adverse events through machine learning techniques. *Computational and structural biotechnology journal*, 15:26–47, 2017.

[70] Rizhen Wei, Chuhan Li, Noa Fogelson, and Ling Li. Prediction of conversion from mild cognitive impairment to alzheimer's disease using mri and structural network features. *Frontiers in aging neuroscience*, 8:76, 2016.

[71] Jonathan Young, Marc Modat, Manuel J Cardoso, Alex Mendelson, Dave Cash, Sebastien Ourselin, Alzheimer's Disease Neuroimaging Initiative, et al. Accurate multimodal probabilistic prediction of conversion to alzheimer's disease in patients with mild cognitive impairment. *NeuroImage: Clinical*, 2:735–745, 2013.

[72] Lara C Foland-Ross, Matthew D Sacchet, Gautam Prasad, Brooke Gilbert, Paul M Thompson, and Ian H Gotlib. Cortical thickness predicts the first onset of major depression in adolescence. *International Journal of Developmental Neuroscience*, 46:125–131, 2015.

[73] Konstantinos Kamnitsas, Christian Ledig, Virginia FJ Newcombe, Joanna P Simpson, Andrew D Kane, David K Menon, Daniel Rueckert, and Ben Glocker. Efficient multi-scale 3d cnn with fully connected crf for accurate brain lesion segmentation. *Medical image analysis*, 36:61–78, 2017.

[74] Mohammad Havaei, Axel Davy, David Warde-Farley, Antoine Biard, Aaron Courville, Yoshua Bengio, Chris Pal, Pierre-Marc Jodoin, and Hugo Larochelle. Brain tumor segmentation with deep neural networks. *Medical image analysis*, 35:18–31, 2017.

[75] Sérgio Pereira, Adriano Pinto, Victor Alves, and Carlos A Silva. Brain tumor segmentation using convolutional neural networks in mri images. *IEEE transactions on medical imaging*, 35(5):1240–1251, 2016.

[76] Khalid Usman and Kashif Rajpoot. Brain tumor classification from multi-modality mri using wavelets and machine learning. *Pattern Analysis and Applications*, 20(3):871–881, 2017.

[77] Christian Salvatore, Antonio Cerasa, Isabella Castiglioni, F Gallivanone, A Augimeri, M Lopez, G Arabia, M Morelli, MC Gilardi, and A Quattrone. Machine learning on brain mri data for differential diagnosis of parkinson's disease and progressive supranuclear palsy. *Journal of Neuroscience Methods*, 222:230–237, 2014.

[78] Amicie de Pierrefeu, Tommy Löfstedt, C Laidi, Fouad Hadj-Selem, Julie Bourgin, Tomas Hajek, Filip Spaniel, Marian Kolenic, Philippe Ciuciu, Nora Hamdani, et al. Identifying a neuroanatomical signature of schizophrenia, reproducible across sites and stages, using machine learning with structured sparsity. *Acta Psychiatrica Scandinavica*, 138(6):571–580, 2018.

[79] Sergi Valverde, Mariano Cabezas, Eloy Roura, Sandra González-Villà, Deborah Pareto, Joan C Vilanova, Lluís Ramió-Torrentà, Àlex Rovira, Arnau Oliver, and Xavier Lladó. Improving automated multiple sclerosis lesion segmentation with a cascaded 3d convolutional neural network approach. *NeuroImage*, 155:159–168, 2017.

[80] Tom Brosch, Lisa YW Tang, Youngjin Yoo, David KB Li, Anthony Traboulsee, and Roger Tam. Deep 3d convolutional encoder networks with shortcuts for multiscale feature integration applied to multiple sclerosis lesion segmentation. *IEEE transactions on medical imaging*, 35(5):1229–1239, 2016.

[81] Shuang Gao, Vince D Calhoun, and Jing Sui. Machine learning in major depression: From classification to treatment outcome prediction. *CNS neuroscience & therapeutics*, 24(11):1037–1052, 2018.

[82] Ronny Redlich, Nils Opel, Dominik Grotegerd, Katharina Dohm, Dario Zaremba, Christian Bürger, Sandra Münker, Lisa Mühlmann, Patricia Wahl, Walter Heindel, et al. Prediction of individual response to electroconvulsive therapy via machine learning on structural magnetic resonance imaging data. *JAMA psychiatry*, 73(6):557–564, 2016.

[83] F Kurth, E Luders, and C Gaser. Voxel-based morphometry. *Brain Mapping*, 1:345–349, 2015.

[84] Shihui Chen, Jian Zhang, Xiaolei Ruan, Kan Deng, Jianing Zhang, Dongfang Zou, Xiaoming He, Feng Li, Guo Bin, Hongwu Zeng, et al. Voxel-based morphometry analysis and machine learning based classification in pediatric mesial temporal lobe epilepsy with hippocampal sclerosis. *Brain Imaging and Behavior*, pages 1–10, 2019.

[85] Yasmeen Farouk, Sherine Rady, and Hossam Faheem. Statistical features and voxel-based morphometry for alzheimer's disease classification. In *2018 9th International Conference on Information and Communication Systems (ICICS)*, pages 133–138. IEEE, 2018.

[86] Ali K Bourisly, Ahmed El-Beltagi, Jigi Cherian, Grace Gejo, Abrar Al-Jazzaf, and Mohammad Ismail. A voxel-based morphometric magnetic resonance imaging study of the brain detects age-related gray matter volume changes in healthy subjects of 21–45 years old. *The neuroradiology journal*, 28(5):450–459, 2015.

[87] Hiroshi Matsuda. Voxel-based morphometry of brain mri in normal aging and alzheimer's disease. *Aging and disease*, 4(1):29, 2013.

[88] Jennifer L Whitwell. Voxel-based morphometry: an automated technique for assessing structural changes in the brain. *Journal of Neuroscience*, 29(31):9661–9664, 2009.

[89] IC Wright, PK McGuire, J-B Poline, JM Travere, RM Murray, CD Frith, RSJ Frackowiak, and KJ Friston. A voxel-based method for the statistical analysis of gray and white matter density applied to schizophrenia. *Neuroimage*, 2(4):244–252, 1995.

[90] John Ashburner and Karl J Friston. Voxel-based morphometry—the methods. *Neuroimage*, 11(6):805–821, 2000.

[91] Samrah Ahmed, Clare Loane, Sara Bartels, Giovanna Zamboni, Clare Mackay, Ian Baker, Masud Husain, Sian Thompson, Michael Hornberger, and Christopher Butler. Lateral parietal contributions to memory impairment in posterior cortical atrophy. *NeuroImage: Clinical*, 20:252–259, 2018.

[92] Alexandre Savio, M Teresa García-Sebastián, D Chyzyk, Carmen Hernández, Manuel Graña, A Sistiaga, A LóPez De Munain, and Jorge Villanúa. Neurocognitive disorder detection based on feature vectors extracted from vbm analysis of structural mri. *Computers in biology and medicine*, 41(8):600–610, 2011.

[93] G Castellano, L Bonilha, LM Li, and F Cendes. Texture analysis of medical images. *Clinical radiology*, 59(12):1061–1069, 2004.

[94] Jaber Juntu, Jan Sijbers, Steve De Backer, Jeny Rajan, and Dirk Van Dyck. Machine learning study of several classifiers trained with texture analysis features to differentiate benign from malignant soft-tissue tumors in t1-mri images. *Journal of Magnetic Resonance Imaging: An Official Journal of the International Society for Magnetic Resonance in Medicine*, 31(3):680–689, 2010.

[95] Evangelia I Zacharaki, Sumei Wang, Sanjeev Chawla, Dong Soo Yoo, Ronald Wolf, Elias R Melhem, and Christos Davatzikos. Classification of brain tumor type and grade using mri texture and shape in a machine learning scheme. *Magnetic Resonance in*

Medicine: An Official Journal of the International Society for Magnetic Resonance in Medicine, 62(6):1609–1618, 2009.

[96] MS De Oliveira, MLF Balthazar, A D'abreu, CL Yasuda, BP Damasceno, F Cendes, and G Castellano. Mr imaging texture analysis of the corpus callosum and thalamus in amnestic mild cognitive impairment and mild alzheimer disease. *American Journal of Neuroradiology*, 32(1):60–66, 2011.

[97] TA Santos, CEB Maistro, CB Silva, MS Oliveira, MC França, and G Castellano. Mri texture analysis reveals bulbar abnormalities in friedreich ataxia. *American Journal of Neuroradiology*, 36(12):2214–2218, 2015.

[98] Zahra Karimaghaloo, Hassan Rivaz, Douglas L Arnold, D Louis Collins, and Tal Arbel. Temporal hierarchical adaptive texture crf for automatic detection of gadolinium-enhancing multiple sclerosis lesions in brain mri. *IEEE transactions on medical imaging*, 34(6):1227–1241, 2014.

[99] Khan M Iftekharuddin, Shaheen Ahmed, and Jakir Hossen. Multiresolution texture models for brain tumor segmentation in mri. In *2011 Annual International Conference of the IEEE Engineering in Medicine and Biology Society*, pages 6985–6988. IEEE, 2011.

[100] Robert M Haralick et al. Statistical and structural approaches to texture. *Proceedings of the IEEE*, 67(5):786–804, 1979.

[101] Olivier Yu, Nathalie Parizel, Laure Pain, Blandine Guignard, Bernard Eclancher, Yres Mauss, and Daniel Grucker. Texture analysis of brain mri evidences the amygdala activation by nociceptive stimuli under deep anesthesia in the propofol–formalin rat model. *Magnetic resonance imaging*, 25(1):144–146, 2007.

[102] Olaf Sporns. From simple graphs to the connectome: networks in neuroimaging. *Neuroimage*, 62(2):881–886, 2012.

[103] Mikail Rubinov and Olaf Sporns. Complex network measures of brain connectivity: uses and interpretations. *Neuroimage*, 52(3):1059–1069, 2010.

[104] Zhijiang Wang, Zhengjia Dai, Gaolang Gong, Changsong Zhou, and Yong He. Understanding structural-functional relationships in the human brain: a large-scale network perspective. *The Neuroscientist*, 21(3):290–305, 2015.

[105] Fani Deligianni, Gaël Varoquaux, Bertrand Thirion, David J Sharp, Christian Ledig, Robert Leech, and Daniel Rueckert. A framework for inter-subject prediction of functional connectivity from structural networks. *IEEE transactions on medical imaging*, 32(12):2200–2214, 2013.

[106] Shu-Hsien Chu, Keshab K Parhi, and Christophe Lenglet. Function-specific and enhanced brain structural connectivity mapping via joint modeling of diffusion and functional mri. *Scientific reports*, 8(1):4741, 2018.

[107] Maxim Zaitsev, Burak Akin, Pierre LeVan, and Benjamin R Knowles. Prospective motion correction in functional mri. *Neuroimage*, 154:33–42, 2017.

[108] Xiaoping Hu, Tuong Huu Le, Todd Parrish, and Peter Erhard. Retrospective estimation and correction of physiological fluctuation in functional mri. *Magnetic resonance in medicine*, 34(2):201–212, 1995.

[109] Peter Jezzard. Physiological noise: strategies for correction. *Functional MRI*, pages 1173–1181, 2000.

[110] Michael K Stehling, Robert Turner, and Peter Mansfield. Echo-planar imaging: magnetic resonance imaging in a fraction of a second. *Science*, 254(5028):43–50, 1991.

[111] David Parker, Xueqing Liu, and Qolamreza R Razlighi. Optimal slice timing correction and its interaction with fmri parameters and artifacts. *Medical image analysis*, 35:434–445, 2017.

[112] PR Bannister, SM Smith, M Brady, and M Jenkinson. Spatio-temporal realignment of fmri data. In *Eighth Int. Conf. on Functional Mapping of the Human Brain*, 2002.

[113] André Collignon, Frederik Maes, Dominique Delaere, Dirk Vandermeulen, Paul Suetens, and Guy Marchal. Automated multi-modality image registration based on information theory. In *Information processing in medical imaging*, volume 3, pages 263–274, 1995.

[114] John Ashburner, Karl Friston, et al. The role of registration and spatial normalisation in detecting activations in functional imaging. *CLINICAL MRI*, 7(1):26–27, 1997.

[115] Geoffrey M Boynton, Stephen A Engel, Gary H Glover, and David J Heeger. Linear systems analysis of functional magnetic resonance imaging in human v1. *Journal of Neuroscience*, 16(13):4207–4221, 1996.

[116] Ron D Frostig, Edmund E Lieke, Daniel Y Ts'o, and Amiram Grinvald. Cortical functional architecture and local coupling between neuronal activity and the microcirculation revealed by in vivo high-resolution optical imaging of intrinsic signals. *Proceedings of the National Academy of Sciences*, 87(16):6082–6086, 1990.

[117] Martin A Lindquist, Ji Meng Loh, Lauren Y Atlas, and Tor D Wager. Modeling the hemodynamic response function in fmri: efficiency, bias and mis-modeling. *Neuroimage*, 45(1):S187–S198, 2009.

[118] Gary H Glover. Deconvolution of impulse response in event-related bold fmri1. *Neuroimage*, 9(4):416–429, 1999.

[119] Jingyuan E Chen and Gary H Glover. Functional magnetic resonance imaging methods. *Neuropsychology review*, 25(3):289–313, 2015.

[120] Peter A Bandettini, Andrzej Jesmanowicz, Eric C Wong, and James S Hyde. Processing strategies for time-course data sets in functional mri of the human brain. *Magnetic resonance in medicine*, 30(2):161–173, 1993.

[121] Karl J Friston, Andrew P Holmes, Keith J Worsley, J-P Poline, Chris D Frith, and Richard SJ Frackowiak. Statistical parametric maps in functional imaging: a general linear approach. *Human brain mapping*, 2(4):189–210, 1994.

[122] Martin M Monti. Statistical analysis of fmri time-series: a critical review of the glm approach. *Frontiers in human neuroscience*, 5:28, 2011.

[123] Jean-Baptiste Poline and Matthew Brett. The general linear model and fmri: does love last forever? *Neuroimage*, 62(2):871–880, 2012.

[124] Xiaowei Zhuang, Zhengshi Yang, Karthik R Sreenivasan, Virendra R Mishra, Tim Curran, Rajesh Nandy, and Dietmar Cordes. Multivariate group-level analysis for task fmri data with canonical correlation analysis. *NeuroImage*, 194:25–41, 2019.

[125] Martin A Lindquist et al. The statistical analysis of fmri data. *Statistical science*, 23(4):439–464, 2008.

[126] Babak A Ardekani and Iwao Kanno. Statistical methods for detecting activated regions in functional mri of the brain. *Magnetic Resonance Imaging*, 16(10):1217–1225, 1998.

[127] David Colquhoun. An investigation of the false discovery rate and the misinterpretation of p-values. *Royal Society open science*, 1(3):140216, 2014.

[128] Thomas E Nichols. Multiple testing corrections, nonparametric methods, and random field theory. *Neuroimage*, 62(2):811–815, 2012.

[129] Keith J Worsley, Alan C Evans, Sean Marrett, and P Neelin. A three-dimensional statistical analysis for cbf activation studies in human brain. *Journal of Cerebral Blood Flow & Metabolism*, 12(6):900–918, 1992.

[130] Thomas E Nichols and Andrew P Holmes. Nonparametric permutation tests for functional neuroimaging: a primer with examples. *Human brain mapping*, 15(1):1–25, 2002.

[131] Christopher R Genovese, Nicole A Lazar, and Thomas Nichols. Thresholding of statistical maps in functional neuroimaging using the false discovery rate. *Neuroimage*, 15(4):870–878, 2002.

[132] Yoav Benjamini and Yosef Hochberg. Controlling the false discovery rate: a practical and powerful approach to multiple testing. *Journal of the Royal statistical society: series B (Methodological)*, 57(1):289–300, 1995.

[133] Russell A Poldrack, Jeanette A Mumford, and Thomas E Nichols. *Handbook of functional MRI data analysis*. Cambridge University Press, 2011.

[134] Frederik Barkhof, Sven Haller, and Serge ARB Rombouts. Resting-state functional mr imaging: a new window to the brain. *Radiology*, 272(1):29–49, 2014.

[135] Maria Carmela Padula, Marie Schaer, Elisa Scariati, Maude Schneider, Dimitri Van De Ville, Martin Debbané, and Stephan Eliez. Structural and functional connectivity in the default mode network in 22q11. 2 deletion syndrome. *Journal of neurodevelopmental disorders*, 7(1):23, 2015.

[136] Yijun Liu, Jia-Hong Gao, Mario Liotti, Yonglin Pu, and Peter T Fox. Temporal dissociation of parallel processing in the human subcortical outputs. *Nature*, 400(6742):364, 1999.

[137] Giulio Tononi, Olaf Sporns, and Gerald M Edelman. A measure for brain complexity: relating functional segregation and integration in the nervous system. *Proceedings of the National Academy of Sciences*, 91(11):5033–5037, 1994.

[138] Michael D Fox and Marcus E Raichle. Spontaneous fluctuations in brain activity observed with functional magnetic resonance imaging. *Nature reviews neuroscience*, 8(9):700, 2007.

[139] Dardo Tomasi, Gene-Jack Wang, and Nora D Volkow. Energetic cost of brain functional connectivity. *Proceedings of the National Academy of Sciences*, 110(33):13642–13647, 2013.

[140] Qi-Hong Zou, Chao-Zhe Zhu, Yihong Yang, Xi-Nian Zuo, Xiang-Yu Long, Qing-Jiu Cao, Yu-Feng Wang, and Yu-Feng Zang. An improved approach to detection of amplitude of low-frequency fluctuation (alff) for resting-state fmri: fractional alff. *Journal of neuroscience methods*, 172(1):137–141, 2008.

[141] Li An, Qing-Jiu Cao, Man-Qiu Sui, Li Sun, Qi-Hong Zou, Yu-Feng Zang, and Yu-Feng Wang. Local synchronization and amplitude of the fluctuation of spontaneous brain activity in attention-deficit/hyperactivity disorder: a resting-state fmri study. *Neuroscience bulletin*, 29(5):603–613, 2013.

[142] Liu Yang, Yan Yan, Yonghao Wang, Xiaochen Hu, Jie Lu, Piu Chan, Tianyi Yan, and Ying Han. Gradual disturbances of the amplitude of low-frequency fluctuations (alff) and fractional alff in alzheimer spectrum. *Frontiers in neuroscience*, 12:975, 2018.

[143] Martin Küblböck, Michael Woletz, Anna Höflich, Ronald Sladky, Georg S Kranz, André Hoffmann, Rupert Lanzenberger, and Christian Windischberger. Stability of low-frequency fluctuation amplitudes in prolonged resting-state fmri. *Neuroimage*, 103:249–257, 2014.

[144] Yufeng Zang, Tianzi Jiang, Yingli Lu, Yong He, and Lixia Tian. Regional homogeneity approach to fmri data analysis. *Neuroimage*, 22(1):394–400, 2004.

[145] Rongfeng Qi, Long Jiang Zhang, Qiang Xu, Jianhui Zhong, Shengyong Wu, Zhiqiang Zhang, Wei Liao, Ling Ni, Zongjun Zhang, Huafu Chen, et al. Selective impairments of resting-state networks in minimal hepatic encephalopathy. *PloS one*, 7(5):e37400, 2012.

[146] Lili Jiang, Ting Xu, Ye He, Xiao-Hui Hou, Jinhui Wang, Xiao-Yan Cao, Gao-Xia Wei, Zhi Yang, Yong He, and Xi-Nian Zuo. Toward neurobiological characterization of functional homogeneity in the human cortex: regional variation, morphological association and functional covariance network organization. *Brain Structure and Function*, 220(5):2485–2507, 2015.

[147] Qiu-Feng Chen, Hua-Jun Chen, Jun Liu, Tao Sun, and Qun-Tai Shen. Machine learning classification of cirrhotic patients with and without minimal hepatic encephalopathy based on regional homogeneity of intrinsic brain activity. *PloS one*, 11(3):e0151263, 2016.

[148] Xiaopeng Song, Yi Zhang, and Yijun Liu. Frequency specificity of regional homogeneity in the resting-state human brain. *PloS one*, 9(1):e86818, 2014.

[149] Cornelis P Lanting, Emile de Kleine, Dave RM Langers, and Pim van Dijk. Unilateral tinnitus: changes in connectivity and response lateralization measured with fmri. *PloS one*, 9(10):e110704, 2014.

[150] Dardo Tomasi and Nora D Volkow. Functional connectivity density mapping. *Proceedings of the National Academy of Sciences*, 107(21):9885–9890, 2010.

[151] Sophie Achard, Raymond Salvador, Brandon Whitcher, John Suckling, and ED Bullmore. A resilient, low-frequency, small-world human brain functional network with highly connected association cortical hubs. *Journal of Neuroscience*, 26(1):63–72, 2006.

[152] Yong He, Zhang J Chen, and Alan C Evans. Small-world anatomical networks in the human brain revealed by cortical thickness from mri. *Cerebral cortex*, 17(10):2407–2419, 2007.

[153] Masahiro Hata, Hiroaki Kazui, Toshihisa Tanaka, Ryouhei Ishii, Leonides Canuet, Roberto D Pascual-Marqui, Yasunori Aoki, Shunichiro Ikeda, Hideki Kanemoto, Kenji Yoshiyama, et al. Functional connectivity assessed by resting state eeg correlates with

cognitive decline of alzheimer's disease–an eloreta study. *Clinical Neurophysiology*, 127(2):1269–1278, 2016.

[154] Xiaofei Hu, Yuchao Jiang, Xiaomei Jiang, Jiuquan Zhang, Minglong Liang, Jing Li, Yanling Zhang, Dezhong Yao, Cheng Luo, and Jian Wang. Altered functional connectivity density in subtypes of parkinson's disease. *Frontiers in human neuroscience*, 11:458, 2017.

[155] Luigi A Maglanoc, Nils Inge Landrø, Rune Jonassen, Tobias Kaufmann, Aldo Cordova-Palomera, Eva Hilland, and Lars T Westlye. Data-driven clustering reveals a link between symptoms and functional brain connectivity in depression. *Biological Psychiatry: Cognitive Neuroscience and Neuroimaging*, 4(1):16–26, 2019.

[156] Marcus E Raichle. The restless brain. *Brain connectivity*, 1(1):3–12, 2011.

[157] Michael G Hart, Stephen J Price, and John Suckling. Functional connectivity networks for preoperative brain mapping in neurosurgery. *Journal of neurosurgery*, 126(6):1941–1950, 2016.

[158] Vesa Kiviniemi, Juha-Heikki Kantola, Jukka Jauhiainen, Aapo Hyvärinen, and Osmo Tervonen. Independent component analysis of nondeterministic fmri signal sources. *Neuroimage*, 19(2):253–260, 2003.

[159] Christian F Beckmann, Marilena DeLuca, Joseph T Devlin, and Stephen M Smith. Investigations into resting-state connectivity using independent component analysis. *Philosophical Transactions of the Royal Society B: Biological Sciences*, 360(1457):1001–1013, 2005.

[160] Aapo Hyvärinen and Erkki Oja. Independent component analysis: algorithms and applications. *Neural networks*, 13(4-5):411–430, 2000.

[161] Svante Wold, Kim Esbensen, and Paul Geladi. Principal component analysis. *Chemometrics and intelligent laboratory systems*, 2(1-3):37–52, 1987.

[162] Abd-Krim Seghouane and Asif Iqbal. The adaptive block sparse pca and its application to multi-subject fmri data analysis using sparse mcca. *Signal Processing*, 153:311–320, 2018.

[163] Ola Friman, Magnus Borga, Peter Lundberg, and Hans Knutsson. Exploratory fmri analysis by autocorrelation maximization. *NeuroImage*, 16(2):454–464, 2002.

[164] Abd-Krim Seghouane and Andrzej Cichocki. Bayesian estimation of the number of principal components. *Signal Processing*, 87(3):562–568, 2007.

[165] Magnus O Ulfarsson and Victor Solo. Dimension estimation in noisy pca with sure and random matrix theory. *IEEE transactions on signal processing*, 56(12):5804–5816, 2008.

[166] Bernhard Schölkopf, Alexander Smola, and Klaus-Robert Müller. Nonlinear component analysis as a kernel eigenvalue problem. *Neural computation*, 10(5):1299–1319, 1998.

[167] Bertrand Thirion, Gaël Varoquaux, Elvis Dohmatob, and Jean-Baptiste Poline. Which fmri clustering gives good brain parcellations? *Frontiers in neuroscience*, 8:167, 2014.

[168] Yulia Golland, Polina Golland, Shlomo Bentin, and Rafael Malach. Data-driven clustering reveals a fundamental subdivision of the human cortex into two global systems. *Neuropsychologia*, 46(2):540–553, 2008.

[169] Megan H Lee, Carl D Hacker, Abraham Z Snyder, Maurizio Corbetta, Dongyang Zhang, Eric C Leuthardt, and Joshua S Shimony. Clustering of resting state networks. *PloS one*, 7(7):e40370, 2012.

[170] Raymond Salvador, John Suckling, Martin R Coleman, John D Pickard, David Menon, and ED Bullmore. Neurophysiological architecture of functional magnetic resonance images of human brain. *Cerebral cortex*, 15(9):1332–1342, 2005.

[171] Dietmar Cordes, Vic Haughton, John D Carew, Konstantinos Arfanakis, and Ken Maravilla. Hierarchical clustering to measure connectivity in fmri resting-state data. *Magnetic resonance imaging*, 20(4):305–317, 2002.

[172] Pierre Bellec, Pedro Rosa-Neto, Oliver C Lyttelton, Habib Benali, and Alan C Evans. Multi-level bootstrap analysis of stable clusters in resting-state fmri. *Neuroimage*, 51(3):1126–1139, 2010.

[173] Martijn Van Den Heuvel, Rene Mandl, and Hilleke Hulshoff Pol. Normalized cut group clustering of resting-state fmri data. *PloS one*, 3(4):e2001, 2008.

[174] Ed Bullmore and Olaf Sporns. Complex brain networks: graph theoretical analysis of structural and functional systems. *Nature reviews neuroscience*, 10(3):186, 2009.

[175] Fabrizio de Vico Fallani, Jonas Richiardi, Mario Chavez, and Sophie Achard. Graph analysis of functional brain networks: practical issues in translational neuroscience. *Philosophical Transactions of the Royal Society B: Biological Sciences*, 369(1653):20130521, 2014.

[176] Nathalie Tzourio-Mazoyer, Brigitte Landeau, Dimitri Papathanassiou, Fabrice Crivello, Olivier Etard, Nicolas Delcroix, Bernard Mazoyer, and Marc Joliot. Automated anatomical labeling of activations in spm using a macroscopic anatomical parcellation of the mni mri single-subject brain. *Neuroimage*, 15(1):273–289, 2002.

[177] Christian Georg Habeck. Basics of multivariate analysis in neuroimaging data. *JoVE (Journal of Visualized Experiments)*, (41):e1988, 2010.

[178] Jonathan D Cohen, Nathaniel Daw, Barbara Engelhardt, Uri Hasson, Kai Li, Yael Niv, Kenneth A Norman, Jonathan Pillow, Peter J Ramadge, Nicholas B Turk-Browne, et al. Computational approaches to fmri analysis. *Nature neuroscience*, 20(3):304, 2017.

[179] Jarrod A Lewis-Peacock and Kenneth A Norman. Multi-voxel pattern analysis of fmri data. *The cognitive neurosciences*, 911:920, 2013.

[180] Robert W Cox, Andrzej Jesmanowicz, and James S Hyde. Real-time functional magnetic resonance imaging. *Magnetic resonance in medicine*, 33(2):230–236, 1995.

[181] Ranganatha Sitaram, Tomas Ros, Luke Stoeckel, Sven Haller, Frank Scharnowski, Jarrod Lewis-Peacock, Nikolaus Weiskopf, Maria Laura Blefari, Mohit Rana, Ethan Oblak, et al. Closed-loop brain training: the science of neurofeedback. *Nature Reviews Neuroscience*, 18(2):86, 2017.

[182] Joe Kamiya. The first communications about operant conditioning of the eeg. *Journal of Neurotherapy*, 15(1):65–73, 2011.

[183] Jonathan Wolpaw and Elizabeth Winter Wolpaw. *Brain-computer interfaces: principles and practice*. OUP USA, 2012.

[184] Martin J McKeown, Scott Makeig, Greg G Brown, Tzyy-Ping Jung, Sandra S Kindermann, Anthony J Bell, and Terrence J Sejnowski. Analysis of fmri data by blind separation into independent spatial components. *Human brain mapping*, 6(3):160–188, 1998.

[185] Nathaniel D Daw et al. Trial-by-trial data analysis using computational models. *Decision making, affect, and learning: Attention and performance XXIII*, 23(1), 2011.

[186] Narender Ramnani, Timothy EJ Behrens, Will Penny, and Paul M Matthews. New approaches for exploring anatomical and functional connectivity in the human brain. *Biological psychiatry*, 56(9):613–619, 2004.

[187] Karl J Friston. Functional and effective connectivity in neuroimaging: a synthesis. *Human brain mapping*, 2(1-2):56–78, 1994.

[188] Christian Hohenfeld, Cornelius J Werner, and Kathrin Reetz. Resting-state connectivity in neurodegenerative disorders: Is there potential for an imaging biomarker? *NeuroImage: Clinical*, 18:849–870, 2018.

[189] Juan Zhou, Siwei Liu, Kwun Kei Ng, and Juan Wang. Applications of resting-state functional connectivity to neurodegenerative disease. *Neuroimaging Clinics*, 27(4):663–683, 2017.

[190] Hai Lin, Xiaodong Cai, Doudou Zhang, Jiali Liu, Peng Na, and Weiping Li. Functional connectivity markers of depression in advanced parkinson's disease. *NeuroImage: Clinical*, 25:102130, 2020.

[191] Julia Schumacher, Luis R Peraza, Michael Firbank, Alan J Thomas, Marcus Kaiser, Peter Gallagher, John T O'Brien, Andrew M Blamire, and John-Paul Taylor. Dynamic functional connectivity changes in dementia with lewy bodies and alzheimer's disease. *NeuroImage: Clinical*, 22:101812, 2019.

[192] Kristin K Lottman, Timothy J Gawne, Nina V Kraguljac, Jeffrey F Killen, Meredith A Reid, and Adrienne C Lahti. Examining resting-state functional connectivity in first-episode schizophrenia with 7t fmri and meg. *NeuroImage: Clinical*, 24:101959, 2019.

[193] Canhua Wang, Zhiyong Xiao, and Jianhua Wu. Functional connectivity-based classification of autism and control using svm-rfecv on rs-fmri data. *Physica Medica*, 65:99–105, 2019.

[194] Valeria Saccà, Alessia Sarica, Fabiana Novellino, Stefania Barone, Tiziana Tallarico, Enrica Filippelli, Alfredo Granata, Carmelina Chiriaco, Roberto Bruno Bossio, Paola Valentino, et al. Evaluation of machine learning algorithms performance for the prediction of early multiple sclerosis from resting-state fmri connectivity data. *Brain imaging and behavior*, 13(4):1103–1114, 2019.

[195] Atif Riaz, Muhammad Asad, Eduardo Alonso, and Greg Slabaugh. Deepfmri: End-to-end deep learning for functional connectivity and classification of adhd using fmri. *Journal of Neuroscience Methods*, page 108506, 2020.

[196] Xiaoxiao Wang, Xiao Liang, Zhoufan Jiang, Benedictor Alexander Nguchu, Yawen Zhou, Yanming Wang, Huijuan Wang, Yu Li, Yuying Zhu, Feng Wu, et al. Decoding and mapping task states of the human brain via deep learning. *arXiv preprint arXiv:1801.09858*, 2018.

[197] Dong Wen, Zhenhao Wei, Yanhong Zhou, Guolin Li, Xu Zhang, and Wei Han. Deep learning methods to process fmri data and their application in the diagnosis of cognitive impairment: a brief overview and our opinion. *Frontiers in neuroinformatics*, 12:23, 2018.

[198] Yuhui Du, Zening Fu, and Vince D Calhoun. Classification and prediction of brain disorders using functional connectivity: promising but challenging. *Frontiers in neuroscience*, 12:525, 2018.

[199] Meenakshi Khosla, Keith Jamison, Gia H. Ngo, Amy Kuceyeski, and Mert R. Sabuncu. Machine learning in resting-state fmri analysis. *Magnetic Resonance Imaging*, 64:101 – 121, 2019. Artificial Intelligence in MRI.

[200] Vince D Calhoun, Robyn Miller, Godfrey Pearlson, and Tulay Adalı. The chronnectome: time-varying connectivity networks as the next frontier in fmri data discovery. *Neuron*, 84(2):262–274, 2014.

[201] Kamalaker Dadi, Mehdi Rahim, Alexandre Abraham, Darya Chyzhyk, Michael Milham, Bertrand Thirion, Gaël Varoquaux, Alzheimer's Disease Neuroimaging Initiative, et al. Benchmarking functional connectome-based predictive models for resting-state fmri. *NeuroImage*, 192:115–134, 2019.

[202] Basudeb Mondal and Kajal De. An overview applications of graph theory in real field. *International Journal of Scientific Research in Computer Science, Engineering and Information Technology*, 2(5):751–759, 2017.

[203] Donatello Conte, Pasquale Foggia, Carlo Sansone, and Mario Vento. Thirty years of graph matching in pattern recognition. *International journal of pattern recognition and artificial intelligence*, 18(03):265–298, 2004.

[204] Johannes Köbler, Uwe Schöning, and Jacobo Torán. The graph isomorphism problem: Its structural complexity. 1993. *Progr. Theoret. Comput. Sci*, 1993.

[205] Robert G Busacker and Thomas Lorie Saaty. Finite graphs and networks: an introduction with applications. 1965.

[206] Alfred V Aho and John E Hopcroft. *The design and analysis of computer algorithms*. Pearson Education India, 1974.

[207] John E. Hopcroft and Robert Endre Tarjan. Av log v algorithm for isomorphism of triconnected planar graphs. *Journal of Computer and System Sciences*, 7(3):323–331, 1973.

[208] John E Hopcroft and Jin-Kue Wong. Linear time algorithm for isomorphism of planar graphs (preliminary report). In *Proceedings of the sixth annual ACM symposium on Theory of computing*, pages 172–184, 1974.

[209] Eugene M Luks. Isomorphism of graphs of bounded valence can be tested in polynomial time. *Journal of computer and system sciences*, 25(1):42–65, 1982.

[210] Ion Stefan Filotti and Jack N Mayer. A polynomial-time algorithm for determining the isomorphism of graphs of fixed genus. In *Proceedings of the twelfth annual ACM symposium on Theory of computing*, pages 236–243, 1980.

[211] László Babai, D Yu Grigoryev, and David M Mount. Isomorphism of graphs with bounded eigenvalue multiplicity. In *Proceedings of the fourteenth annual ACM symposium on Theory of computing*, pages 310–324, 1982.

[212] Eugene M Luks. Parallel algorithms for permutation groups and graph isomorphism. In *27th Annual Symposium on Foundations of Computer Science (sfcs 1986)*, pages 292–302. IEEE, 1986.

[213] Charles J Colbourn. On testing isomorphism of permutation graphs. *Networks*, 11(1):13–21, 1981.

[214] Xiaoyi Jiang and Horst Bunke. Optimal quadratic-time isomorphism of ordered graphs. *Pattern Recognition*, 32(7):1273–1283, 1999.

[215] David B Blumenthal and Johann Gamper. On the exact computation of the graph edit distance. *Pattern Recognition Letters*, 2018.

[216] Xiaoyi Jiang and Horst Bunke. Graph matching. In *Case-based reasoning on images and signals*, pages 149–173. Springer, 2008.

[217] Min-Soo Kim and Jiawei Han. A particle-and-density based evolutionary clustering method for dynamic networks. *Proceedings of the VLDB Endowment*, 2(1):622–633, 2009.

[218] Julien Lerouge, Zeina Abu-Aisheh, Romain Raveaux, Pierre Héroux, and Sébastien Adam. New binary linear programming formulation to compute the graph edit distance. *Pattern Recognition*, 72:254–265, 2017.

[219] Derek Justice and Alfred Hero. A binary linear programming formulation of the graph edit distance. *IEEE Transactions on Pattern Analysis and Machine Intelligence*, 28(8):1200–1214, 2006.

[220] Kaspar Riesen and Horst Bunke. Approximate graph edit distance computation by means of bipartite graph matching. *Image and Vision computing*, 27(7):950–959, 2009.

[221] Mostafa Darwiche, Donatello Conte, Romain Raveaux, and Vincent t'Kindt. A local branching heuristic for solving a graph edit distance problem. *Computers & Operations Research*, 106:225–235, 2019.

[222] Matteo Fischetti and Andrea Lodi. Local branching. *Mathematical programming*, 98(1-3):23–47, 2003.

[223] Sebastien Bougleux, Luc Brun, Vincenzo Carletti, Pasquale Foggia, Benoit Gaüzère, and Mario Vento. Graph edit distance as a quadratic assignment problem. *Pattern Recognition Letters*, 87:38–46, 2017.

[224] Giorgio Levi. A note on the derivation of maximal common subgraphs of two directed or undirected graphs. *Calcolo*, 9(4):341, 1973.

[225] James J McGregor. Backtrack search algorithms and the maximal common subgraph problem. *Software: Practice and Experience*, 12(1):23–34, 1982.

[226] Horst Bunke and Kim Shearer. A graph distance metric based on the maximal common subgraph. *Pattern recognition letters*, 19(3-4):255–259, 1998.

[227] Walter D Wallis, Peter Shoubridge, M Kraetz, and D Ray. Graph distances using graph union. *Pattern Recognition Letters*, 22(6-7):701–704, 2001.

[228] Horst Bunke. On a relation between graph edit distance and maximum common subgraph. *Pattern Recognition Letters*, 18(8):689–694, 1997.

[229] Mirtha-Lina Fernández and Gabriel Valiente. A graph distance metric combining maximum common subgraph and minimum common supergraph. *Pattern Recognition Letters*, 22(6):753–758, 2001.

[230] Rohit Singh, Jinbo Xu, and Bonnie Berger. Pairwise global alignment of protein interaction networks by matching neighborhood topology. In *Annual International Conference on Research in Computational Molecular Biology*, pages 16–31. Springer, 2007.

[231] Rohit Singh, Jinbo Xu, and Bonnie Berger. Global alignment of multiple protein interaction networks with application to functional orthology detection. *Proceedings of the National Academy of Sciences*, 105(35):12763–12768, 2008.

[232] Jon M Kleinberg. Authoritative sources in a hyperlinked environment. *Journal of the ACM (JACM)*, 46(5):604–632, 1999.

[233] Vincent D Blondel, Anahí Gajardo, Maureen Heymans, Pierre Senellart, and Paul Van Dooren. A measure of similarity between graph vertices: Applications to synonym extraction and web searching. *SIAM review*, 46(4):647–666, 2004.

[234] Giorgos Kollias, Shahin Mohammadi, and Ananth Grama. Network similarity decomposition (nsd): A fast and scalable approach to network alignment. *IEEE Transactions on Knowledge and Data Engineering*, 24(12):2232–2243, 2011.

[235] Giorgos Kollias, Madan Sathe, Olaf Schenk, and Ananth Grama. Fast parallel algorithms for graph similarity and matching. *Journal of Parallel and Distributed Computing*, 74(5):2400–2410, 2014.

[236] Zeina Abu-Aisheh, Romain Raveaux, Jean-Yves Ramel, and Patrick Martineau. A parallel graph edit distance algorithm. *Expert Systems with Applications*, 94:41–57, 2018.

[237] Leyuan Wang and John D Owens. Fast gunrock subgraph matching (gsm) on gpus. *arXiv preprint arXiv:2003.01527*, 2020.

[238] Bas O Fagginger Auer and Rob H Bisseling. A gpu algorithm for greedy graph matching. In *Facing the Multicore-Challenge II*, pages 108–119. Springer, 2012.

[239] JH Her and F Pellegrini. Efficient and scalable parallel graph partitioning. *Parallel Computing*, 2010.

[240] Rob Patro and Carl Kingsford. Global network alignment using multiscale spectral signatures. *Bioinformatics*, 28(23):3105–3114, 2012.

[241] Arif M Khan, David F Gleich, Alex Pothen, and Mahantesh Halappanavar. A multithreaded algorithm for network alignment via approximate matching. In *Proceedings of the International Conference on High Performance Computing, Networking, Storage and Analysis*, page 64. IEEE Computer Society Press, 2012.

[242] Danielle S Bassett and Edward T Bullmore. Human brain networks in health and disease. *Current opinion in neurology*, 22(4):340, 2009.

[243] Matthew Lawrence Stanley, Malaak Nasser Moussa, Brielle Paolini, Robert Gray Lyday, Jonathan H Burdette, and Paul J Laurienti. Defining nodes in complex brain networks. *Frontiers in computational neuroscience*, 7:169, 2013.

[244] Silke Dodel, J Michael Herrmann, and Theo Geisel. Functional connectivity by cross-correlation clustering. *Neurocomputing*, 44:1065–1070, 2002.

[245] Francisco Pereira, Jennifer M Walz, Ertan Cetingul, Sandra Sudarsky, Mariappan Nadar, and Ruchika Prakash. Creating group-level functionally-defined atlases for diagnostic classification. In *2013 International Workshop on Pattern Recognition in Neuroimaging*, pages 29–32. IEEE, 2013.

[246] Madiha J Jafri, Godfrey D Pearlson, Michael Stevens, and Vince D Calhoun. A method for functional network connectivity among spatially independent resting-state components in schizophrenia. *Neuroimage*, 39(4):1666–1681, 2008.

[247] Olaf Sporns. *Networks of the Brain*. MIT press, 2010.

[248] Danielle Smith Bassett and ED Bullmore. Small-world brain networks. *The neuroscientist*, 12(6):512–523, 2006.

[249] Sophie Achard and Ed Bullmore. Efficiency and cost of economical brain functional networks. *PLoS Comput Biol*, 3(2):e17, 2007.

[250] Kiho Im, Rudolph Pienaar, Jong-Min Lee, Joon-Kyung Seong, Yu Yong Choi, Kun Ho Lee, and P Ellen Grant. Quantitative comparison and analysis of sulcal patterns using sulcal graph matching: a twin study. *Neuroimage*, 57(3):1077–1086, 2011.

[251] Faguo Yang and Frithjof Kruggel. Optimization algorithms for labeling brain sulci based on graph matching. In *Computer Vision, 2007. ICCV 2007. IEEE 11th International Conference on*, pages 1–7. IEEE, 2007.

[252] Faguo Yang and Frithjof Kruggel. A graph matching approach for labeling brain sulci using location, orientation, and shape. *Neurocomputing*, 73(1):179–190, 2009.

[253] Ying Huang, Zhibin He, Lei Guo, Tianming Liu, and Tuo Zhang. Multi-view graph matching of cortical landmarks. In *International Conference on Medical Image Computing and Computer-Assisted Intervention*, pages 84–92. Springer, 2019.

[254] Tuo Zhang, Xiao Li, Lin Zhao, Ying Huang, Zhibin He, Lei Guo, and Tianming Liu. Group-wise graph matching of cortical gyral hinges. In *International Conference on Medical Image Computing and Computer-Assisted Intervention*, pages 75–83. Springer, 2019.

[255] Yusuf Osmanlıoğlu, Birkan Tunç, Drew Parker, Mark A Elliott, Graham L Baum, Rastko Ciric, Theodore D Satterthwaite, Raquel E Gur, Ruben C Gur, and Ragini Verma. System-level matching of structural and functional connectomes in the human brain. *Neuroimage*, 199:93–104, 2019.

[256] Zhenyu Tang, Di Jiang, Hongming Li, and Yong Fan. Matching functional connectivity patterns for spatial correspondence detection in fmri registration. In *Augmented Reality Environments for Medical Imaging and Computer-Assisted Interventions*, pages 249–257. Springer, 2013.

[257] Yusuf Osmanlıoğlu, Jacob A Alappatt, Drew Parker, Junghoon Kim, and Ragini Verma. A graph based similarity measure for assessing altered connectivity in traumatic brain injury. In *International MICCAI Brainlesion Workshop*, pages 189–198. Springer, 2018.

[258] Kuo-Chin Fan, Cheng-Wen Liu, and Yuan-Kai Wang. A fuzzy bipartite weighted graph matching approach to fingerprint verification. In *Systems, Man, and Cybernetics, 1998. 1998 IEEE International Conference on*, volume 5, pages 4363–4368. IEEE, 1998.

[259] Pengyu Hong, Roy Wang, and Thomas Huang. Learning patterns from images by combining soft decisions and hard decisions. In *Computer Vision and Pattern Recognition, 2000. Proceedings. IEEE Conference on*, volume 1, pages 78–83. IEEE, 2000.

[260] Martin Lades, Jan C Vorbruggen, Joachim Buhmann, Jörg Lange, Christoph Von Der Malsburg, Rolf P Wurtz, and Wolfgang Konen. Distortion invariant object recognition in the dynamic link architecture. *IEEE Transactions on computers*, 42(3):300–311, 1993.

[261] Ponnuthurai N Suganthan and Hong Yan. Recognition of handprinted chinese characters by constrained graph matching. *Image and Vision Computing*, 16(3):191–201, 1998.

[262] Andrea Torsello and Edwin R Hancock. Computing approximate tree edit distance using relaxation labeling. *Pattern Recognition Letters*, 24(8):1089–1097, 2003.

[263] Stefano Berretti, Alberto Del Bimbo, and Enrico Vicario. Efficient matching and indexing of graph models in content-based retrieval. *IEEE Transactions on Pattern Analysis and Machine Intelligence*, 23(10):1089–1105, 2001.

[264] Francesc Serratosa, Xavier CortéS, and Albert Solé-Ribalta. Component retrieval based on a database of graphs for hand-written electronic-scheme digitalisation. *Expert Systems with Applications*, 40(7):2493–2502, 2013.

[265] Stefan Fischer, Kaspar Gilomen, and Horst Bunke. Identification of diatoms by grid graph matching. *Structural, Syntactic, and Statistical Pattern Recognition*, pages 335–370, 2002.

[266] Kim Shearer, Horst Bunke, and Svetha Venkatesh. Video indexing and similarity retrieval by largest common subgraph detection using decision trees. *Pattern Recognition*, 34(5):1075–1091, 2001.

[267] Pasquale Foggia, Gennaro Percannella, and Mario Vento. Graph matching and learning in pattern recognition in the last 10 years. *International Journal of Pattern Recognition and Artificial Intelligence*, 28(01):1450001, 2014.

[268] Mario Vento. A long trip in the charming world of graphs for pattern recognition. *Pattern Recognition*, 48(2):291–301, 2015.

[269] Lopamudra Mukherjee, Vikas Singh, Jiming Peng, Jinhui Xu, Michael J Zeitz, and Ronald Berezney. Generalized median graphs: Theory and applications. In *Computer Vision, 2007. ICCV 2007. IEEE 11th International Conference on*, pages 1–8. IEEE, 2007.

[270] Lopamudra Mukherjee, Vikas Singh, Jiming Peng, Jinhui Xu, Michael J Zeitz, and Ronald Berezney. Generalized median graphs and applications. *Journal of Combinatorial Optimization*, 17(1):21–44, 2009.

[271] Leonardo M Musmanno and Celso C Ribeiro. Heuristics for the generalized median graph problem. *European Journal of Operational Research*, 254(2):371–384, 2016.

[272] Stephanie Sandor and Richard Leahy. Surface-based labeling of cortical anatomy using a deformable atlas. *IEEE transactions on medical imaging*, 16(1):41–54, 1997.

[273] Sylvain Jaume, Benoît Macq, and Simon K Warfield. Labeling the brain surface using a deformable multiresolution mesh. In *International Conference on Medical Image Computing and Computer-Assisted Intervention*, pages 451–458. Springer, 2002.

[274] Belaggoune Mohamed, Oukid Saliha, and Benblidia Nadjia. Ontology driven graph matching approach for automatic labeling brain cortical sulci. *IT4OD*, page 162, 2014.

[275] Kirsten Judith Behnke, Maryam E Rettmann, Dzung L Pham, Dinggang Shen, Susan M Resnick, Christos Davatzikos, and Jerry L Prince. Automatic classification of sulcal regions of the human brain cortex using pattern recognition. In *Medical Imaging 2003: Image Processing*, volume 5032, pages 1499–1511. International Society for Optics and Photonics, 2003.

[276] Matthieu Perrot, Denis Riviere, and Jean-Francois Mangin. Identifying cortical sulci from localization, shape and local organization. In *Biomedical Imaging: From Nano to Macro, 2008. ISBI 2008. 5th IEEE International Symposium on*, pages 420–423. IEEE, 2008.

[277] Gabriele Lohmann and D Yves von Cramon. Automatic labelling of the human cortical surface using sulcal basins. *Medical image analysis*, 4(3):179–188, 2000.

[278] Bruce Fischl, André Van Der Kouwe, Christophe Destrieux, Eric Halgren, Florent Ségonne, David H Salat, Evelina Busa, Larry J Seidman, Jill Goldstein, David Kennedy, et al. Automatically parcellating the human cerebral cortex. *Cerebral cortex*, 14(1):11–22, 2004.

[279] Fabien Vivodtzev, Lars Linsen, Bernd Hamann, Kenneth Joy, and Bruno Olshausen. Brain mapping using topology graphs obtained by surface segmentation. *Scientific Visualization: The Visual Extraction of Knowledge from Data*, pages 35–48, 2006.

[280] Yonggang Shi, Zhuowen Tu, Allan L Reiss, Rebecca A Dutton, Agatha D Lee, Albert M Galaburda, Ivo Dinov, Paul M Thompson, and Arthur W Toga. Joint sulci detection using graphical models and boosted priors. In *Biennial International Conference on Information Processing in Medical Imaging*, pages 98–109. Springer, 2007.

[281] J-F Mangin, Fabrice Poupon, Édouard Duchesnay, Denis Rivière, Arnaud Cachia, D Louis Collins, Alan C Evans, and Jean Régis. Brain morphometry using 3d moment invariants. *Medical Image Analysis*, 8(3):187–196, 2004.

[282] Zhuowen Tu, Songfeng Zheng, Alan L Yuille, Allan L Reiss, Rebecca A Dutton, Agatha D Lee, Albert M Galaburda, Ivo Dinov, Paul M Thompson, and Arthur W Toga.

Automated extraction of the cortical sulci based on a supervised learning approach. *IEEE Transactions on Medical Imaging*, 26(4):541–552, 2007.

[283] C-H Lo and H-S Don. 3-d moment forms: their construction and application to object identification and positioning. *IEEE Transactions on Pattern Analysis and Machine Intelligence*, 11(10):1053–1064, 1989.

[284] Sergi Valverde, Arnau Oliver, Eloy Roura, Sandra González-Villà, Deborah Pareto, Joan C Vilanova, Lluís Ramió-Torrentà, Àlex Rovira, and Xavier Lladó. Automated tissue segmentation of mr brain images in the presence of white matter lesions. *Medical image analysis*, 35:446–457, 2017.

[285] F Kruggel. Techniques in analyzing the neocortical fine-structure. *Medical Imaging Systems*, 5:255–279, 2005.

[286] Paolo Cignoni, Fabio Ganovelli, Claudio Montani, and Roberto Scopigno. Reconstruction of topologically correct and adaptive trilinear isosurfaces. *Computers & Graphics*, 24(3):399–418, 2000.

[287] Faguo Yang and Frithjof Kruggel. Automatic segmentation of human brain sulci. *Medical Image Analysis*, 12(4):442–451, 2008.

[288] Yong Zhou, Paul M Thompson, and Arthur W Toga. Extracting and representing the cortical sulci. *IEEE Computer Graphics and Applications*, 19(3):49–55, 1999.

[289] Horst Bunke, Xiaoyi Jiang, and Abraham Kandel. On the minimum common supergraph of two graphs. *Computing*, 65(1):13–25, 2000.

[290] Miquel Ferrer, Ernest Valveny, and Francesc Serratosa. Median graphs: A genetic approach based on new theoretical properties. *Pattern Recognition*, 42(9):2003–2012, 2009.

[291] Michel Neuhaus and Horst Bunke. A quadratic programming approach to the graph edit distance problem. In *GbRPR*, pages 92–102. Springer, 2007.

[292] Adam Schenker, Abraham Kandel, Horst Bunke, and Mark Last. *Graph-theoretic techniques for web content mining*, volume 62. World Scientific, 2005.

[293] Xiaoyi Jiang, Andreas Munger, and Horst Bunke. An median graphs: properties, algorithms, and applications. *IEEE Transactions on Pattern Analysis and Machine Intelligence*, 23(10):1144–1151, 2001.

[294] Miquel Ferrer, Ernest Valveny, and Francesc Serratosa. Median graphs: A genetic approach based on new theoretical properties. *Pattern Recognition*, 42(9):2003–2012, 2009.

[295] Adel Hlaoui and Shengrui Wang. A new median graph algorithm. *Graph based representations in pattern recognition*, pages 225–234, 2003.

[296] Miquel Ferrer Sumsi. *Theory and Algorithms on the Median Graph: application to Graph-Based Classification and Clustering*. PhD thesis, Universitat Autònoma de Barcelona, 2008.

[297] Miquel Ferrer, Ernest Valveny, and Francesc Serratosa. Median graph: A new exact algorithm using a distance based on the maximum common subgraph. *Pattern Recognition Letters*, 30(5):579–588, 2009.

[298] Miquel Ferrer, Ernest Valveny, Francesc Serratosa, Kaspar Riesen, and Horst Bunke. An approximate algorithm for median graph computation using graph embedding. In *Pattern Recognition, 2008. ICPR 2008. 19th International Conference on*, pages 1–4. IEEE, 2008.

[299] Miquel Ferrer, Ernest Valveny, Francesc Serratosa, Kaspar Riesen, and Horst Bunke. Generalized median graph computation by means of graph embedding in vector spaces. *Pattern Recognition*, 43(4):1642–1655, 2010.

[300] Nicola Rebagliati, Albert Solé-Ribalta, Marcello Pelillo, and Francesc Serratosa. On the relation between the common labelling and the median graph. *Structural, Syntactic, and Statistical Pattern Recognition*, pages 107–115, 2012.

[301] Steven Gold and Anand Rangarajan. A graduated assignment algorithm for graph matching. *IEEE Transactions on pattern analysis and machine intelligence*, 18(4):377–388, 1996.

[302] Panagiotis Papadimitriou, Ali Dasdan, and Hector Garcia-Molina. Web graph similarity for anomaly detection. *Journal of Internet Services and Applications*, 1(1):19–30, 2010.

[303] Brian P Kelley, Bingbing Yuan, Fran Lewitter, Roded Sharan, Brent R Stockwell, and Trey Ideker. Pathblast: a tool for alignment of protein interaction networks. *Nucleic acids research*, 32(suppl_2):W83–W88, 2004.

[304] Mehmet Koyutürk, Yohan Kim, Umut Topkara, Shankar Subramaniam, Wojciech Szpankowski, and Ananth Grama. Pairwise alignment of protein interaction networks. *Journal of Computational Biology*, 13(2):182–199, 2006.

[305] Tijana Milenković and Nataša Pržulj. Uncovering biological network function via graphlet degree signatures. *Cancer informatics*, 6:CIN–S680, 2008.

[306] Nataša Pržulj. Biological network comparison using graphlet degree distribution. *Bioinformatics*, 23(2):e177–e183, 2007.

[307] Wei Hu, Yuzhong Qu, and Gong Cheng. Matching large ontologies: A divide-and-conquer approach. *Data & Knowledge Engineering*, 67(1):140–160, 2008.

[308] Giorgos Kollias, Madan Sathe, Shahin Mohammadi, and Ananth Grama. A fast approach to global alignment of protein-protein interaction networks. *BMC research notes*, 6(1):35, 2013.

[309] Lawrence Page, Sergey Brin, Rajeev Motwani, and Terry Winograd. The pagerank citation ranking: Bringing order to the web. Technical report, Stanford InfoLab, 1999.

[310] Craig Silverstein, Sergey Brin, and Rajeev Motwani. Beyond market baskets: Generalizing association rules to dependence rules. *Data mining and knowledge discovery*, 2(1):39–68, 1998.

[311] Matthias Rupp, Ewgenij Proschak, and Gisbert Schneider. Kernel approach to molecular similarity based on iterative graph similarity. *Journal of chemical information and modeling*, 47(6):2280–2286, 2007.

[312] Maritza Hernandez, Arman Zaribafiyan, Maliheh Aramon, and Mohammad Naghibi. A novel graph-based approach for determining molecular similarity. *arXiv preprint arXiv:1601.06693*, 2016.

[313] Adnan Anwar and Abdun Naser Mahmood. Anomaly detection in electric network database of smart grid: graph matching approach. *Electric Power Systems Research*, 133:51–62, 2016.

[314] Nitish Korula and Silvio Lattanzi. An efficient reconciliation algorithm for social networks. *Proceedings of the VLDB Endowment*, 7(5):377–388, 2014.

[315] Huda Nassar and David F Gleich. Multimodal network alignment. In *Proceedings of the 2017 SIAM International Conference on Data Mining*, pages 615–623. SIAM, 2017.

[316] Karthik Kambatla, Georgios Kollias, and Ananth Grama. Efficient large-scale graph analysis in mapreduce. *PMAA*, 2012.

[317] Mohsen Bayati, Margot Gerritsen, David F Gleich, Amin Saberi, and Ying Wang. Algorithms for large, sparse network alignment problems. In *Data Mining, 2009. ICDM'09. Ninth IEEE International Conference on*, pages 705–710. IEEE, 2009.

[318] Shaikh Arifuzzaman, Maleq Khan, and Madhav Marathe. Distributed-memory parallel algorithms for counting and listing triangles in big graphs. *arXiv preprint arXiv:1706.05151*, 2017.

[319] Giorgos Kollias, Shahin Mohammadi, and Ananth Grama. Network similarity decomposition (nsd): A fast and scalable approach to network alignment. *IEEE Transactions on Knowledge and Data Engineering*, 24(12):2232–2243, 2012.

[320] Ümit V Çatalyürek, Florin Dobrian, Assefaw Gebremedhin, Mahantesh Halappanavar, and Alex Pothen. Distributed-memory parallel algorithms for matching and coloring. In *Parallel and Distributed Processing Workshops and Phd Forum (IPDPSW), 2011 IEEE International Symposium on*, pages 1971–1980. IEEE, 2011.

[321] Md Mostofa Ali Patwary, Rob H Bisseling, and Fredrik Manne. Parallel greedy graph matching using an edge partitioning approach. In *Proceedings of the fourth international workshop on High-level parallel programming and applications*, pages 45–54. ACM, 2010.

[322] Daniel D Lee and H Sebastian Seung. Learning the parts of objects by non-negative matrix factorization. *Nature*, 401(6755):788–791, 1999.

[323] John E Richards and Wanze Xie. Chapter one-brains for all the ages: structural neurodevelopment in infants and children from a life-span perspective. *Advances in child development and behavior*, 48:1–52, 2015.

[324] Duygu Tosun, Maryam E Rettmann, and Jerry L Prince. Mapping techniques for aligning sulci across multiple brains. *Medical image analysis*, 8(3):295–309, 2004.

[325] Mario Saiano, Laura Pellegrino, Maura Casadio, Susanna Summa, Eleonora Garbarino, Valentina Rossi, Daniela Dall'Agata, and Vittorio Sanguineti. Natural interfaces and virtual environments for the acquisition of street crossing and path following skills in adults with autism spectrum disorders: a feasibility study. *Journal of neuroengineering and rehabilitation*, 12(1):17, 2015.

[326] Benjamin Zablotsky, Lindsey I Black, Matthew J Maenner, Laura A Schieve, and Stephen J Blumberg. Estimated prevalence of autism and other developmental disabilities following questionnaire changes in the 2014 national health interview survey. (87), 2015. Journal Issue.

[327] Helena Brentani, Cristiane Silvestre de Paula, Daniela Bordini, Deborah Rolim, Fabio Sato, Joana Portolese, Maria Clara Pacifico, and James T McCracken. Autism spectrum disorders: an overview on diagnosis and treatment. *Revista brasileira de psiquiatria*, 35:S62–S72, 2013.

[328] Mark Plitt, Kelly Anne Barnes, and Alex Martin. Functional connectivity classification of autism identifies highly predictive brain features but falls short of biomarker standards. *NeuroImage: Clinical*, 7:359–366, 2015.

[329] John D Medaglia. Graph theoretic analysis of resting state functional mr imaging. *Neuroimaging Clinics*, 27(4):593–607, 2017.

[330] Ruoxuan Cui, Manhua Liu, Alzheimer's Disease Neuroimaging Initiative, et al. Rnn-based longitudinal analysis for diagnosis of alzheimer's disease. *Computerized Medical Imaging and Graphics*, 73:1–10, 2019.

[331] M Deepika Nair, MS Sinta, and M Vidya. A study on various deep learning algorithms to diagnose alzheimer's disease. In *International Conference on ISMAC in Computational Vision and Bio-Engineering*, pages 1705–1710. Springer, 2018.

[332] Parisa Forouzannezhad, Alireza Abbaspour, Chen Fang, Mercedes Cabrerizo, David Loewenstein, Ranjan Duara, and Malek Adjouadi. A survey on applications and analysis methods of functional magnetic resonance imaging for alzheimer's disease. *Journal of Neuroscience Methods*, 317:121–140, 2019.

[333] Ali Khazaee, Ata Ebrahimzadeh, and Abbas Babajani-Feremi. Identifying patients with alzheimer's disease using resting-state fmri and graph theory. *Clinical Neurophysiology*, 126(11):2132–2141, 2015.

[334] Junhua Li, Yu Sun, Yi Huang, Anastasios Bezerianos, and Rongjun Yu. Machine learning technique reveals intrinsic characteristics of schizophrenia: an alternative method. *Brain imaging and behavior*, pages 1–11, 2018.

[335] Sergey M Plis, Md Faijul Amin, Adam Chekroud, Devon Hjelm, Eswar Damaraju, Hyo Jong Lee, Juan R Bustillo, KyungHyun Cho, Godfrey D Pearlson, and Vince D Calhoun. Reading the (functional) writing on the (structural) wall: Multimodal fusion of brain structure and function via a deep neural network based translation approach reveals novel impairments in schizophrenia. *NeuroImage*, 181:734–747, 2018.

[336] Rami F Algunaid, Ali H Algumaei, Muhammad A Rushdi, and Inas A Yassine. Schizophrenic patient identification using graph-theoretic features of resting-state fmri data. *Biomedical Signal Processing and Control*, 43:289–299, 2018.

[337] Conor Liston. 115. neuroimaging biomarkers predicting distinct subtypes of anhedonic behavior in depression. *Biological Psychiatry*, 83(9):S47, 2018.

[338] David C Steffens, Lihong Wang, and Godfrey D Pearlson. Functional connectivity predictors of acute depression treatment outcome. *International psychogeriatrics*, pages 1–5, 2019.

[339] Tingting Xu, Kathryn R Cullen, Bryon Mueller, Mindy W Schreiner, Kelvin O Lim, S Charles Schulz, and Keshab K Parhi. Network analysis of functional brain connectivity

in borderline personality disorder using resting-state fmri. *NeuroImage: Clinical*, 11:302–315, 2016.

[340] Feng Liu, Wenbin Guo, Jean-Paul Fouche, Yifeng Wang, Wenqin Wang, Jurong Ding, Ling Zeng, Changjian Qiu, Qiyong Gong, Wei Zhang, and Huafu Chen. Multivariate classification of social anxiety disorder using whole brain functional connectivity. *Brain Structure and Function*, 220(1):101–115, 2015.

[341] Yan Tang, Weixiong Jiang, Jian Liao, Wei Wang, and Aijing Luo. Identifying individuals with antisocial personality disorder using resting-state fmri. *PloS one*, 8(4):e60652, 2013.

[342] Sarah Parisot, Sofia Ira Ktena, Enzo Ferrante, Matthew Lee, Ricardo Guerrero, Ben Glocker, and Daniel Rueckert. Disease prediction using graph convolutional networks: Application to autism spectrum disorder and alzheimer's disease. *Medical image analysis*, 48:117–130, 2018.

[343] Anibal Sólon Heinsfeld, Alexandre Rosa Franco, R Cameron Craddock, Augusto Buchweitz, and Felipe Meneguzzi. Identification of autism spectrum disorder using deep learning and the abide dataset. *NeuroImage: Clinical*, 17:16–23, 2018.

[344] Alexandre Abraham, Michael P Milham, Adriana Di Martino, R Cameron Craddock, Dimitris Samaras, Bertrand Thirion, and Gael Varoquaux. Deriving reproducible biomarkers from multi-site resting-state data: an autism-based example. *NeuroImage*, 147:736–745, 2017.

[345] AR Jac Fredo, Afrooz Jahedi, Maya Reiter, and Ralph-Axel Müller. Diagnostic classification of autism using resting-state fmri data and conditional random forest. *Age (years)*, 12(2.76):6–41, 2018.

[346] Amirali Kazeminejad and Roberto C Sotero. Topological properties of resting-state fmri functional networks improve machine learning-based autism classification. *Frontiers in Neuroscience*, 12, 2018.

[347] Robert X Smith, Kay Jann, Mirella Dapretto, and Danny JJ Wang. Imbalance of functional connectivity and temporal entropy in resting-state networks in autism spectrum disorder: A machine learning approach. *Frontiers in neuroscience*, 12, 2018.

[348] Hailong Li, Nehal A Parikh, and Lili He. A novel transfer learning approach to enhance deep neural network classification of brain functional connectomes. *Frontiers in neuroscience*, 12:491, 2018.

[349] Maryam Akhavan Aghdam, Arash Sharifi, and Mir Mohsen Pedram. Combination of rs-fmri and smri data to discriminate autism spectrum disorders in young children using deep belief network. *Journal of digital imaging*, pages 1–9, 2018.

[350] Cameron Craddock, Yassine Benhajali, Carlton Chu, Francois Chouinard, Alan Evans, András Jakab, Budhachandra Singh Khundrakpam, John David Lewis, Qingyang Li, Michael Milham, Chaogan Yan, and Pierre Bellec. The neuro bureau preprocessing initiative: open sharing of preprocessed neuroimaging data and derivatives. *Neuroinformatics*, 2013.

[351] František Váša, Edward T Bullmore, and Ameera X Patel. Probabilistic thresholding of functional connectomes: Application to schizophrenia. *Neuroimage*, 172:326–340, 2018.

[352] Martijn P van den Heuvel, Siemon C de Lange, Andrew Zalesky, Caio Seguin, BT Thomas Yeo, and Ruben Schmidt. Proportional thresholding in resting-state fmri functional connectivity networks and consequences for patient-control connectome studies: Issues and recommendations. *Neuroimage*, 152:437–449, 2017.

[353] Wayne W Zachary. An information flow model for conflict and fission in small groups. *Journal of anthropological research*, 33(4):452–473, 1977.

[354] U Brandes, D Delling, and M Gaertler. Go rke. *R., Hoefer, M., Nikoloski, Z. and Wagner, D., On modularity clustering. IEEE Trans. Knowl. Data Eng*, 20:172–188, 2008.

[355] Hongyang Gao, Yongjun Chen, and Shuiwang Ji. Learning graph pooling and hybrid convolutional operations for text representations. *arXiv preprint arXiv:1901.06965*, 2019.

[356] Stephen Phillips and Kostas Daniilidis. All graphs lead to rome: Learning geometric and cycle-consistent representations with graph convolutional networks. *arXiv preprint arXiv:1901.02078*, 2019.

[357] Yunsheng Bai, Hao Ding, Yizhou Sun, and Wei Wang. Convolutional neural networks for fast approximation of graph edit distance. *arXiv preprint arXiv:1809.04440*, 2018.

[358] Sijie Yan, Yuanjun Xiong, and Dahua Lin. Spatial temporal graph convolutional networks for skeleton-based action recognition. *arXiv preprint arXiv:1801.07455*, 2018.

[359] Rianne van den Berg, Thomas N Kipf, and Max Welling. Graph convolutional matrix completion. *stat*, 1050:7, 2017.

[360] Ashesh Jain, Amir R Zamir, Silvio Savarese, and Ashutosh Saxena. Structural-rnn: Deep learning on spatio-temporal graphs. In *Proceedings of the IEEE Conference on Computer Vision and Pattern Recognition*, pages 5308–5317, 2016.

[361] Mikael Henaff, Joan Bruna, and Yann LeCun. Deep convolutional networks on graph-structured data. *arXiv preprint arXiv:1506.05163*, 2015.

[362] Yujia Li, Daniel Tarlow, Marc Brockschmidt, and Richard Zemel. Gated graph sequence neural networks. *arXiv preprint arXiv:1511.05493*, 2015.

[363] David K Duvenaud, Dougal Maclaurin, Jorge Iparraguirre, Rafael Bombarell, Timothy Hirzel, Alán Aspuru-Guzik, and Ryan P Adams. Convolutional networks on graphs for learning molecular fingerprints. In *Advances in neural information processing systems*, pages 2224–2232, 2015.

[364] Michaël Defferrard, Xavier Bresson, and Pierre Vandergheynst. Convolutional neural networks on graphs with fast localized spectral filtering. In *Advances in Neural Information Processing Systems*, pages 3844–3852, 2016.

[365] Mathias Niepert, Mohamed Ahmed, and Konstantin Kutzkov. Learning convolutional neural networks for graphs. In *International conference on machine learning*, pages 2014–2023, 2016.

[366] Yotam Hechtlinger, Purvasha Chakravarti, and Jining Qin. Convolutional neural networks generalization utilizing the data graph structure. 2016.

[367] Michael Edwards and Xianghua Xie. Graph convolutional neural network. In Edwin R. Hancock Richard C. Wilson and William A. P. Smith, editors, *Proceedings of the British Machine Vision Conference (BMVC)*, pages 114.1–114.11. BMVA Press, September 2016.

[368] Ryan A Rossi, Rong Zhou, and Nesreen K Ahmed. Deep feature learning for graphs. *arXiv preprint arXiv:1704.08829*, 2017.

[369] CJ Stam. Characterization of anatomical and functional connectivity in the brain: a complex networks perspective. *International Journal of Psychophysiology*, 77(3):186–194, 2010.

[370] Bashar Awad Al-Shboul, Heba Hakh, Hossam Faris, Ibrahim Aljarah, and Hamad Alsawalqah. Voting-based classification for e-mail spam detection. *Journal of ICT Research and Applications*, 10(1):29–42, 2016.

[371] Isha Gandhi and Mrinal Pandey. Hybrid ensemble of classifiers using voting. In *2015 international conference on green computing and Internet of Things (ICGCIoT)*, pages 399–404. IEEE, 2015.